INVESTIGATION OF RESIDUAL STRESSES AFTER SHOT PEENING PROCESSING

by

Siavash Ghanbari

A Dissertation

Submitted to the Faculty of Purdue University

In Partial Fulfillment of the Requirements for the degree of

Doctor of Philosophy

School of Materials Engineering

West Lafayette, Indiana

December 2019

THE PURDUE UNIVERSITY GRADUATE SCHOOL
STATEMENT OF COMMITTEE APPROVAL

Dr. David Bahr, Chair
School of Materials Engineering

Dr. Anter El-Azab
School of Materials Engineering

Dr. David Johnson
School of Materials Engineering

Dr. Michael Sangid
School of Materials Engineering
School of Aeronautics and Astronautics

Approved by:
Dr. David Bahr

Dedicated to Raheleh and my Parents

For their supports and encouragements

ACKNOWLEDGMENTS

First, thank to my advisor, professor David Bahr, for all his guidances, suggestions, advises, attentions and his endless support that he has given me over the past four years. I would like to express my gratitude to the committee members, Prof. Anter El-Azab, Prof. David Johnson and Prof. Michael Sangid for their helps and suggestions. I also would like to thank Prof. Jeffrey Youngblood for our productive research collaboration. I would like to thank my research collaborators specially Daniel Chadwick and Raheleh Mohammad Rahimi. I would like to thank the school of Materials Engineering staff, specifically Vicki Cline. Also, I would like to thank all my fellow members in our research group and MSE department. Finally, I would like to express my sincere gratitude to my wife, Raheleh, and my parents for their helps in all steps of my life.

This research was supported by Jack Champaigne of EI Incorporated, Jim Wheeler of Progressive Surface, the Center for Surface Engineering Enhancement at Purdue University (CSEE), Cummins Fuel Systems, Indiana Manufacturing, and Metal Improvement.

TABLE OF CONTENTS

LIST OF TABLES

LIST OF FIGURES

ABSTRACT

Mechanical surface treatments using an elastic-plastic cold working process can develop residual stresses on the surface of a workpiece. Compressive residual stresses on the surface increase resistance against surface crack propagation, so the overall mechanical performance can be improved by this technique. Compressive residual stresses can be created by different methods such as hammering, rolling, and shot peening. Shot peening is a well-established method to induce compressive residual stresses in the metallic components using cold working, and often ascribed to being beneficial to fatigue life in the aerospace and automobile industries. In this method, the surface is bombarded by high-velocity spherical balls which cause plastic deformation of the substrate, leading to a residual compressive stress after shot peening on the surface of the part. Computational modeling is an appropriate and effective way which can predict the amount of produced residual stresses and plastic deformation to obtain surface roughness after shot peening simulation. Finally, an experimental method to measure the magnitude of the residual stress using a nanoindentation technique was developed. The experimental indentation method was compared to both computational predictions (in aluminum) and with x-ray diffraction measurements of stress (in an alloy steel). The current study validates the relation between the nanoindentation method and numerical simulation for assessing the surface residual stresses resulting from single or multiple shot peening processes.

CHAPTER 1. INTRODUCTION

1.1. Introduction to Shot peening

Shot peening is a cold working process in which random impacts are made by small spherical particles on metal components. Shot peening contains multiple impacts on the metal substrate so each impact causes a small elastic-plastic deformation which creates compressive or tensile residual stresses. Typically, the velocity of a shot at the component is 50-70 m/s. Compressive residual stresses are developed by plastically deforming the metallic substrate and elastic deformation will be recovered by unloading of the impacting shot. Wohlfahrt showed two types of residual stresses that developed during the shot peening process, first a direct plastic elongation of the primary layer of the peened surface due to multiple shot dents and the second one is the elastic-plastic deformation that creates compressive residual stresses with a maximum intensity within the substrate [1]. The second residual stresses theory can be defined as a Hertzian pressure. In reality a combination of these two processes develops residual stresses after shot peening. The residual stresses have a maximum value below the surface at half of the dent radius [2].

This cold working process and residual stresses help to prolong the fatigue life. Fatigue cracks propagate along the surface with the application of tensile stresses, so compressive residual stresses on the substrate improve fatigue life. The important parameters in the shot peening process are: angle of the shot, velocity, material hardness, yield strength and friction [2]. Many researchers have focused on the numerical and experimental studies of residual stress distribution as well as the effect of the shot peening processing parameters on the stresses, often using numerical methods such as the Finite Element Method (FEM). This method is a quick approach to predict residual stresses with acceptable results.

Different experimental methods have been developed to measure residual stresses such as drilling [3], layer removal [4], X-ray diffraction [5] and magnetic methods [6]. But all these methods have some issues. Drilling and surface removal methods as examples are destructive methods, and the test accuracy is affected by many parameters during the experiments. X-ray method is unusable for amorphous materials in addition to the penetration depth limit in this method. Nanoindentation is a machine indentation technique which can be used to measure the mechanical properties of bulk materials in small scales. The metal substrate after shot peening is

affected by the residual stresses, which will change yielding and plastic straining [7, 8, 9]. Nanoindentation parameters such as hardness [10, 11, 12], loading and unloading behavior [13] and contacted pile-up area [14] are effected by residual stresses, although some researchers showed residual stresses don't always effect hardness [12]. Some new methods were developed by Suresh et al. [15] in order to measure the residual stresses by nanoindentation method. In this method for obtaining the equibiaxial residual stresses both stress-free and stressed samples should be compared with each other [15]. Lee at all suggested a new method to obtain the equibiaxial residual stresses by using stress relaxation with the shear plastic deformation [16]. Swadener et al found that residual stresses have more effect on spherical indentation than sharp indentation such as Berkovich tip [17].

1.2. Principle of Nanoindentation

The fundamental objective of nanoindentation experiment is to obtain hardness and elastic modulus from load and unloading curves. Usually, in load-depth curves. The depth of the penetration is reported from zero to a maximum number, then a load is returned from the maximum to the zero. After unloading, the materials try to recover their original shape, but some small parts cannot be recovered because of the plastic deformation.

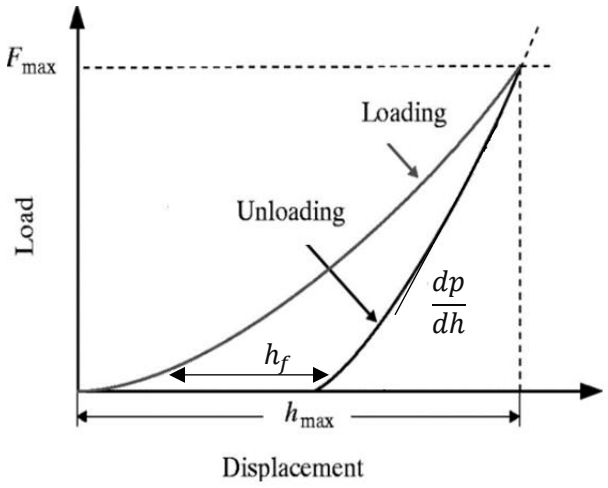

Figure 1- 1 Schematic of loading and unloading curves, nanoindentation method.

The cross-section profile of nanoindentation is shown in Figure 1- 1. Oliver-Pharr method is developed to measure hardness and modulus from the load depth-curves. The hardness H and reduced modulus E_r are defined by following equations [18, 19]:

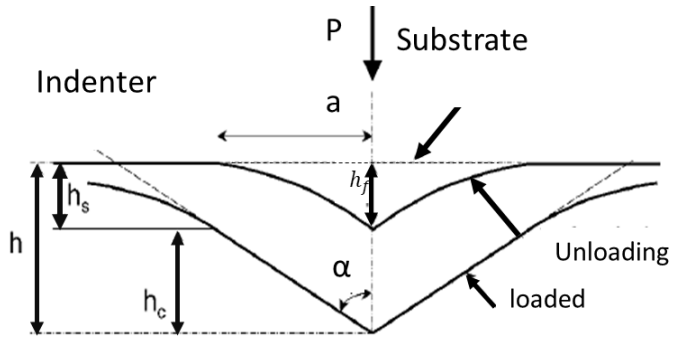

Figure 1- 2 Schematic of elastic plastic deformation after indentation.

$$H=\frac{P_{max}}{A_c} \qquad \text{Equation 1- 1}$$

$$E_r=\frac{S\sqrt{\pi}}{2\beta\sqrt{A_c}} \qquad \text{Equation 1- 2}$$

where A_c is the contact area, S is the stiffness at the initial unloading, P_{max} is the maximum load and β is a constant which is related to the geometry of the indenter for example for Berkovich tip β =1.034. A load-depth curve has three important parts which are shown in Figure 1- 1. These parameters are maximum load F_{max}, maximum displacement h_{max}, permanent plastic deformation h_f, contact depth hc and stiffness which is equal to the slope or $\frac{d_p}{d_h}$. Accuracy of these parameters is very important to calculate of hardness and modulus. Unloading curve can be shown by the power law relation:

$$p = \alpha(H - H_f)^m \qquad \text{Equation 1- 3}$$

where α and m are constant, usually exponent of this equation is between 1.2≤m≤1.6 [17]. Unloading process which is shown in Figure 2- 2. In this figure the amount of sink in is shown by h_s. If we assume that the pile-up area is negligible for elastic-plastic materials, then h_s will be:

$$h_s=\frac{\epsilon.\ P_{max}}{S} \qquad \text{Equation 1- 4}$$

where ϵ is a geometry factor of the indenter and contact depth between the indenter and materials is h_c:

$$h_c = h_{max} - \frac{\epsilon . P_{max}}{S}$$ Equation 1- 5

and the projected area of the indenter on the specimen is a function of h_c which is equal to the [20, 21]:

$$A_c = \sum_{n=0}^{8} C_n \ (h_c)^{2-n}$$ Equation 1- 6

By obtaining of the contact area, hardness and elastic modulus can be estimated and the effective elastic modulus can be determined by:

$$\frac{1}{E_{eff}} = \frac{1-\vartheta^2}{E} + \frac{1-\vartheta_i^2}{E_i}$$ Equation 1- 7

where E and E_i are the elastic modulus of the sample and indenter respectively, and also ϑ and ϑ_i are the Poisson's ratios respectively. Elastic deformation occurs in both sample and indenter and so effective elastic modulus will be calculated. Also, unloading stiffness can be calculated from effective modulus which is equal to:

$$S = \beta \frac{2}{\sqrt{\pi}} E_{eff} \sqrt{A}$$ Equation 1- 8

this equation can be used for all axisymmetric indenter and all geometry and shape of the indenter [2]. In this equation β is a constant that is related to the axial symmetry for indenters. Materials hardness also can be determined by combining Eq (1-8) and Eq (1-1) and taking $\beta = 1$ leads to another equation for hardness as a fallowing equation [19]:

$$\frac{4}{\pi} \frac{P_{max}}{S^2} = \frac{H}{E_{eff}^2}$$ Equation 1- 9

1.3. Effect of Residual Stresses on Indentation

Nanoindentation has been used to examine the effect of the residual stresses on the specimen. Modulus and hardness were observed to increase by applying compressive residual stresses and decreases by tensile stresses experimentally. But modulus should be the intrinsic property of the materials, therefore it has to be constant. So, this error is resulted from the pile-up area around the indentation. By calculating correct contact area, hardness and elastic modulus are independent of the residual stresses [22, 20]. However, Residual stresses can change the load-depth curves. By

assuming the same dent depth, the loading curve for compressive residual stresses is a higher than the stress-free sample. Also, oppositely the load-depth curve is lower for tensile residual stresses in comparison with free stress sample [23, 24]. Additionally, unloading curves for tensile and compressive residual stresses will be shifted to the right or left respectively [23].

1.4. Cold Working effect on Indentation

Materials after cold working exhibit pile-up area around the indent point which is the result of incompressibility after cold working [25, 26] therefore the height of the pile-up is important for when assessing the contact area of the impression after indentation. Pile-up also increases as the included angle of the indenter decreases.

1.5. Shot Peening Analytical Analysis

Combining of the Hertzian contact theory and elastic- plastic theory is the first approach to model a shot impact as an analytical model [2, 3]. Al-Hassani developed bending and axial stress to obtain residual stresses by adding source stress. But finding the proper boundary conditions is a crucial step. For this reason, one effective way to define the accurate boundary is considering the low coverage of the material surface for shot peening. Khaboua showed that this assumption for some materials such as aluminum cannot be right because of their complex plastic behavior [27]. Hence source stress was assumed as a cosine function in this method [28]. Shen and Alturi developed an analytical model for linear hardening materials [29].

1.6. Elastic Loading Condition

In the analytical modeling of shot peening some assumptions need to be considered. Materials are isotropic, the substrate and body are semi- infinite, materials are strain rate dependent and strain hardening dependent, velocity and impact trajectory is perpendicular to the substrate there is no friction between the ball and surface and indenter is a perfect spherical shape. Two different models can be assumed for the indenter: deformable body and analytically rigid body. In order to obtain the stress value under the impact condition, Hertzian contact theory or maximum normal elastic pressure is shown as following [30]:

$$p = \frac{1}{\pi}\left[\frac{5}{2}\pi k\rho v^2 E_0^4\right]^{\frac{1}{5}}$$ Equation 1- 10

In this equation v is the initial velocity E_0 is the relative modulus and K is efficiency constant which is related to the thermal dissipation. Maximum elastic residual stresses are shown as following equation as well:

$$\sigma_{11}^e = p(1+v)\left[\frac{X_3}{r_e}\, tan^{-1}\, \frac{X_3}{r_e}\ \text{-1}\right] + p_2 \frac{r_e^2}{(r_e^2+x_3^2)}$$ Equation 1- 11

$$\sigma_{22}^e = p(1+v)\left[\frac{X_3}{r_e}\, tan^{-1}\, \frac{X_3}{r_e}\ \text{-1}\right] + p_2 \frac{r_e^2}{(r_e^2+x_3^2)}$$ Equation 1- 12

$$\sigma_{33}^e = -p\left[1+\frac{{x_3}^2}{r_e}\right]^{-1}$$ Equation 1- 13

In these equations x_3 direction along impact direction, r_e is the maximum radius of the elastic contact.

1.7. Plastic Deformation

Shot peening deforms the substrate plastically during the impingement. The relation between the plastic deformation and strain rate are defined by Johnson-Cook equation. In Johnson-Cook equation, both strain rate and strain hardening are considered. This equation has been used in many high strain rate applications such as shot peening [30, 31].

$$\sigma = [\text{A}+\text{B}(\bar{\varepsilon}^N)\ [1+\text{Cln}\ (\frac{\dot{\bar{\varepsilon}}}{\dot{\bar{\varepsilon}}_0})]\ [1-(\frac{T-T_0}{T_M-T})^M]$$ Equation 1- 14

In this equation A, B, C, m and n are materials constant, $\bar{\varepsilon}$ and T_0 are reference amounts and both $\dot{\bar{\varepsilon}}$ and T terms are under examination condition and finally T_m is the melting temperature. Regarding to the plastic stress deviators, residual stresses are shown as following.

$$\sigma_{11}^r = \frac{1}{3}\left(\sigma_i^p - 2\sigma_i^p - \Delta\sigma_i^p\right)$$ Equation 1- 15

$$\sigma_{22}^r = \frac{1}{3}\left(\sigma_i^p - 2\sigma_i^p - \Delta\sigma_i^p\right)$$ Equation 1- 16

$$\sigma_{33}^{r} = -2\sigma_{11}^{r}$$ Equation 1- 17

1.8. Almen Modeling and Almen Intensity

When an impact occurs between two solid materials, two possibilities can be considered. The first one is the perfect elastic impact, in this case all potential energy is transmitted into the reversed kinetic energy. The second possibility is the elastic-plastic deformation. In this situation, some portion of the energy is transmitted to the reversed kinetic energy, but the other part causes plastic deformation. Therefore, the restitution or recovery coefficient for impact can be calculated as the following equation [32]:

$$e_r = \frac{V_2 \sin \alpha}{V_1 \sin \alpha}$$ Equation 1- 18

In this equation m is equal to the shot particles mass, V_1 is impact velocity, V_2 is returning velocity and α impact angle. The e_r parameter which depends on the material hardness and contact properties which is between 0 and 1. Minimum or maximum number represent perfect plastic and elastic contact respectively [32]. Spinning and sliding can happened during the shot peening so in this condition only the penetration considered as the deformation mechanism to avoid more complications and energy differences after impact can be expressed by the following equation:

$$W_p + W_d = \frac{mV_i^2(1-e_r^2)}{2}$$ Equation 1- 19

in this equation W_p is the energy which is needed for plastic deformation and W_d is the energy loss such as heat and vibration during the impact. Regarding the energy transfer to the sample during the shot peening, standard test strips were developed by Almen and Black [33]. This test consists of two parts which is called Almen strips and Almen gage. In this test a thin sample of the metal is subjected to the plastic deformation by shot peening on one of its sides. Then the sample will be bended after releasing from the rigid substrate. Almen measured the arc height at the center of the sample during the shot peening process. Higher arc measurement shows higher kinetic energy has been transferred to the sample. Simulation of the Almen gage can help us to improve shot peening quality and parameters such as incubation time for shot peening, velocity, diameter of shot particles and effect of strain rate.

1.9. Fatigue Improvement by Shot Peening

The majority of experimental results for failure analysis show cracks propagate from the surface or very close to the surface. Shot peening can prevent the crack growth on the surface by producing compressive residual stresses but numerous factors can reduce shot peening capability to improve fatigue life [34]. Therefore, understanding the shot peening process and results require more details about residual stresses corresponding to the microstructure. Shot peening process is subjected to different important parameters such as mass of the impact ball, ball diameter, impact velocity and angle of the impacts. As a results broad statistical variation for impingement can be considered during the shot peening. Higher residual stresses are equal to the higher impingement coverage which is desirable but higher coverage cause surface damage and reversed crack growth into the materials specially in a slim sample. Also stress concentration around harder solid solution particles or intermetallic components increase the risk of the crack nucleation around those particles [34]. In this way measuring of the residual stresses in different location with reliable method is very important. Obtaining the optimum of shot peening parameters and impingement coverage by computer modeling and nanoindentation method not only will increase the material performance but also decrease any disadvantage of shot peening due to the excess of the residual stresses on the surface.

1.10. Effect of the Temperature and Plastic Deformation after Shot Peening

Under the loading condition, temperature and plastic deformation can release compressive residual stresses after shot peening because of stress relaxation or creep mechanism **[34, 35]** [53,54]. Monotonic and cycling relaxation release compressive residual stresses as a result of shot peening process is not effective enough, however stress amplitude should be high enough to release compressive residual stresses [54]. Modeling of shot peening and temperature dependent cyclic loading can help to find the certain amount of stress or strain amplitude to avoid complete stress relaxation and increase general life enhancement.

1.11. Modeling dynamic or static analysis

Finite element simulation provides a wide range of stress analysis after shot peening. Modeling can be multiple shots or a single shot. Multiple random impacts are favorable for shot peening

process due to the shot peening random nature. Also, shot peening simulation can be carried out using a dynamic explicit or quasi-static procedure. During explicit dynamic modeling, initial shot velocity should be assigned. For implicit quasi static modeling, displacement of the shot should be assigned during the simulation, therefore dimple size should be determined. Each method has an advantage and disadvantage. The advantage of dynamic simulation is related to the explicit integration, which can handle nonlinear problems. Therefore, constant calculation is not needed to obtain a tangent stiffness matrix. Consequently, for large analysis dynamic explicit is more efficient in compare with quasi-static model. Also, this model is more realistic in comparison with the quasi-static model for shot peening simulation. Shot peening has a dynamic nature and it has preassigned velocity due to the back pressure in the nozzle. However, there is one drawback in the use of the dynamic explicit model. During dynamic impact simulation (small model dimensions) stress waves are reflected at the boundary into the system. Guagliano et al. solved this problem by averaging the stress [36]. There are some other techniques to solve this problem such as damping technique [37] or non-reflecting boundary [38, 39, 40]. In this research averaging technique and nonreflecting boundary were used.

1.12. Materials Modeling

The material model for shot peening simulation can be range from isotropic, kinematic, or combined models (kinematic and isotropic) hardening. Many researches showed using only kinematic hardening cause small maximum compressive residual stresses in comparing with isotropic hardening [41, 42]. This phenomenon is related to the reverse plastic flow which cannot be captured by the isotropic hardening model [43]. Al-Hassani and Meguid showed due to the nature of shot peening and plastic strain rates up to (5×10^{6} 1/s) ~ (6×10^{6} 1/s) there is a difference between dynamic simulation with strain rate sensitivity and quasi-static model [44, 45]. Some researchers found using a strain rate effects reduced plastic deformation in shot peened surface and using strain rate effect and power-law cause unusual high compressive residual stresses [40, 46]. They showed that the main reason for overestimation for cyclic impact is not related to the strain rate effect, but also this is related to cyclic deformation and Bauschinger effect which was not considered during simulation [47]. They showed using combined isotropic and kinematic hardening has a good correlation with experimental results for shot peening process due to the cyclic hardening and deformation [40, 39, 48, 47]. In this research work in chapter IV combine

kinematic and isotropic hardening was used for multiple random impacts modeling. In chapter II small domain 300μm×300μm has been used for shot peening simulation. For full coverage, three basic rows of shot particles were designed. In this simulation, the Johnson cook model was used in aluminum substrate to include strain rate hardening. In experimental studies shown by Jayaraman [49] Johnson-Cook model is valid for large plastic strains with high strain rate 5×10^5 ~6×10^6 1/s such as shot peening [40]. Johnson-Cook model relates the elastic-plastic stress and strain with high strain hardening and strain rate phenomena for some materials such as aluminum and Inconel [50]. Eitobgy showed shot peening simulation with Johnson-Cook model for target materials with strain rate hardening has a good and realistic behavior [51]. In conclusion, Johnson-cook equation is the model shows good correlation of impact and drop-test which enables to capture work hardening effect due to the plastic deformation, the only drawback of this model is related to the hot working (high temperature) due to the recrystallization which is not the case in this research [52].

1.13. Conclusion

This background setting the stage for the remainder of the thesis has focused on the creation, and evaluation of residual stresses after shot peening process. Nanoindentation is a promising experimental technique to extract the related mechanical behavior while determining residual stresses. In the next chapters residual stress will be measured by nanoindentation technique with comparing contact area between stressed sample and stress-free sample. This technique has the capability to evaluate hardness and residual stresses under the impingement surface after shot peening. Also, nanoindentation results will be validated by X-ray technique. Finite element simulation can predict the experimental results and shot peening parameters such as velocity, impact diameter, impact angle and exposure time. Finally, in this research random impact modeling was developed to create a link between model shot energy to Almen strip intensities and the better understanding of residual stresses and surface characterization.

CHAPTER 2. RESIDUAL STRESS ASYMMETRY IN THIN SHEETS OF DOUBLE-SIDE SHOT PEENED ALUMINUM

A portion of this chapter is previously published in journal of Journal of Materials Engineering and Performance by Siavash Ghanbari, Michael D. Sangid, David F. Bahr as " Residual Stress Asymmetry in Thin Sheets of Double-Sided Shot Peened Aluminum", 28, Issue 5, pp 3094–3104, 2019. https://doi.org/10.1007/s11665-019-04066-3

A portion of this chapter is previously published in journal of Fatigue & Fracture of Engineering Materials & Structures by Daniel J Chadwick, Siavash Ghanbari, David F Bahr, Michael D Sangidas as " Crack incubation in shot peened AA7050 and mechanism for fatigue enhancement", 41, Issue 1, pp 71–83, 2018. https://doi.org/10.1111/ffe.12652

2.1.Abstract

The local mechanical properties and residual stresses of a double side shot peened aluminum alloy AA7050-T7451 sheet were measured by nanoindentation and simulated by the finite element method (FEM). The variation of the pile-up area around the indentation due to residual stresses, as well as changes in hardness as a function of cold working, was assessed. Numerical simulations were conducted to investigate the residual stress profile. When the indentation contact area was corrected to account for pile-up induced from residual stresses the hardness increased about 10% over the range of depths at which compressive residual stresses exist, indicating some strain hardening did occur. The maximum compressive residual stress for the second shot peened surface is on the order of 10% higher than the first surface; this is ascribed to the sequencing during the peening process, in which the first side peening influenced the stress throughout the part thickness for these thin plate structures. The ability to couple FEM simulations and rapid experimental assessments of residual stresses and hardness allows for future prediction of part thickness effects in double-side peening processes.

2.2. Introduction

Shot peening is a well-established and cost-effective method to induce compressive residual stresses in metallic components using localized cold working, often leading to increases in fatigue life [53]. The important parameters in the shot peening process include properties of the shot itself (i.e. the shot mass, hardness and size); parameters such as the velocity of the shot and the angle at

which the shot impacts the surface; and finally the properties of the material being processed, such as the sample hardness (or yield strength), strain hardening behavior, and the friction between the shot and sample [53]. Compressive residual stresses develop as an elastic response to the plastic deformation of the metallic substrate. Wohlfahrt showed two types of residual stresses develop during the shot peening process, the first is a result of the direct plastic elongation of the primary tangential layer of the peened surface due to multiple shot impacts and the second is a consequence of the elastic-plastic deformation that creates compressive residual stresses perpendicular to the free surface with a maximum intensity within the substrate [1], which can be modeled as a Hertzian pressure. The net residual compressive stresses have a maximum value below the surface at a depth on the order of half of the residual impression radius [2].

Many researchers have carried out numerical and experimental studies for predicting or measuring the residual stresses distribution as well as the effect of the shot peening processing parameters on the resulting stress distribution. The Finite Element Method (FEM) provides a rapid method to predict residual stresses with acceptable results for multiple impacts analyses. Both axisymmetric 2D dynamic models for plastic deformation with rigid spherical impact [54, 55] and periodic symmetric cells with 3D modeling have been developed [56, 57, 45, 37]. The effect of peening coverage and impact ball position on the residual stress profile have been established [58, 59]. Other important parameters during shot peening such as peening energy, rigid shot properties and plastic deformation of the substrate have been studied [60, 61], and commercial examples of simulations of shot peening [62] are available using a range of packaged software [60, 61, 62, 39, 36].

Several experimental methods exist to obtain residual stresses at a length scale appropriate to shot peened parts, such as hole drilling [3], layer removal [4], X-ray diffraction [63] and magnetic methods [6] as well as combinations of these methods. Drilling and surface removal methods are accurate but destructive methods, and the test accuracy can be affected by many parameters during the experiments. X-ray diffraction methods based on the lattice strains provide effective means to quantify residual stress near the free surface (with the X-ray energy determining the depth of penetration). X-ray diffraction can be used with an iterative surface removal technique, such as electropolishing, to quantify residual stress as a function of depth via layer removal, but this method is most appropriate for thick specimens. In the case of thin and double side shot peened materials, distortion can occur during layer removal due to balancing internal stresses. High energy

X-ray diffraction techniques exist to determine residual stress throughout a workpiece, but these methods require a synchrotron radiation source [64, 65]. Nanoindentation (instrumented indentation) can be used to measure the mechanical properties of bulk materials on small scales [66]. The metal substrate after shot peening is affected by the residual stresses, which may change yielding and plastic straining behavior [66, 7, 8, 9]. Nanoindentation parameters such as hardness [10, 23, 67], loading and unloading behavior [68] and the residual pile-up area [13] can be affected by residual stresses. Suresh et al. [15] developed an analysis procedure to extract equibiaxial residual stresses from nanoindentation by comparing the loading profile of stress-free and stressed samples [15]. Lee et al. suggested equibiaxial residual stresses could be identified by using stress relaxation with knowledge of the shear plastic deformation during indentation [16]. Swadener et al. found that biaxial residual stresses have a more significant effect on spherical indentation than sharp indentations such as the Berkovich tip [17]. In order to further investigate the material response during nanoindentation characterization, numerical approaches have been developed for indentation analysis based on the fact that the contact area and contact depth are affected by the pile-up area, which can be correlated with the elastic strains and associated residual stresses present in the material [69, 70].

In the current work, we have developed an experimental procedure to quantify residual stresses using nanoindentation, which is then applied to a double side shot peened specimen. Additionally, finite element modeling was used to model the double side shot peened and nanoindentation process to illuminate residual stress prediction and the effect of the residual stresses on the mechanics of the indentation, respectively.

2.3.Materials, Specimens and Test Procedure

2.3.1 Nanoindentation method

Figure 2- 1 shows a schematic of the nanoindentation process, wherein the depth of the penetration of a tip into a softer material is monitored during the process of loading, holding at a fixed load, and subsequently unloaded, creating what is conventionally referred to as a load-depth curve. After unloading, the material recovers the elastic deformation, leaving a residual impression of the indentation. The schematic profile of an impression in cross section is shown in Figure 2- 1. for the case where there is neither pile up nor sink in around the indentation volume. The Oliver-Pharr

method is commonly used to extract hardness and modulus from load depth-curves. The hardness H and reduced modulus E_r are defined by [17, 69, 70, 18, 19, 20, 21]:

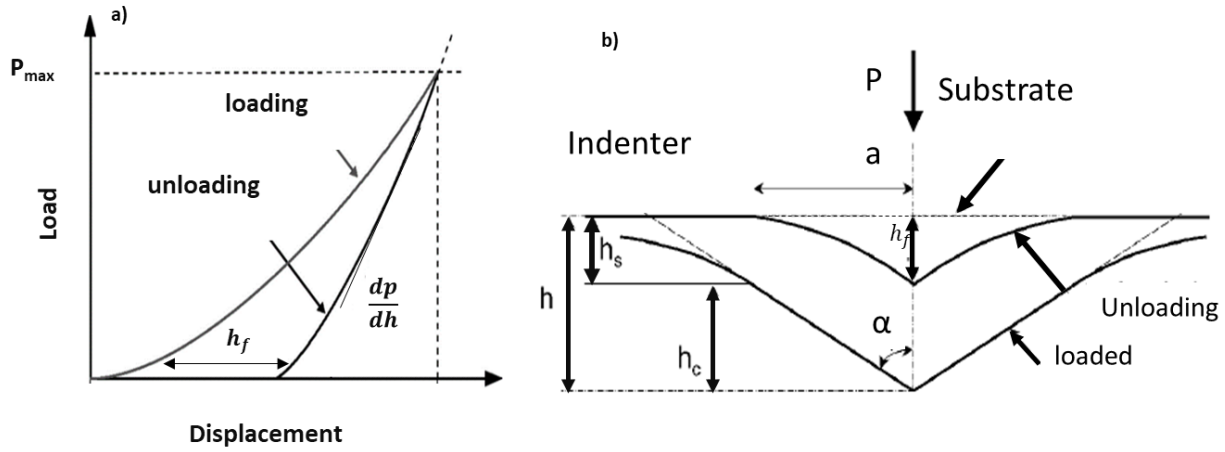

Figure 2- 1 a) Schematic of nanoindentation loading and unloading curves, b) Schematic of elastic plastic deformation after indentation.

$$H=\frac{P_{max}}{A_{c(h_c)}} \qquad \text{Equation 2- 1}$$

$$E_r=\frac{S\sqrt{\pi}}{2\beta\sqrt{A_c}} \qquad \text{Equation 2- 2}$$

where A_c is the projected contact area, S is the stiffness at the initial unloading, P_{max} is the maximum load and β is a constant related to the geometry of the indenter, for example for a Berkovich tip β =1.034.

It is important to note that A is conventionally determined by performing indentations into materials of known elastic modulus and minimal pile-up, and then creating a calibration curve that relates contact depth to the projected contact area of the tip. The contact depth h_c can be found knowing P_{max}, S, and the maximum displacement h_{max}, using

$$h_c=h_{max}-\frac{\epsilon.\ P_{max}}{S} \qquad \text{Equation 2- 3}$$

where ϵ is a constant related to the shape of the indenter (about 0.75 for the Berkovich tip) [19]. Finally, the elastic modulus of the sample can be obtained from the reduced modulus, E_r

$$\frac{1}{E_r} = \frac{1-\nu^2}{E} + \frac{1-\nu_i^2}{E_i}$$ Equation 2- 4

where E and E_i are the elastic modulus of the sample and indenter respectively, also ν and ν_i are the Poisson ratios of the sample and indenter, respectively [19].

2.3.2 Effect of residual stresses on Indentation and residual stress determination

Nanoindentation load-depth curves, and the residual impression left by an indentation, are effected by the residual stresses in the specimen. Figure 2- 2 schematically shows the expected changes for loading conditions in materials with residual stresses. The experimentally perceived elastic modulus and hardness determined from an unloading slope analysis can appear to increase by applying compressive residual stresses and decrease in the presence of tensile stresses. But, since the modulus is an intrinsic property of the material, it must be constant; this perceived error results from the pile-up area around the indentation, which for most metals is increased around the indentation impression by the application of biaxial compressive stresses. By calculating or measuring the correct contact area by determining the effective contact depth, hardness and elastic modulus are generally found to be independent of the residual stresses [21, 71, 13, 8, 72] using a correction such as

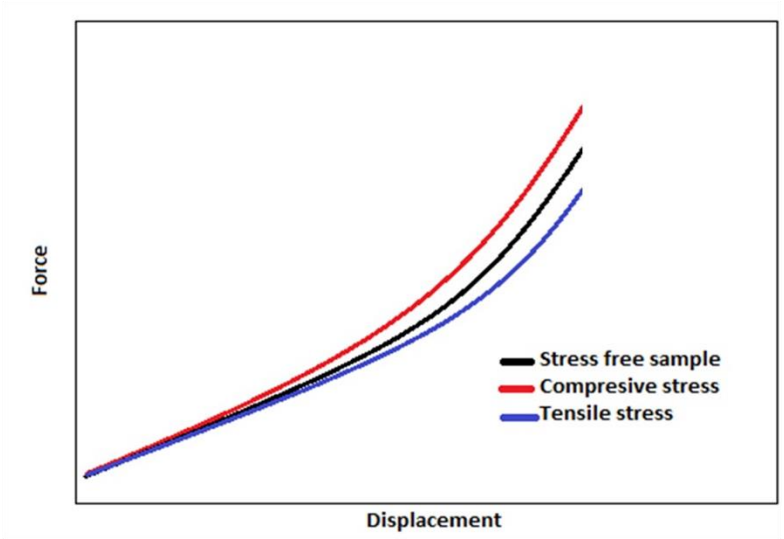

Figure 2- 2 Schematic loading curves for tensile and compressive residual stresses compare with the stress-free sample.

$$h_c = h_{primary} + h_{pileup} = h_{primary} + \frac{h_{pileup-1} + h_{pileup-2} + h_{pileup-3}}{3}$$ Equation 2- 5

(where 1,2 and 3 subscripts are the three edges of the pile-up area, which are shown in the inset of Figure 2- 3 for an indent impression) then the corrected contact depth is used to determine the real contact area in Eq. 1. Based on the Suresh and Giannakopoulos model [15], residual stresses on the sample can be found by comparing the relative contacts areas for the same loading conditions of the stressed sample and stress-free sample as:

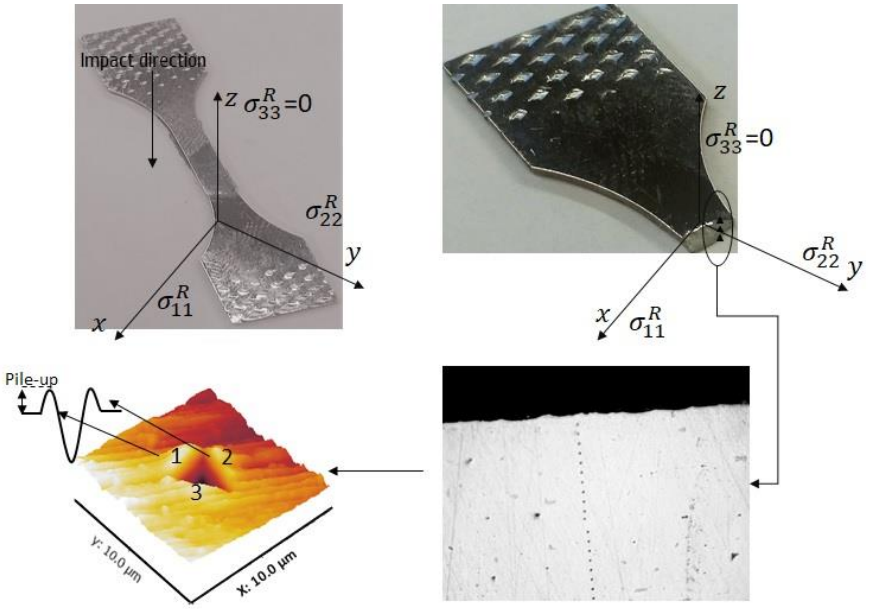

Figure 2- 3 Sample used for double side shot peening and the surface used for indentation on the cross-section area highlighting the residual impression.

$$\sigma_t = H\left(\frac{A_0}{A} - 1\right)$$ Equation 2- 6

$$\sigma_c = \frac{H}{\sin\alpha}\left(1 - \frac{A_0}{A}\right)$$ Equation 2- 7

Where Eq (2-6) is used to account for compressive stresses and Eq (2-7) for tensile stresses. Here, α is the effective half angle of the indenter tip, for the Berkovich tip 24.7°, and A_0 and A are the projected contact area for stress free and stressed samples, respectively. The Suresh model assumes a biaxial surface residual stresses and a homogenous substrate [26, 73]. Tsui et al. showed uniaxial and biaxial residual stresses have the same influence on the contact area [23]. Based on the Suresh

model and Tsui et al investigation, the equibiaxial residual stress state leads to hardness results that will generally exceed the hardness for materials under uniaxial residual stresses by approximately 10-20% [24, 28]. When the shot peening process results in uniform coverage over the specimen's surface, then stress and strain tensor can be shown as [74, 75]:

$$\sigma^{rs} = \begin{pmatrix} \sigma(z) & - & - \\ - & \sigma(z) & - \\ - & - & \emptyset \end{pmatrix} \quad \text{Equation 2- 8}$$

$$\varepsilon = \begin{pmatrix} - & - & - \\ - & - & - \\ - & - & \varepsilon(z) \end{pmatrix} \quad \text{Equation 2- 9}$$

These stress and strain tensors are demonstrated in a coordinate system shown in Figure 2- 3, where the dash lines represent a value close to zero and Ø indicates a value denoted as a zero due to the traction free surface boundary conditions. Also, the tensors exhibit values that are independent of the X and Y direction on the impact plane, once 100% shot peening coverage is reached. In the present paper, by cutting the sample to access the cross section, the residual stress was spatially determined along the thickness of the sample based on the Suresh model (with qualitative support based on the morphology of the post-indentation impression); and then the results were compared by double sided shot peening simulation. This is elaborated upon in part 2-5.

2.3.3 Shot peening process

Flat dog bone samples of aluminum alloy AA7050-T7451 with a nominal thickness of 1.6 mm and a gauge section 3 mm in width and 10 mm in length with an overall length of 48 mm were polished with 1200 SiC paper (Figure 2- 3) [76]. The double side shot peening was carried out by a commercial supplier using Z150 ceramic shot with an average diameter on the order of 150 µm. The shot peening nozzle was a V-type model, the accelerating air pressure was 41.4 kPa, and a 152.4 mm standoff distance was used. The first side of the coupons were peened, then the part flipped, and the reverse side was peened using the same conditions [77].

2.3.4 Sample preparation and nanoindentation

A cross-section of the sample normal to the shot peened surface was cut for both shot peened and unpeened samples with a diamond saw. The cross-sectioning releases stress with directional components perpendicular to the cutting surface, while the other two directions still maintain their residual stress. The cross section was ground through 1200 grit paper, followed by polishing with 6 and 3 μm diamond paste. Nanoindentation was carried out using a Hysitron TI950 system with a Berkovich tip, the tests were conducted in depth control mode with a maximum depth of 320nm, using 50nm/s loading and unloading rates and a 20s dwell time at the maximum depth. The partial unload method was used to evaluate modulus and hardness as a function of depth for any given indent, and the indents were spaced in a line pattern with 30 μm distances from edge to edge. The indentation tip area function was calibrated with fused quartz. Post-indent impressions exhibited some pile-up, therefore post indentation imaging was used Eq (2-5) to determine the effective contact depth and true contact area.

2.3.5 Shot peening modeling

The FEM method was used to simulate multiple shots impinging upon the substrate using a strain rate dependent elastic-plastic formulation. The simulation consisted of rigid spherical bodies with 150 μm diameter impacting an aluminum 7050 sheet for the substrate. ABAQUS/Explicit was used for finite element modeling. A simulation of a single side shot peened sample with dimensions of a standard Almen strip (76 mm long, 19 mm wide, and 1.3 mm thick) was run, and the stress profile as a function of depth was compared to that of a simulation of a unit cell of 300 μm x 300 μm x 1600 μm. The stress profiles of the two simulations were similar, and so for computational efficiency, subsequently all simluations were performed on the smaller unit cell. A mesh sensitivity analysis was conducted to determine the mesh size, and the unit cell was selected to ensure 100% coverage of the peened surface. The simulation set-up is consistent with peening simulations in literature [78]. For conducting the double side shot peening two steps were defined. The first side of peening was simulated, and then the first step's results in terms of strain and strain at the integration points of each element were transferred to the second step as a predefined field for the initial state of the model [78]. Non-linear geometry was assigned in ABAQUS to control the large distortion and plastic deformation. For boundary conditions, each opposite side of the

impact at each step was fixed in all directions ($U_X=U_Y=U_Z=0$) and four sides of the unit were fixed in the X and Y directions ($U_X=U_Y=0$). In this study, the effect of temperature due to friction during shot peening was not considered, due to the relatively low coefficient friction. Hence, adiabatic heating was negligible and therefore the effect of temperature on shot peening was not considered The Johnson-Cook equation was used for relating stress and plastic strain, accounting for strain hardening and strain rate dependency

$$\sigma = [A+B\varepsilon_p^n)\ [1+C\ln\ (\frac{\dot{\varepsilon_p}}{\dot{\varepsilon_0}})]\ [1-(\frac{T-T_0}{T_M-T})^m] \qquad \text{Equation 2- 10}$$

In this equation *A,B,C, m* and *n* are materials constants, material properties and model parameters are shown in Table 2- 1and Table 2- 2 respectively. ε_p is the equivalent plastic strain, $\dot{\varepsilon_0}$ and $\dot{\varepsilon_p}$ are the reference strain rate value and applied strain rate, respectively, T_m, T and T_0 are melting temperature, current temperature in the simulation and reference temperature, respectively. The residual stress values were averaged along the peening direction on the unit cell, in order to depict the residual stresses in the material as shown in Figure 2- 4. Finally, the residual stresses developed by the FEM simulation were compared with experimental measurements.

Table 2- 1 Physical and material properties of Aluminum 7050 used for this study [79]

Property	**Aluminum 7050**	**Dimond**
Elastic Modulus	71.7 GPa	1220 GPa
Yield stress	500 MPa	1200 MPa
Shear modulus	26.9 GPa	470 GPa
Ultimate strength	524 MPa	2800 MPa
Density	2.8 $\frac{gr}{cm^3}$	3.52 $\frac{gr}{cm^3}$

Table 2- 2 Materials parameters used for Johnson-Cook equation [79].

Material parameter	**A**	**B**	**n**	**m**	$\dot{\varepsilon_0}$
Aluminum 7050	500 MPa	530 MPa	0.58	1.1	1

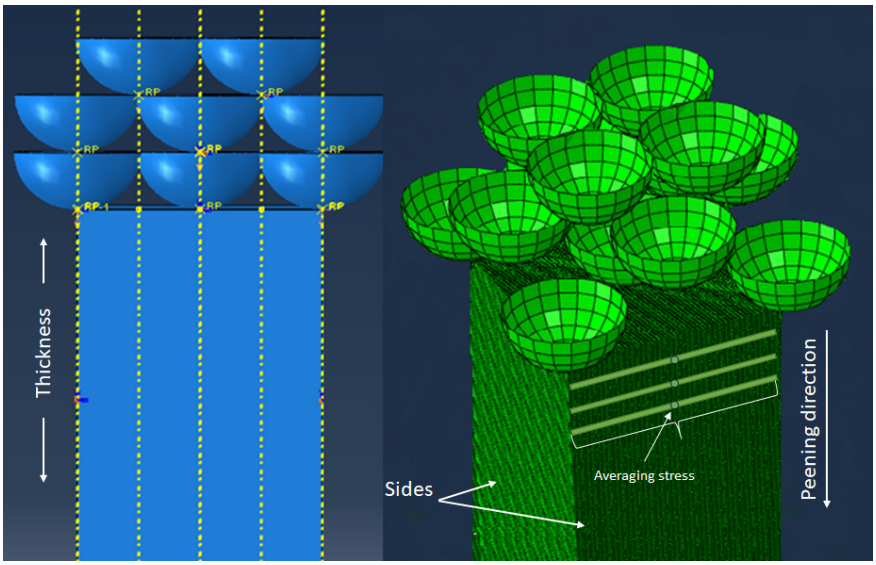

Figure 2- 4 FE unit cell model under multiple impacts.

For multiple impacts on a given surface, three basic rows in each step are defined for shot particles interacting with the top surface. Each row is horizontal and the space between rows are equal. The second and third rows cover the interstitial space of each lower layer. The rigid spherical shot in each row impinges upon the surface without interaction with each other. The FE model for shot peening is shown in Figure 2- 4.

2.3.6 Nanoindentation modeling

A 3D model of nanoindentation with Berkovich tip was conducted to study of the load-depth curves and comparing the load-depth curves between stress-free sample and stressed sample. The result of the shot peened sample close to the shot peened surface in an Abaqus was transferred to the dynamic step in order to do the nanoindentation simulation. In this FEM modeling for stressed-sample simulation, compressive stress tensor was considered in a pre-boundary condition section. Assigned compressive stress tensor was equal to the residual stress tensor that was close to the simulated shot peened surface.

$$\sigma^{rs}\,(Mpa) = \begin{pmatrix} -437 & -10 & +8.5 \\ -10 & -45 & -6.9 \\ +8.5 & -6.9 & -436 \end{pmatrix}$$

The standard Berkovich tip was used for modeling with elastic Dimond physical properties which is shown in Table 2- 1. Substrate was modeled as a cube with measures 30 µm ×30 µm and the depth of the 40 µm. The cube was modeled with C3D8R hexagonal elements. The very fine mesh was considered around indent point in order to reduce computational time and study of stress and strain around and beneath of the indentation. Nonlinear geometry and Johnson-Cook model were defined for strain-rate effects during indentation for the substrate, same as the shot peening simulation in the section 2.2.5. Physical and materials properties for aluminum substrate has been defined in Table 2- 1 and Table 2- 2. Both loading and unloading indentation process were simulated in one dynamic step. The simulation was considered as a displacement or a depth control mode same as real nanoindentation test. The contact behavior was defined as a surface to surface contact. In this model indenter and substrate surface was chosen as a master and slave surface respectively. Indenter was considered as a diamond rigid body. For boundary conditions the bottom of the cube was fixed in all directions (ux=uy=uz) and indenter was fixed in X and Z directions (UX=UZ =0). According to the reference the friction coefficient was considered as a 0.6 during simulation [80]. Nanoindentation setup simulation has been shown in Figure 2- 5.

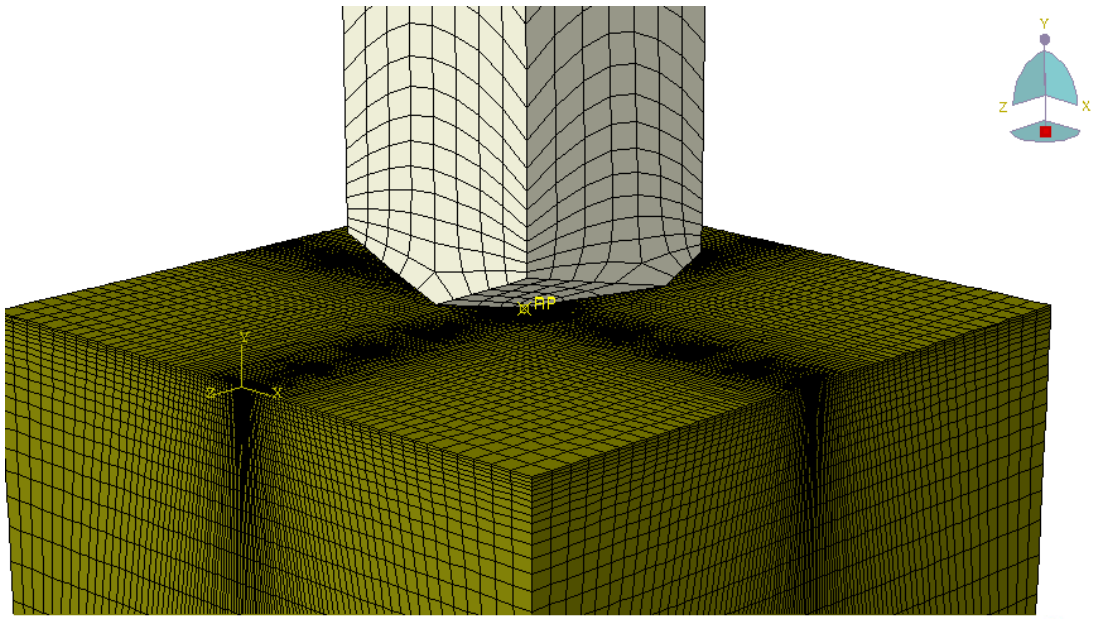

Figure 2- 5 Nanoindentation modeling setup Berkovich tip.

2.4.Results and Discussion

The results will present the experimental measurements of the material's hardness as a function of position across the entire thickness of the aluminum sheet, including the residual stresses extracted from the pile up around the indentations. Then the residual stresses from the FEM simulation of the double side shot peened sample will be presented and compared to the results of the nanoindentation experiment.

2.4.1 Nanoindentation experiment and hardness measurements

A cross section of the sample, shown in Figure 2- 6 was used to measure both the hardness profile as well as the residual plastic deformation around each indentation. Compressive residual stresses should lead to more pile up around an indentation [8], and the indentations near the peened surfaces exhibited higher pile up around a given indentation than those near the center of the sample which is shown in Figure 2- 7. In order to minimize any bias during the residual stress calculation, indentations were placed at the same distance from the surface in both the peened and un-peened samples. The measured hardness for both samples is shown in Figure 2- 8. The hardness values were corrected by considering pile-up height through Eq. (5) and Eq. (1). A smoothed average of hardness from six indent positions after shot peening is shown by the dashed in Figure 2- 8. The hardness increases near each surface compared with the center of the specimen. The hardness in the first 100 μm of the sample thickness on each side varies between 2.3 to 2.0 GPa. There is a minimum hardness in the center, ranging from 1.7 to 2.0 GPa, which is very similar to the average hardness of 2.0 GPa for the stress-free sample. Due to the small size of the indentations, it is likely that there is an indentation size effect, leading to a measured hardness which is higher than would be found using a larger Vickers or Rockwell indentation. However, since all indentations were performed in depth control, the relative difference in hardness should be independent of the indentation size.

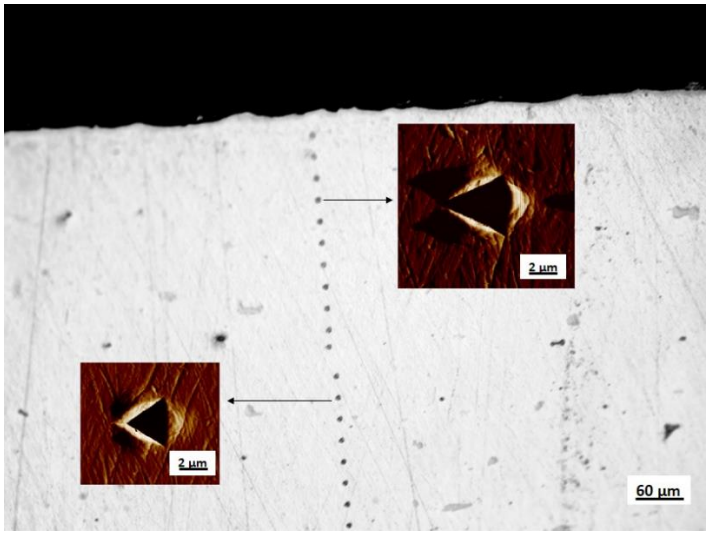

Figure 2- 6 Nanoindentation pattern in double side peened aluminum 7050, insets show scanning probe images of pile up around impressions.

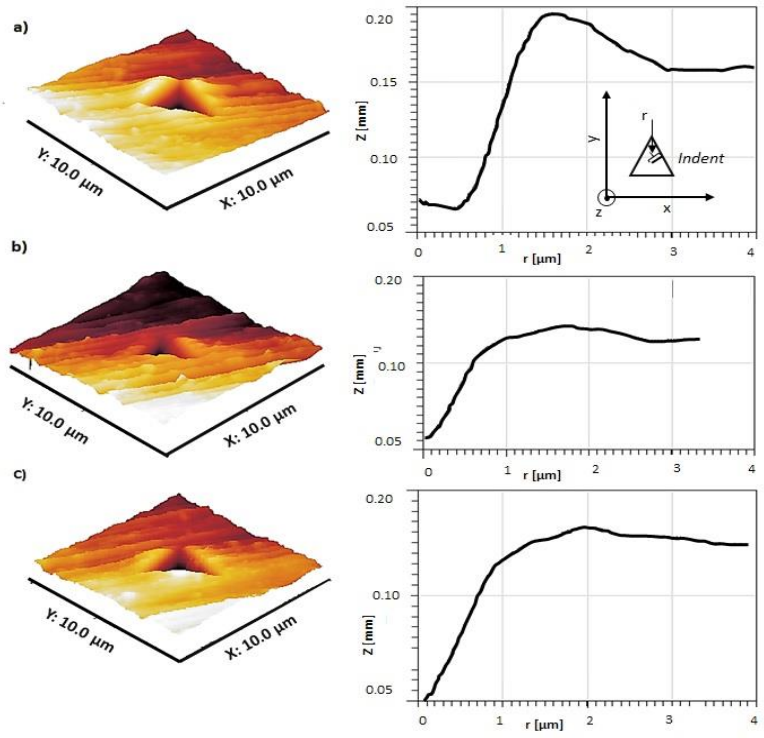

Figure 2- 7 Topography of 2D image for typical indentation a) indent point located close to the surface with compressive residual stress, b) indent point located in stress free sample and c) indent point located in the center with tensile residual stress.

To verify that the hardness when measuring the contact area was appropriate, the parameter P/S^2 was also assessed. Examining the hardness and modulus calculation, if H/E^2 is measured, then the contact area cancels out, such that P/S^2 is directly proportional to H/E^2. Since modulus is a constant, and will not be influenced by either plastic deformation or the residual stresses (at least at this moderate level of stresses), then changes in P/S^2 are proportional to H. A similar increase of approximately 10% was observed in the P/S^2 data, lending credence to the suitability of using the measured area to determine hardness in the case of a varying residual stress within the sample and pointing towards a future use of simply using the P/S^2 parameter to assess hardness in peened sample cross sections.

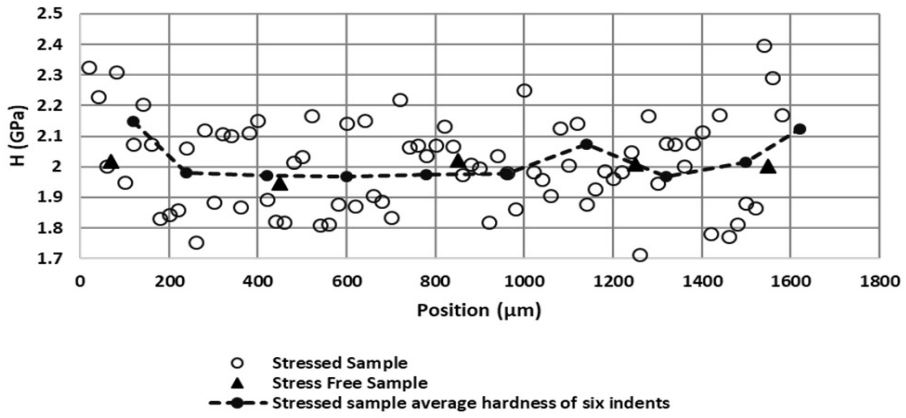

Figure 2- 8 Hardness profile obtained beneath the impact, along the width of the sample (surface to surface) by nanoindentation method.

Obtaining residual stress based on the Suresh and Giannakopoulos model requires comparing stressed and stress-free samples, here taken as a peened and as-received sample [7]. Generally, one would expect a compressive residual stress sub-surface to a depth on the order of the shot diameter, and then a smaller magnitude tensile stress within the center of the sample. Figure 2- 9 shows the loading segment of experimental load-depth curves for the peened and un-peened samples. Load-depth curves near the surfaces are "higher" than indents in stress free samples, while load-depth curves in the center of the sheet are "lower" than the stress-free samples. Using Eqs. 6 and 7, the expected residual stress can then be extracted from each indentation position.

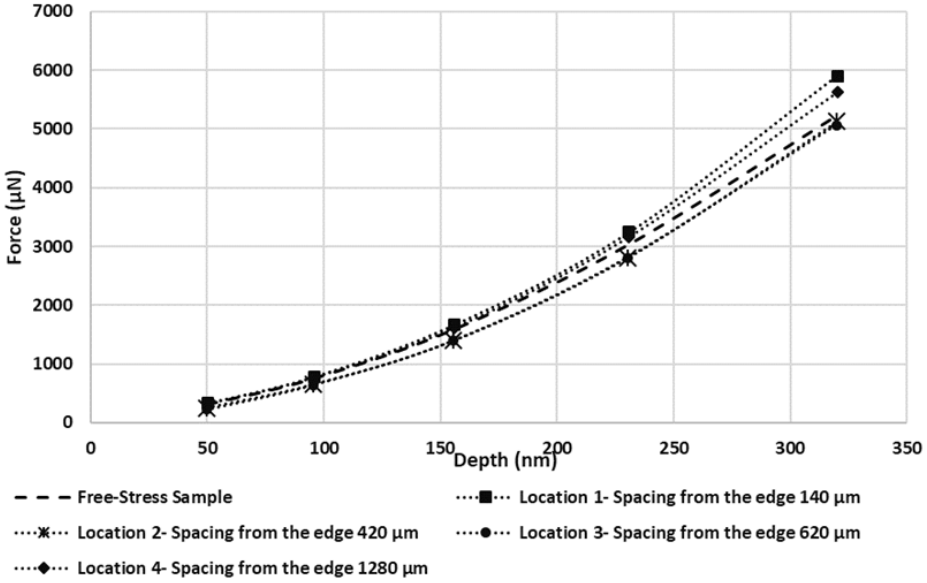

Figure 2- 9 Experimental loading curves obtained by nanoindentation for four typical points along the cross section.

2.4.2 Comparing nanoindentation simulation and experiment

The modeling results in the Figure 2- 10 shows that the load-depth curve for compressive residual stresses is higher than the stress-free modeling result. As a discussed in the previous section compressive residual stresses alter both contact area and the depth of the indentation. Therefore, for a fixed indentation depth, higher indentation force is needed for stressed sample with the compressive residual stresses in comparison to the stress-free sample. The experimental results showed that the maximum indentation force for stressed sample after shot peening was about 5850 µN corresponding to the 350 nm indentation depth. The same results had been observed in the modeling with 5800 µN and 3980 µN indentation force for stressed sample and stress-free sample in the same indentation depth respectively. In this result small differences might actually draw attention to the metallurgical parameters during experiments such as grain boundaries, defects, and work hardening rate. Also, it can be explained by idealized elastic-plastic behavior pretended in finite element simulation. In order to further highlight, the pile-up area in modeling result and the experimental result have been compared in Figure 2- 11 . As can be seen in this figure, maximum height of the pile-up area in the simulation and experiment were calculated about 16 µm and 18 µm respectively. In the finite element simulation, plastic deformation occurs where the

proportionate stress is equal to the yield strength of the materials which was defined as a Johnson Cooke model based on the Eq 2-10. It can be seen from Figure 2- 11 both simulation and experimental measurements for the pile-up height are in good agreement with each other. As a mentioned in the introduction part, a significant issue for the stress measurement is related to the pile-up area around the indentation spot. This returns to the contact area, that cause some over estimation due to the elastic contact assumption while there is a pre-existing plastic deformation on the specimen. This situation creates errors for hardness and modulus calculation. Therefore, work hardening phenomena such as shot peening increases pile-up area in nanoindentation experiment due to the incompressibility of materials. Finally, Finite element modeling will be helpful to predict and estimate load-depth curves and pile-up area before experimental measurement.

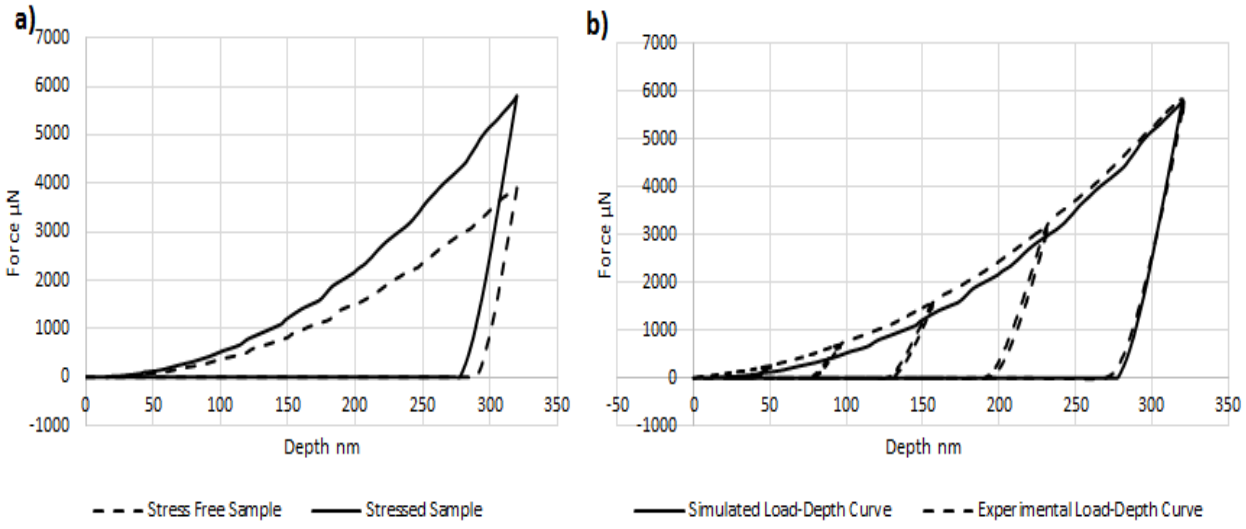

Figure 2- 10 Load-Depth curve obtained by a) finite element simulation and b) comparing nanoindentation and finite element modeling.

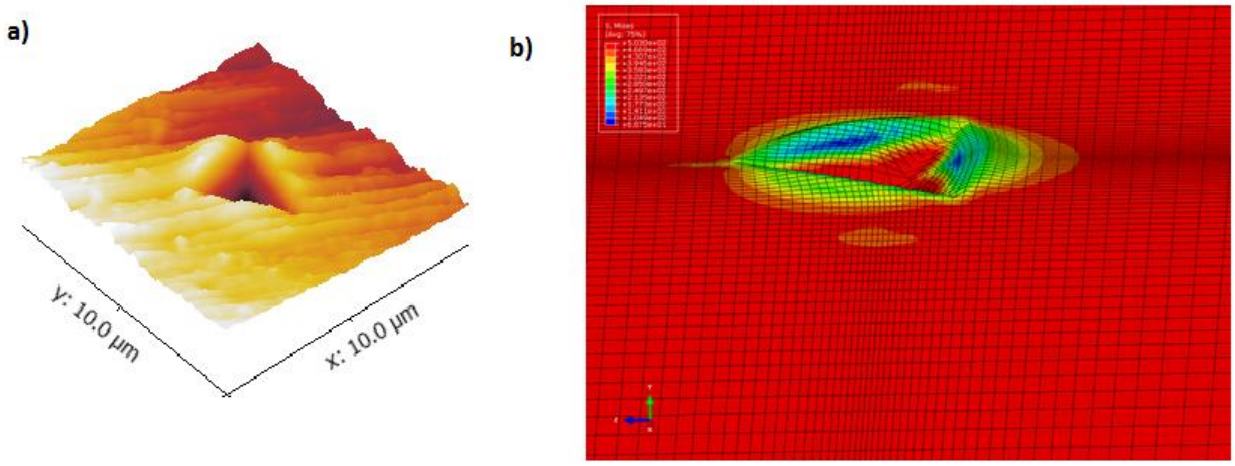

Figure 2- 11 Pile-up area around indent point located in 120 µm distance from the edge a) 3D topography image obtained by nanoindentation method b) pile-up area obtained by simulation with same stress tensor.

2.5.Residual Stress Profiles in Double Side Peened Aluminum

Figure 2- 12 shows the residual stress profile as a function of position within the sample (surface to surface) obtained by nanoindentation using Eq 6 and Eq 7 and the stress determined from the FEM modeling of the shot peening process. Due to the double side shot peening, both sides exhibit a compressive residual stress and the middle of the sample shows a tensile residual stress. In this figure, each black dot represents the stress from a single indentation, and a 6-point smoothing curve represents the average of six indent points with a total spacing of 160 µm, in order to demonstrate the general trend. Point to point variations with the indentation are likely due to the polycrystalline nature of the aluminum, where indenting different grain orientations in aluminum could lead to property measurements on the order of 10% [81], with individual orientation of grains and the presence of constituent particles leading to slight variations (the individual indentation volumes are smaller than the average grain size, which is on the order of 30 µm). Precipitate particles and EBSD map of this research and nanoindentation results have been shown in a previous paper, and we can identify when indentations probe the relatively large intermetallic precipitates (and thus avoid sampling in that area) [77].

In the experimental results, the maximum compressive residual stresses for both sides are 570 and 610 MPa, respectively, and for the simulation, the average stresses (a slab at a given depth, shown in Figure 2- 12) are 420 and 470 MPa. This asymmetry in the stress (even having peened

each side of the samples under the same conditions) is due to the impact of the residual stresses. Because the thickness of the plate is very thin, the shot peening process of the second side after fixing on the rigid body was influenced by the residual stresses imparted throughout the depth of the sample imparted by shot peening of the first side. The main reason is related to the bending due to the balancing of the internal stresses after shot peening, Cao et al. investigated the amount of residual stresses and bending height after shot peening [79]. The simulation of the first shot peening step shows plastic deformation is concentrated on the first side of the sample, while a residual stress develops throughout the thickness. When re-affixed to a base plate for shot peening the second side of the part, the sample is elastically strained to conform to the base plate, leading to an applied stress which then influences the overall residual stress after the second side is peened. Also, as noted in Figure 2- 13 the spatial variation expected in the residual stress is on the order of the variation noted in the experimental data (Figure 2- 12). The maximum residual stresses in the experimental results are located at depths of 80 µm and 100 µm from the edges of the sample from each surface respectively, which is quite similar to the simulation.

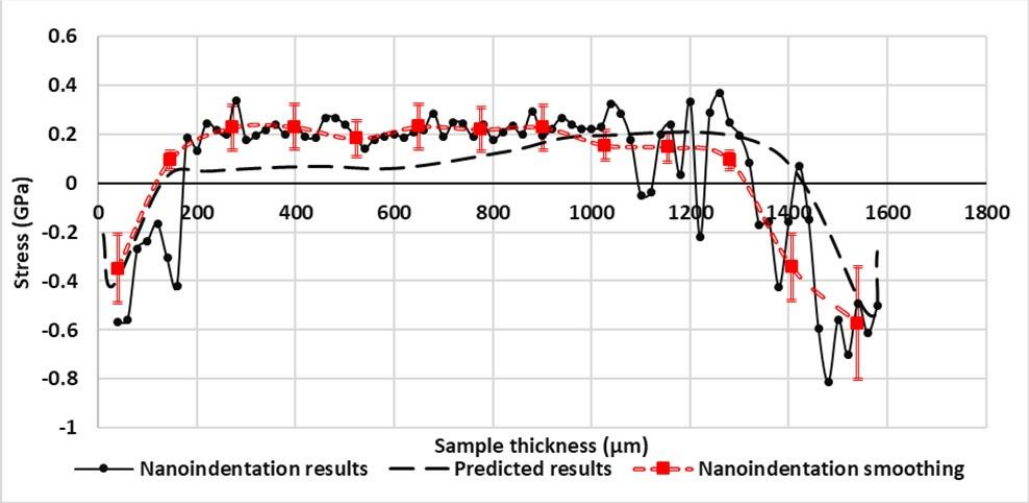

Figure 2- 12 Residual stresses profile measured by nanoindentation and compared to finite element prediction of the double side shot peened samples.

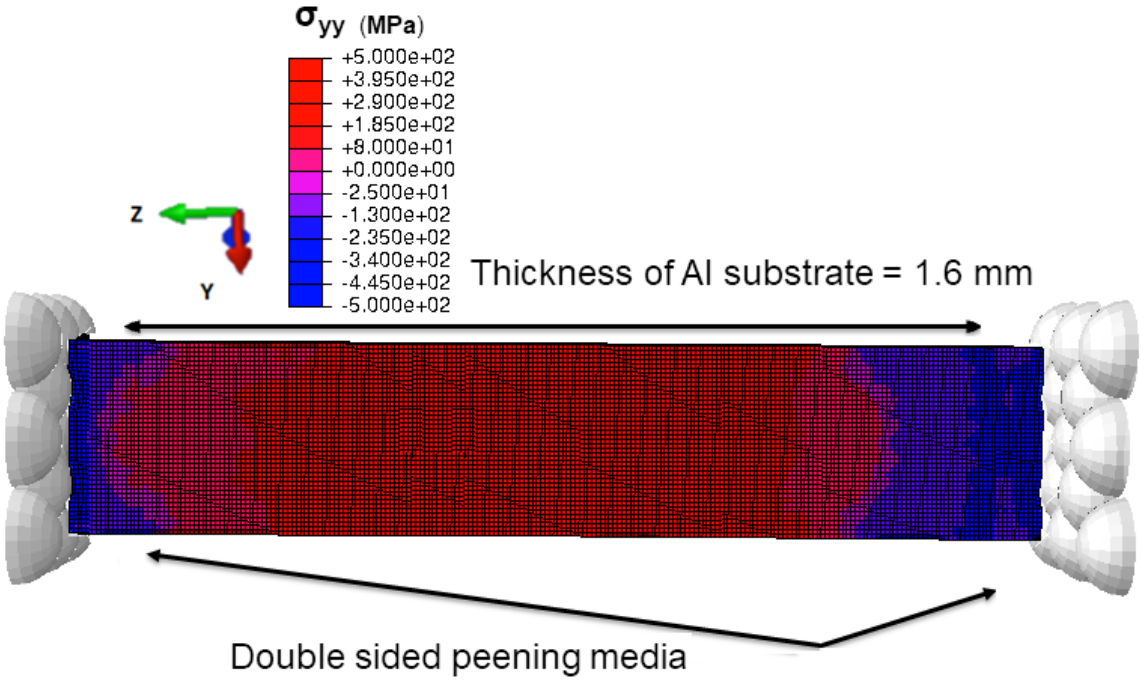

Figure 2- 13 Residual stress profile after double side shot peening simulation (cross section area in a X-plane ~ 100 µm depth) for aluminum 7050 sheet. The left side of the figure was the first to be shot peened in the simulation.

2.6.The effect of elastic and elastoplastic deformation on the contact area

The residual strain or stress on the surface can be elastic or plastic. For equibiaxial elastic field at the surface:

$$|\varepsilon_x^r| = |\varepsilon_y^r| \leq \varepsilon_y^{pl} \qquad \text{Equation 2- 11}$$

$$|\sigma_x^r| = |\sigma_y^r| \leq \sigma_y \qquad \text{Equation 2- 12}$$

where σ_y and ε_y^{pl} are initial yield stress and strain of the substrate. In the second case If we assume there is an elastoplastic deformation on the substrate, then, the surface should yield plastically. As a consequence, we can assign new yield stress to the substrate due to the cold working phenomenon. According to the von Mises criteria effective yield strain and stress are defined as [15]:

$$\varepsilon_e^{pl} = \frac{\sqrt{2}}{3}\sqrt{\left(\varepsilon_z^{pl} - \varepsilon_y^{pl}\right)^2 + \left(\varepsilon_z^{pl} - \varepsilon_x^{pl}\right)^2 + \left(\varepsilon_y^{pl} - \varepsilon_x^{pl}\right)^2} \qquad \text{Equation 2- 13}$$

$$\sigma_e^r = \frac{\sqrt{2}}{2}\sqrt{\left(\sigma_z^r - \sigma_y^r\right)^2 + (\sigma_z^r - \sigma_x^r)^2 + \left(\sigma_y^r - \sigma_x^r\right)^2} \qquad \text{Equation 2- 14}$$

Also, conservative volume during plastic deformation should be satisfied ε_z^{pl}=-2ε_x^{pl}=-2ε_y^{pl}, then for equibiaxial residual strain on the surface, the effective von Mises yield strain can be written as [15]:

$$\varepsilon_e^{pl} = 2\left|\varepsilon_x^{pl}\right| = 2\left|\varepsilon_y^{pl}\right| \qquad \text{Equation 2- 15}$$

substituting Eq (2-15) into the Eq (2-13) and combining with Eq (2-14) a new yield strength on the substrate can be calculated as a function of plastic strain which that residual plastic strain already is included such that [15]:

$$\sigma_y^r = \sigma_e^r = \beta\left(\varepsilon_e^{pl}\right)^n \qquad \text{Equation 2- 16}$$

where n is the strain hardening component and β is the materials constant. For obtaining residual stresses by indentation instrument the main concern that arises is due to the existing of the elastic residual stresses and plastic strain. Plastic deformation will influence the hardness and the pile up, but elastic stresses will also influence the elastic contact area during loading. Hardness when assessing the residual impression cannot capture the change in contact area during loading. After shot peening both elastic residual stresses and residual plastic strain exist on the substrate. According to the Suresh model residual stress calculation has been explained by Eq (2-6) and Eq (2-7) respectively. For these equations, the real contact area has been used which is obtained by Oliver-Pharr method, although this method is developed based on the elastic contact theory such that [19]:

$$p = \frac{2E_{eff}}{(\sqrt{\pi}B)^{\frac{1}{n}}}\left(\frac{n}{n+1}\right)\left[\frac{\Gamma(\frac{n}{2}+\frac{1}{2})}{\Gamma(\frac{n}{2}+1)}\right]^{\frac{1}{n}} h^{1+\frac{1}{n}} \qquad \text{Equation 2- 17}$$

where p is the indentation load, B is related to the indenter shape (area) and n is a materials constant, which n is between 2-6 and Γ is the factorial or gamma function [19]. According to the Oliver-Pharr method elastic contact theory gives the effective indenter shape such that [19]:

$$z(r) = \frac{4pa_{max}}{\pi E_{eff}} \left[\frac{\pi}{2} - E\left(\frac{r}{a_{max}}\right)\right] \qquad \text{Equation 2- 18}$$

In this equation p is the pressure, a_{max} is the contact radius (assuming a cone and a pyramid have similar behavior) and $E\left(\frac{r}{a_{max}}\right)$ is the integral of the second kind evaluated at peak load [19]. They (along with other researchers, see for example [82]) demonstrated that cold working phenomenon or residual plastic strain increases pile-up height around indentation, consequently, there will be some overestimation during contact area calculation. This error is related to the elastic contact analysis (Eq (2-17) and Eq (2-18)) when materials deformed plastically, pile-up is not considered in the contact area (always sink-in occurs due to the elastic deformation, pile-up cannot be modeled [19]). They found pre-strained materials prior to nanoindentation test exhibits pile-up due to the materials surface adjacent during indentation hardening, consequently, materials flow will be in upward direction [19]. Same results with numerical analysis have been shown by Bolshakov and Pharr [67]. According to the Suresh model which considered a real contact area $\frac{A}{A_0}$ to obtain residual stresses, no pile-up considered in the contact area calculation (only elastic contact theory was considered to obtain contact area during the calibration). Residual plastic strain influences on the pile-up deformation explicitly. In conclusion, the residual stress calculation is valid for both residual elastic stresses and residual plastic strain on the surface such as shot peening as far as real contact area has been considered for stress calculations [69, 17, 70]. From figure 7 we can see that the hardness, once adjusted for the pile up, does show an increase over the core material of about 10%; this hardness change is attributed to the plastic strain and work hardening. The additional contact area, which is reflected in the load-depth curve, is how we calculate the magnitude of the elastic residual stresses.

2.7.Nanoindentation After Fatigue and Before Fatigue Test

Shot peening is widely used to enhance fatigue life due to the compressive residual stresses in the metallic substrate. Crack growth and crack incubation before and after fatigue test has been investigated for shot-peened and baseline samples. Sample preparation and details for fatigue test have been described in the Chadwick et al. paper [77]. In this work hardness and reduced modulus has been measured by nanoindentation method in the aluminum matrix and around hard particles after or before shot peening. Indentation test has been conducted on the hard particles (precipitate)

in the aluminum matrix within the line pattern with a spacing of 10~15 µm. Figure 2- 14 and Figure 2- 15 show indentation on the hard particles from one side of the particles to the other side of the particles.

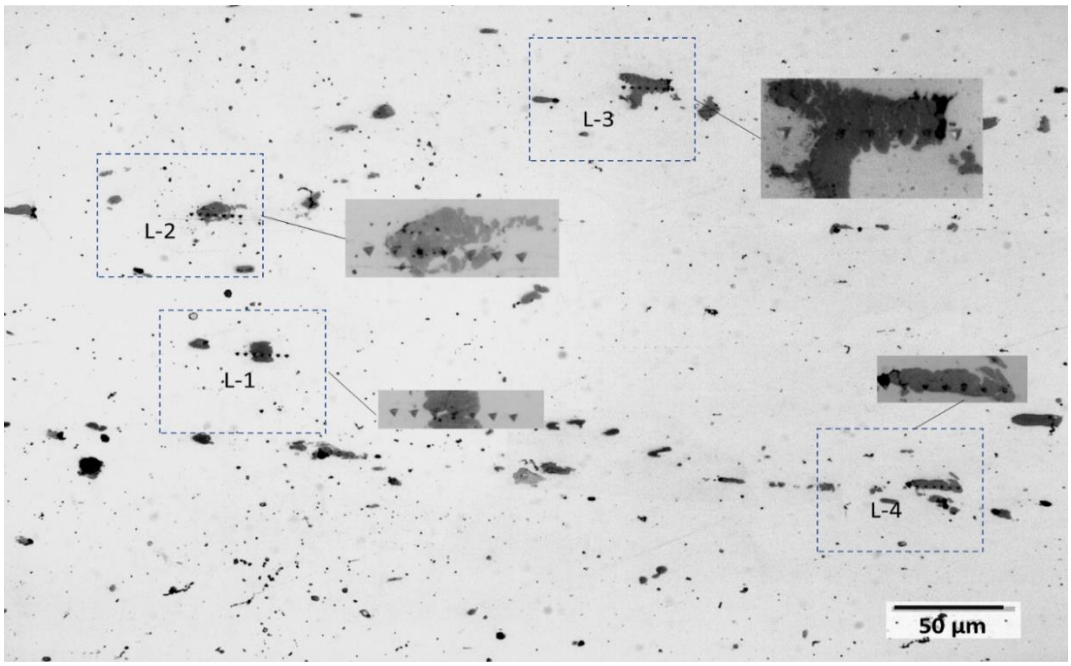

Figure 2- 14 Indentation on the particles and matrix, base line aluminum AA7050-T7451.

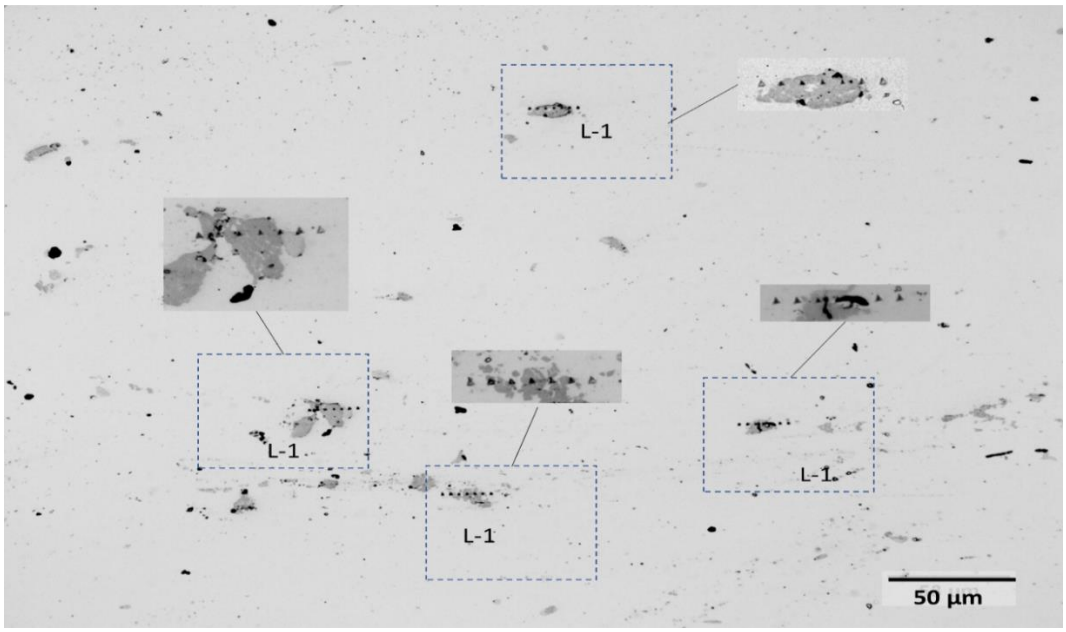

Figure 2- 15 Indentation on the particles and matrix, shot peened sample aluminum AA7050-T7451.

As indicated the hardness values around hard particles have been shown in Figure 2- 16. As can be seen in this figure, hardness values for hard particles in the middle of the curves are higher than two both end sides (left and right) which they are related to the metallic matrix. In this figure, main difference is related to the particle's hardness in shot-peened sample and baseline before shot peening. The average hardness values show significant decreases due to the crack formation after shot peening on the hard particles.

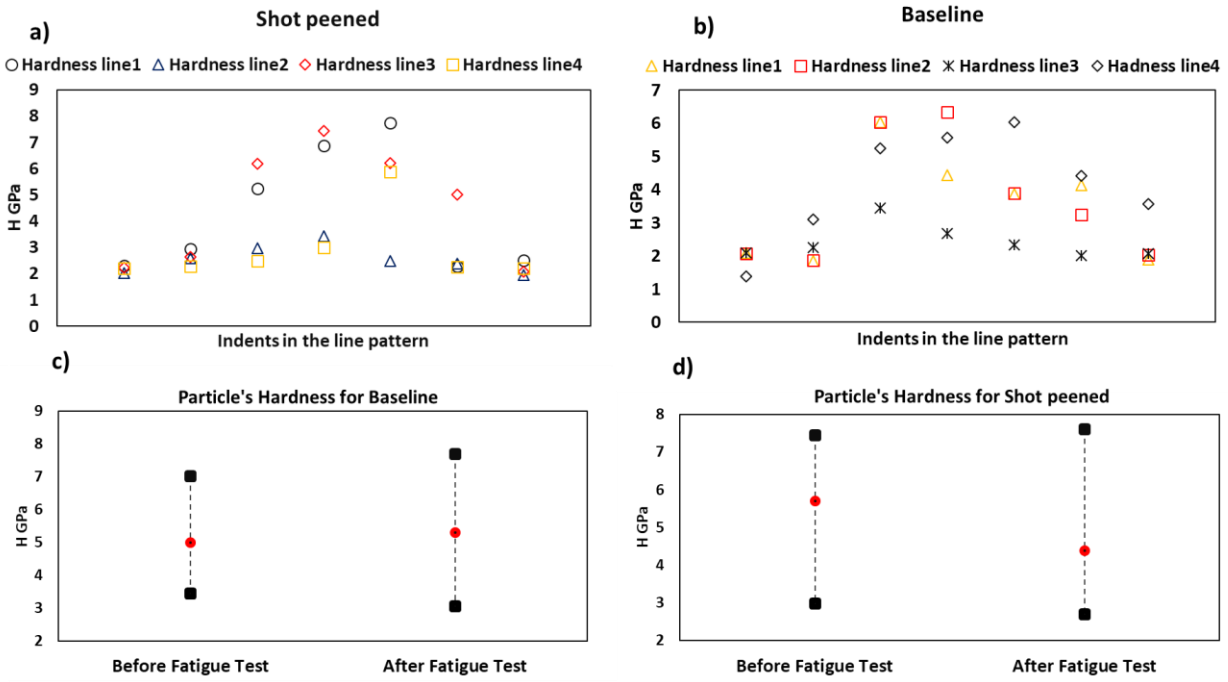

Figure 2- 16 Hardness measurement with nanoindentation method in the line pattern Figure 2- 14 and Figure 2- 15.

Indentation hardness values for hard particles were obtained in the range of 5 GPa and 5.3 GPa before and after fatigue test respectively. A small increase in the hardness after fatigue test can be attributed to the cold working phenomena due to the fatigue test. This cold working after fatigue test can change the contact area and hardness measurement in the nanoindentation test which was explained in section 2.3.1. As can be seen in Figure 2- 16(d) highest average hardness value is related to the shot-peened sample before fatigue test due to the cold working phenomenon. Differently, after fatigue test, the average hardness value of shot peened sample dramatically decreased to the 4.2 GPa. This can be explained by micro-cracks creation on the particles after the fatigue test. Further investigation has been done by comparing reduced modulus around particles

and metallic matrix which they are shown in Figure 2- 17. Reduced modulus in the metallic matrix before shot peening has been measured via nanoindentation test. Figure 2- 17 shows after fatigue test average reduced modulus of the baseline sample is reduced from 96 GPa to the 85 GPa respectively. The main reason is related to the microcracks which they were incubated from hard particles and they were extended to the matrix. Reduced modulus around cracks have been shown in Figure 2- 17, further reduction in the reduced modulus were seen due to the higher compliance of the free surface of the cracks. The shot-peened sample after fatigue test showed higher compliance in comparison to the baseline after fatigue test and baseline near cracks after the fatigue test. This can be attributed to the compressive residual stresses field induced by shot peening that prevents from crack propagation from cracked particles into the matrix of the shot-peened sample.

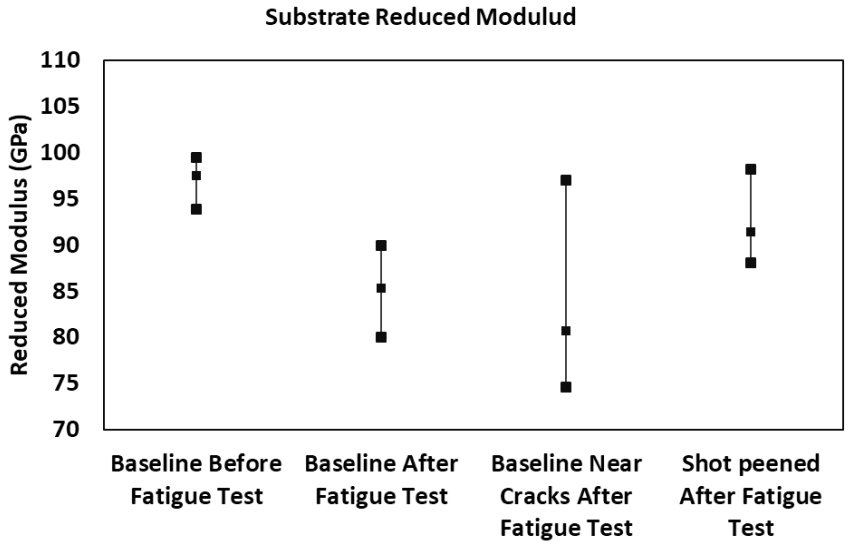

Figure 2- 17 Reduced modulus substrate measured by nanoindentation before and after fatigue test.

2.8.Conclusions

The residual stresses and hardness of a double side shot peened thin aluminum sheet was evaluated using nanoindentation. The generally expected stress profile, with compressive residual stresses at depths approximately 80 μm from the surfaces of both sides and a slight tensile residual stress in the center, was observed. However, an asymmetry in the stress profile was present in the part, even having used the same peening processing conditions for both sides. The hardness of the compressively stressed region increased approximately 10%, from about 2.0 to 2.2 GPa, but this

strain hardened region was constrained to a depth, on the order of the depth over which the compressive residual stresses were present. This simulation and the experimental results compare favorably in terms of the magnitude of the maximum residual stress, the depth of the total compressive stress, and the differences between the “first” and “second” side of the sample. The asymmetry of the residual stress profile is on the order of 10%; with the first side showing a maximum residual stress of approximately 420 MPa and the second side showing a maximum residual stress of 470 MPa. Since there was no significant asymmetry in hardness, this suggests that the dual peening process on thin sheet structures may be influenced by the residual stresses imparted throughout the thickness of the part during the first peening step. Finally, hardness and reduced modulus provided information and foundation for crack initiation and crack incubation by hard particles within shot peened aluminum alloy. The results showed hard particles are damaged due to the shot peening but compressive residual stresses during the fatigue loading prevents crack propagation from hard particles into the metallic matrix.

Acknowledgements

The authors are grateful for the advice and access to commercial shot peening processes provided by Jack Champaign of EI Incorporated and Jim Wheeler of Progressive Surface. Funding was provided by the Center for Surface Engineering Enhancement at Purdue University, an industrial consortium. Additionally, the authors thank Daniel J. Chadwick for the material and specimen preparation.

CHAPTER 3. AN ENERGY-BASED NANOINDENTATION METHOD TO ASSESS LOCALIZED RESIDUAL STRESSES AND MECHANICAL PROPERTIES ON SHOT PEENED MATERIALS

A portion of this chapter is previously published in the Journal of Materials Research by Siavash Ghanbari, David F. Bahr as " An energy-based nanoindentation method to assess localized residual stresses and mechanical properties on shot-peened materials", 34, 7, pp 1121–1129, 2019. https://doi.org/10.1557/jmr.2019.41

3.1. Abstract

Concurrently assessing localized residual stresses and mechanical properties in cases where gradients in stresses and properties (such as those resulting in metallic alloys from shot peening processes) is challenging. Most indentation-based stress measurements assume uniform properties, which is not necessarily the case in this common industrial process. By using the energy envelope describing the total work of indentation by a load-displacement curve from instrumented indentation localized residual stresses after shot peening were evaluated experimentally. A framework is developed to describe the appropriate indentation depth at which to assess properties that effectively defines the volumetric resolution of the method. The residual stresses predicted via the nanoindentation experiment and energy analysis were validated with X-ray measurement of residual stresses on a shot peened 52100 steel. The energy method can be applied directly from the indentation load-displacement curve without considering the contact area.

3.2. Introduction

Determination of localized residual stresses in metallic specimens is important in predicting fatigue lifetime after shot peening. The impact of the peening process on the material's performance is highly dependent on the compressive residual stresses and strain hardening. Excessive residual stresses after peening process can have a destructive influence substantially it can reduce the fatigue lifetime [83]. Residual stresses can currently be measured experimentally using X-ray diffraction-based techniques, hole-drilling, and layer removal [84, 85], but these techniques are limited to mm-scale resolution in lateral dimensions, making relationships to grain-level materials structure challenging, and limiting the ability to correlate to crystal plasticity models. Commercially available depth-sensing indentation techniques (commonly called

nanoindentation) are able to measure hardness (proportional to flow strength), elastic modulus, and other mechanical properties on the μm scale, and several techniques have been developed to concurrently residual stresses by nanoindentation [86, 87].

Nanoindentation relies on interpreting the load-depth record during the penetration of a tip into a sample. Residual stresses can change load-depth curves by altering the amount of material in the "pile-up" around the indenter probe, and subsequently changing the real contact area relative to the depth of penetration [86, 88]. At a given penetration depth the load-depth curve for a sample with a biaxial compressive residual stress is steeper than the stress-free sample and shallower for the tensile residual stresses [89, 90]. Similar behavior occurs for unloading curves; compressive residual stresses shift the unloading curve to shallower penetration depths and oppositely tensile residual stresses shift to higher penetration depths [91, 92]. There is a linear relationship between residual stresses and changes in the real contact area [93]. Many of the models addressing residual stresses are based on self-similar indenters, such as a Vickers or Berkovich tip [86]. Equibiaxial stress can be accounted for as a hydrostatic stress which induces an indentation force. Carlsson and Larson have also presented a model to recognize the residual stresses based on the pile-up area changing contact area [94]. Based on extensive investigations, compressive residual stress increases contact area due to more pile-up and tensile residual stresses decrease the contact area as a consequence of the sinking-in area or less pile-up [94, 93].

Swadener proposed a method to extract the residual stresses from the relationship between hardness and yield stress using spherical indentation probes. However, the model requires *a priori* knowledge of the yield strength and spherical indentation often requires larger tips or flatter samples than self-similar indenter geometries [17].

In this current study a simple approach will be developed to evaluate the localized residual stresses after shot peening using instrumented indentation. Instead of basing the technique on changes in the contact area induced by residual stresses, the indentation energy between a stressed sample and a stress-free sample will be compared. The proposed method can be used directly without the contact area calculation, but of course tip area calibration would be needed to concurrently determine hardness. Wang et al. [95] proposed a residual stress measurement by the energy method using a sharp indenter, however their formulation used indentation angle as a constant parameter, and during the unloading step due to the elastic recovery there would be some

overestimation. Also, Wang et al. assumed that elastic response during unloading is independent of the magnitude of pre-existing residual stresses since the substrate remains purely elastic. However, for elastoplastic materials, particularly after severe deformation such as shot peening, the localized indentation response will be affected due to strain hardening [86]. Therefore, in this current paper to eliminate overestimation during residual stress calculation, instead of the indentation angle, numerical fitting of the load-depth curves were used and also instead of plastic energy, elastoplastic energy (total energy) will be considered for residual stress measurement. The indentation residual stress results will be compared to those determined using X-ray diffraction.

3.3. Materials and Experimental Section

3.3.1 Materials

Flat strip samples of a 52100-steel alloy used for austempering, with a nominal thickness of 6 mm and a width section 18 mm and 20 mm in length were used for this study. The shot peening was carried out by a commercial supplier using steel balls with an average diameter on the order of 1 mm. The shot peening nozzle was a V-type model, the accelerating air pressure was 75 PSI, and 3/8-inch nozzle size was used (English units used based on industrial convention in these processes). After peening there is some residual roughness on the peened surface; this roughness can lead to uncertainties in assessing properties using instrumented indentation. The surface and cross-section were ground through 1200 grit paper, followed by polishing with 6 and 3 μm diamond paste, removing approximately 50-75 um of material. Both the top surface of the shot peened sample (shot peened surface) and a cross section were examined, in addition to the surface of a sample prior to peening.

Nanoindentation was carried out using a Hysitron TI950 system (Hysitron Inc., Minneapolis MN) with a high load head and a Berkovich tip, the tests were conducted in depth control mode with a maximum depth of 350 nm and 1000 nm, using 50 nm/s loading and unloading rates and a 20 s dwell time at maximum depth. The indents were spaced in a rectangular pattern with 40×50 μm distances from edge to edge, and in a line pattern in the cross-section. The indentation tip area function was calibrated with fused quartz.

3.2.2 X-ray measurement of residual stresses

Residual stresses were measured by using the entire Debye-Scherrer ring with a single incident X-ray beam [96, 97]. The residual stresses on the surface changes the diffraction Debye-Scherrer ring on the central angle. The magnitude of the strain can be found from the detected position of Debye-Scherrer ring, and consequently the residual stress can be found by [98]

$$\varepsilon_\delta = \frac{1}{2}\left[(\varepsilon_\delta - \varepsilon_{(\pi+\delta)}) + (\varepsilon_{-\delta} - \varepsilon_{(\pi-\delta)})\right] \quad \text{Equation 3- 1}$$

$$\sigma_x = \frac{E}{(1+\nu)} * \frac{1}{sin\,2\varphi} * \frac{1}{sin\,2\varphi_0} * \left(\frac{\partial\,\varepsilon_\delta}{\partial\ cos\,\delta}\right) \quad \text{Equation 3- 2}$$

where E and ν are the elastic modulus and Poisson ratio respectively, α is the azimuth angle of Debye-Sherrer ring, φ_0 is the incident angles from the Z axis and φ is the complementary angle of the Bragg angle [99]. A Pultstec μ-X360s system X-ray residual stress analyzer (Pulstec USA, Torrance, CA), was used to measure the residual stresses before and after peening. The source of the system was chromium Cr, radiation wavelength of 2.29 $\dot{A}$ (Cr K alpha). This system is capable of mm-scale lateral resolution and a depth resolution on the order of a few $\mu m's$. The residual stresses were measured on the polished samples prior to indentation and were compared with the average of 9 indents over the same general area. In order to measure residual stresses as a function of depth, the specimen was electro-etched in a 3.5% NaCl solution at room temperature (25° C) with a DC current of 0.45 A. The sample was etched, the stress measured, the amount of material removed was measured using a dial gauge micrometer with a resolution of 2 μm, and then this process repeated to generate a stress-depth profile.

3.4. Energy model

The true, or Meyer, hardness (i.e. the mean pressure, defined by the applied load divided by the true contact area during loading) is assumed to be unaffected by any pre-existing elastic residual stresses present in the material, this assumption is common in prior investigations [25, 94, 24]. Similar to the Suresh model [86], differences between a sample with residual stresses and a stress-free sample will impact the subsequent loading curves, shown schematically in Figure 3- 1. An indentation into a material with a compressive residual stresses requires a larger contact force

to reach the same depth of penetration than a similar indentation in a stress-free sample and vice versa for the tensile residual stresses [89, 95, 86, 92].

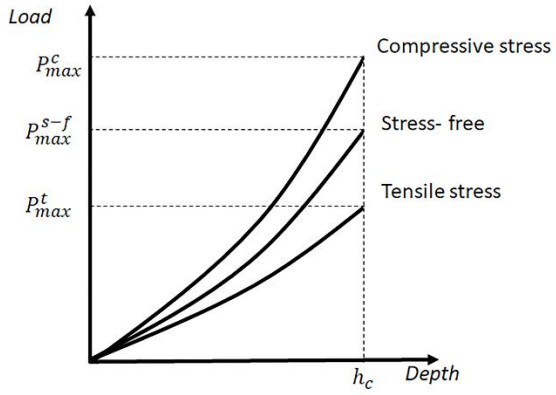

Figure 3- 1 Schematic load-depth curves for indentation loading, comparing stressed sample and stress-free sample.

The elastoplastic energy involved in the indentation can be measured using the load (P) – depth (h) curve, elastoplastic loading is followed by an elastic unloading curve, shown schematically in Figure 3- 2(a). In general, the indentation loading and unloading curves can be described phenomenologically by [100]

$$P = \beta h^m \qquad \text{(loading part, elastoplastic)} \qquad \text{Equation 3- 3}$$

$$P = \beta'(h_{max} - h_r)^{m'} \qquad \text{(unloading, elastic)} \qquad \text{Equation 3- 4}$$

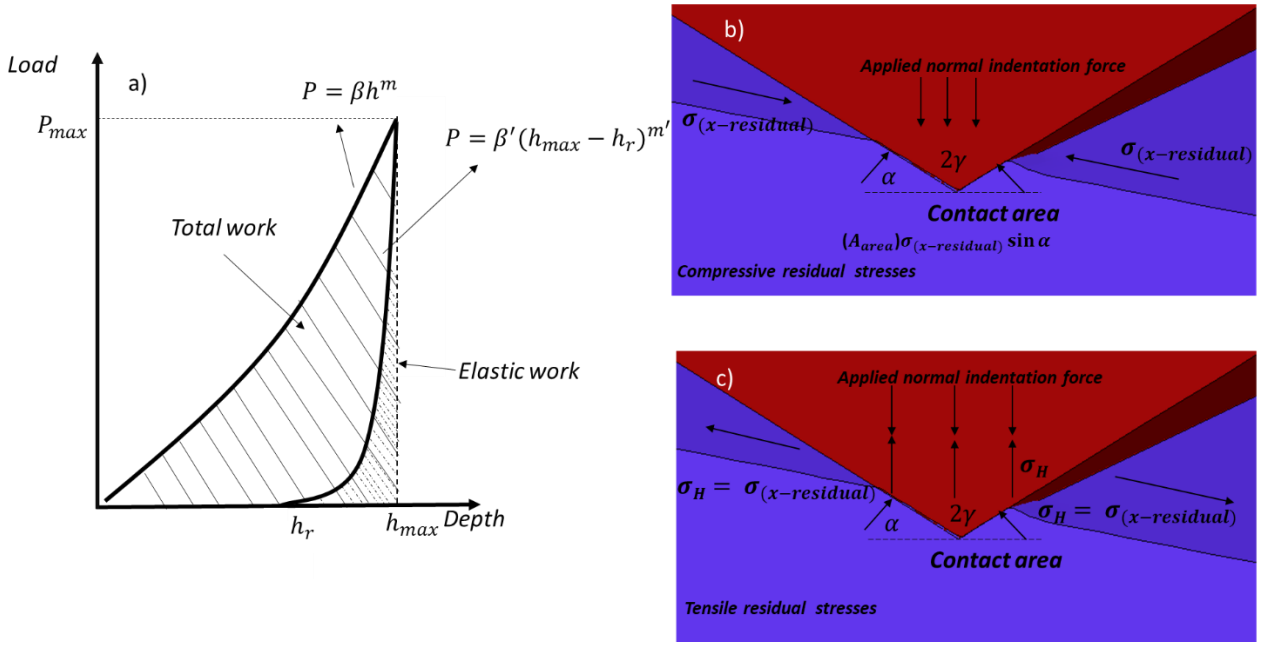

Figure 3- 2 Load displacement curve and residual stress state, (a) Comparing elastoplastic energy area under loading unloading curve, (b) schematic compressive residual stress state at the indentation surface, (c) schematic tensile residual stress state at the indentation surface.

where the h_r is the measured depth, h_{max} is the maximum depth of the indentation, β and β' are material constants which is related to the elastoplastic and elastic properties of the material [25], and m and m' are a constants, connected to the indenter shape and contact nature (*for an ideal conical indenter m = 2*) [89].

Applying a load P to the indenter over a displacement h expresses work done on the system due to the elastoplastic strain, and the unloading part returns the work done by the system as the material elastically recovers [101, 102]. Therefore, the total work (u_{el+pl}) and elastic work of indentation (u_{el}) is the area enclosed by the loading and unloading section respectively. The corresponding equations are

$$u_{el+pl} = \int_0^{h_{max}} \beta h^m \, dh \qquad \text{Equation 3- 5}$$

$$u_{el} = \int_{h_r}^{h_{max}} \beta'(h_{max} - h_r)^{m'} \, dh \qquad \text{Equation 3- 6}$$

based on prior studies [101] of nanoindentation for elastoplastic response with sharp indentation and very small elastic strains in compared with the plastic strains. For a material that strain hardens, prior residual plastic strains can change the localized yield stress. Therefore, for this situation, elastoplastic loading and elastic unloading are not invariant, and they are changed by the prior plastic deformation [103, 104, 86]. After severe plastic deformation, such as shot peening, both elastoplastic and elastic responses during indentation are affected by the residual stresses. Since the total energy (elastoplastic) can be measured, comparing stressed sample and stress-free sample with a given energy level, the indentation can provide the magnitude of the residual stresses. Based on the Suresh model for compressive equibiaxial residual stresses on the indentation surface, hydrostatic stress will be similar to the equibiaxial compressive stresses and uniaxial tensile stress along the indentation direction $-\sigma_x^{res} = -\sigma_y^{res} = -\sigma_z^{res} = -\sigma^{hyd}$ [86]. Due to the tensile and compressive stresses, shown in Figure 3- 2(b), there is (sinα) coefficient that is related to the contact lost between indenter and contact perimeter [86]. Consequently, the upper bound estimation for the maximum load to achieve a given indentation penetration depth between stress free sample and stressed sample can be written as:

$$P_{max}^{c} = P_{max}^{s-f} + \sigma_{res} A_1 \ sin\,\alpha \qquad \text{Equation 3- 7}$$

where $\alpha = (\frac{\pi}{2} - \gamma)$ with γ is the angle of indenter tip, for Berkovich tip $\alpha = 24.7°$, A_1 is a real contact area for stressed sample, P_{max}^{c} and P_{max}^{s-f} are shown in Figure 3- 1. Also for tensile residual stresses Figure 3- 2(c) the same equation can be used for residual stresses $\sigma_x^{res} = \sigma_y^{res} = \sigma_z^{res} = \sigma^{hyd}$, without considering contact loss due to the tensile equibiaxial stresses on the surface and uniaxial tensile stress along the indentation axis

$$P_{max}^{t} = P_{max}^{s-f} - \sigma_{res} A_1 \qquad \text{Equation 3- 8}$$

The total energy at the maximum load $P = P_{max}$ can be calculated by using Eq (3-7) and Eq (3-8) As a result, the work done by compressive and tensile residual stresses on the substrate respectively is

$$U_{el+pl}^{Stressed\ sample} - U_{el+pl}^{Stress-free} = (\ P_{max}^{s-f} + \sigma_{res} A_1 \sin\alpha - P_{max}^{s-f})\ h_{max}$$

(Work done by compressive stress) Equation 3- 9

$$U_{el+pl}^{Stressed\ sample} - U_{el+pl}^{Stress-free} = (P_{max}^{s-f} - \sigma_{res}A_1 - P_{max}^{s-f})\, h_{max}$$

(Work done by tensile stress) Equation 3- 10

After shot peening and cold working, the elastic unloading part during nanoindentation process is also dependent upon residual stresses [86]. Therefore, in order to find the energy contribution of residual stresses, it can be calculated by integrating Eq (3-7) with respect to maximum depth for both stressed sample and stress-free sample

Total work for stressed sample $= \int_0^{h_{max}} (\beta_1 h^{m_1}) dh = \frac{\beta_1 h^{(m_1+1)}}{(m_1+1)} = \frac{P_m^s h_m}{(m_1+1)}$ Equation 3- 11

Total work for stress-free sample $= \int_0^{h_{max}} (\beta_0 h^{m_0}) dh = \frac{\beta_0 h^{(m_0+1)}}{(m_0+1)} = \frac{P_m^{s-f} h_m}{(m_0+1)}$ Equation 3- 12

where, P_{max}^s and P_{max}^{s-f} are the maximum load of indentation for stressed sample and stress-free sample, β and m are the fitting parameters where subscripts 1 and 0 represents stressed sample and stress-free sample respectively. Substituting Eq (3-11) and Eq (3-12) into Eq (3-11) and Eq (3-12), the residual stress can be related to parameters from the indentation load-depth curves as

Compressive residual stresses $(\frac{P_{max}^s h_{max}}{(m_1+1)} - \frac{P_{max}^{s-f} h_{max}}{(m_0+1)}) = (\sigma_{res} A_1 \sin\alpha)\, h_{max}$ Equation 3- 13

Tensile residual stresses $(\frac{P_{max}^s h_{max}}{(m_1+1)} - \frac{P_{max}^{s-f} h_{max}}{(m_0+1)}) = (-\sigma_{res} A_1)\, h_{max}$ Equation 3- 14

3.4.1 Determination of appropriate indentation depth for small scale indentation and residual stress assessment

Indentations can be performed under three different conditions: elastic, elastic-plastic and fully plastic conditions, as described in detail by Tabor [104]. These conditions are separate from any indentation size effect [105] which may be mechanistically related to non-uniform deformation. Indenters always have some spherical asperity at the tip, and so at the lowest loads they may exhibit elastic contact with a substrate (i.e. the Hertzian loading condition of a sphere in contact with a flat). As a spherical asperity on an otherwise self-similar indenter continues to penetrate the surface, the material response is elastic-plastic, and once there is a transition from elastic-plastic behavior to the fully plastic behavior (either through a combination of materials properties or

reaching a self-similar position of the indenter probe), the mean pressure (hardness) becomes constant. In the fully plastic regime with a self-similar indenter, the flow strength of the solid is often estimated as one-third of the hardness [106, 107, 104].

For self-similar indenters in the fully plastic region, pile-up or sinking-in area at contact periphery can develop based on the included angle of the indenter and the strain hardening behavior of the material [106, 25]. While the true hardness is independent of residual stresses in the fully plastic region [94], the projected contact area or pile-up area are dependent upon residual stresses [94, 86, 100]. Numerous studies have shown that the pile-up ratio is a maximum when the fully plastic region is developed, which is often where residual stresses can be extracted [94, 108, 11]. Consequently, for evaluating residual stresses using indentation methods, it is best if the indentation is in the fully plastic region so as to develop a constant ratio of pileup or sinking-in relative to the depth of penetration. Additionally, the indentation should be large enough to eliminate the indentation size effect [105] For this purpose, the relation between contact depth and penetration depth is the key relation to find the transitions from elastic-plastic to fully plastic regimes of the indentation process [106, 107]. Wolf et al. showed by normalizing of contact depth over the indentation depth and plotting against the total penetration depth the ratio plateaus at the value at which the hardness is constant and a fully plastic region is developed [106, 107]. Of course, if one aims to produce a technique applicable to measuring the localized variation in properties, it would be beneficial to measure properties at as small a scale as possible.

For a given position, a cyclic loading and unloading (the "partial load-unload" method) can be used to create the ratio of $\frac{h_c}{h}$ as a function of h (depth of the penetration) [107]. Indentations into the as received 52100 steel were performed, and the resulting hardness and depth ratio is shown in Figure 3- 3. At a depth of indentation exceeding 500 nm the indentation appears to be fully plastic. In order to obtain the most accurate residual stresses the maximum depth of the nanoindentation should be in fully plastic zone, but to be able to map localized properties one would desire the smallest indentation possible in these conditions. The indentation size effect can be calculated by depth-dependent hardness which is shown in Figure 3- 3, which shows that the hardness decreases with increasing depth of the indentation, but plateaus around 250 nm for the material used in this study. Therefore, two maximum depths of indentation, 350 nm and 1000 nm were chosen for

measuring residual stresses with the nanoindentation method and the results were compared with X-ray method to examine the validity of the maximum indentation depth choices.

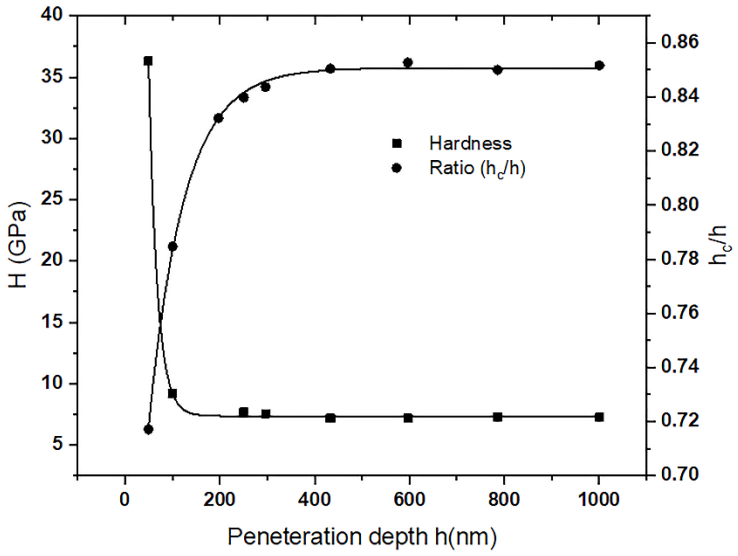

Figure 3- 3 Experimental determination of indentation depth (a) Contact depth over penetration depth ratio obtained from multiple cycling during one single indent, (b) obtaining indentation size effect, hardness as a function of indentation depth. Error bars represent standard deviation of 5 indentations.

3.5. Results and Discussion

3.5.1 Residual stress measurement on the shot peened surface

X-ray diffraction was performed on the as shot peened surface, the mechanically polished surface, and the electro-etched surface, resulting a compressive residual stress of -1490 MPa on the shot peened surface, shown in Figure 3- 4. The depth dependent compressive and tensile residual stresses range between -1250 MPa up to 300 ~ 400 MPa in the interior of the strip.

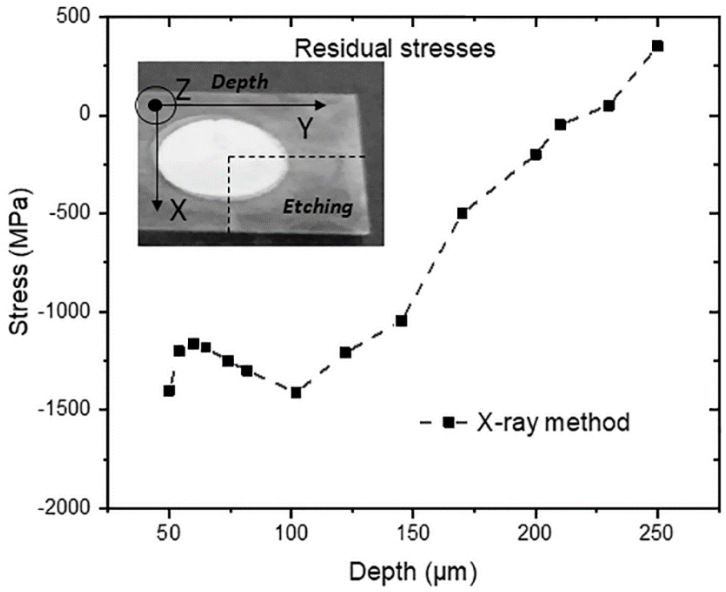

Figure 3- 4 X-ray residual stresses measurement on the corresponding depth with electro-etching method. Error bars the represent instrument precision.

Typical load-displacement curves for 10 indents on the mechanically polished shot peened sample and stress-free sample are shown on Figure 3- 5 with maximum indentation depths of 350 nm and 1000 nm respectively. Fitting curves were applied for each load-depth curve that power law coefficients in Eq (3-1) and Eq (3-2) are shown in Table 3- 1. The loading curves of the shot peened samples (which have a compressive residual stress on the surface) are significantly higher than the stress-free sample. By using Eq. 11. the residual stresses can be estimated corresponding to each indentation impression, shown in Figure 3- 6. Based on the maximum depth of indentation, the average residual stresses on the shot peened surface was -823 MPa and -1220 MPa for maximum indentation depths of 350 nm and 1000 nm respectively. The X-ray result is slightly different from the individual indentation results, especially at the lower indentation depth h_{max} = 350 nm which has more scattered results in comparison with h_{max} = 1000 nm. The main reason for these scatter results for individual indentation return to the X-ray resolution and metallurgical parameters. The X-ray system collects information from an illuminated area on the surface on the order of 1-2 mm^2. Each indent can be impacted by local metallurgical parameters such as grain boundaries, grain orientation and non-uniform distributions of defects. The alloy used for validation in this study had an average grain size of ≈20 μm and therefore each indentation will likely be sampling a different grain but be within one grain (at most two). The higher load (larger

volume sampled) will increase homogenization; the change in residual stresses in each indentation position for maximum depth of indentation h_{max} = 1000 was less than 5%, as shown in Figure 3-6. In general, the residual stresses within h_{max} = 1000 nm and 350 nm are in good agreement with X-ray results.

Table 3- 1 Load-depth parameters (Eq.1) extracted from fitting loading curves.

Maximum indentation depth	Coefficient	Stressed-Indent-1	Stressed-Indent-2	Stressed-Indent-3	Stressed-Indent-4	Stressed-Indent-5	Stressed-Indent-6	Stressed-Indent-7	Stressed-Indent-8	Stressed-Indent-9	Average stress-free
350 nm	β	1.60	1.51	1.40	1.60	1.66	1.62	1.63	1.59	1.63	1.61
350 nm	m	3.24	2.76	8.28	2.21	2.87	1.87	1.83	2.37	1.76	1.51
1000 nm	β	1.76	1.75	1.71	1.71	1.72	1.75	1.72	1.78	1.72	1.72
1000 nm	m	0.84	0.58	1.19	1.23	1.45	1.52	1.45	1.65	1.78	0.59

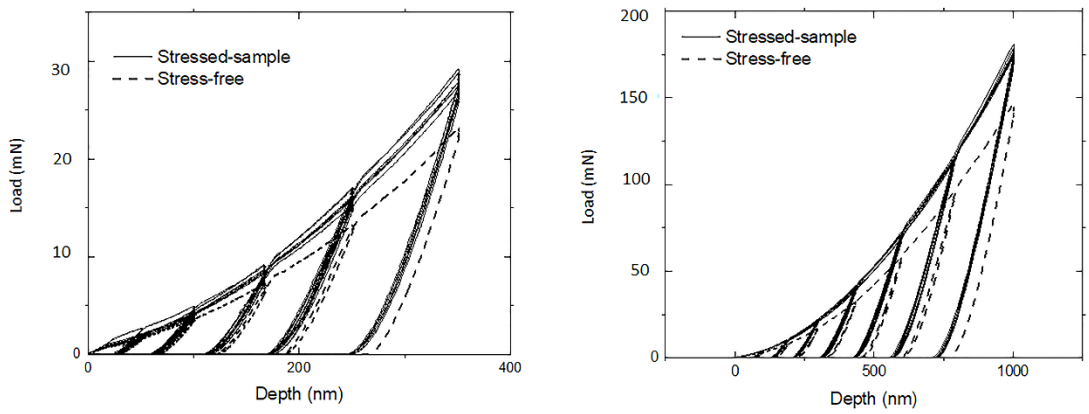

Figure 3- 5 Load-displacement curves for 9 indents on the shot peened sample (solid lines) and the corresponding single indentation on a sample prior to peening (dashed line) to a) maximum indentation depth 350 nm, b) maximum indentation depth 1000nm. Note the stress relaxation during the hold overlaps on the 9 indentations; the magnitude of stress relaxation for any single indent is similar between the stressed and stress-free case.

In order to measure residual stresses by nanoindentation accurately the maximum depth of the indentation should be large enough to eliminate the indentation size effect and it must be in a fully plastic zone, which is mentioned in section 3.3. Indentations in the fully plastic regime will

improve accuracy due to the self-similarity of pile-up or sinking-in area when plasticity dominates the indentation probe. These results are consistent with other investigations [94, 89, 100, 86].

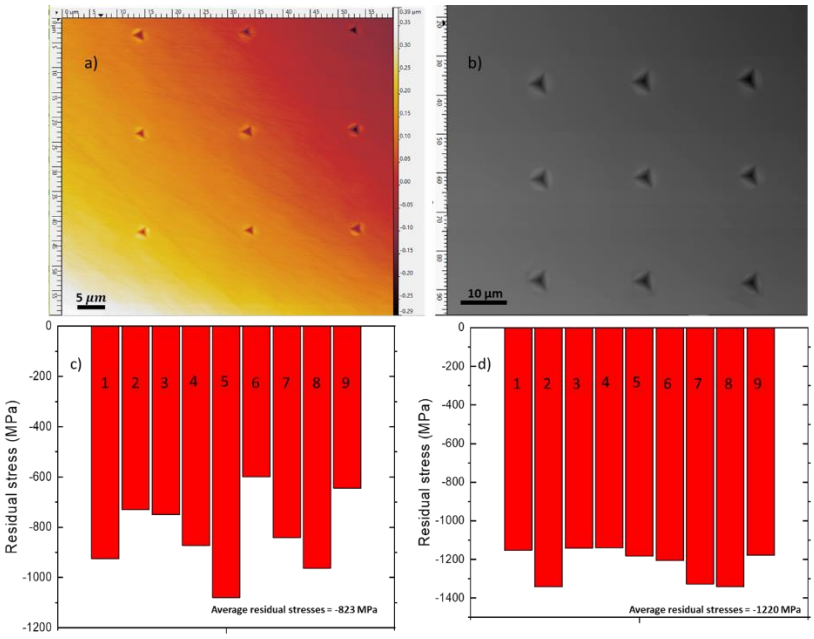

Figure 3- 6 Residual stresses corresponding to the indentation on the shot peened surface obtained by energy model, a and c) maximum indentation depth 350 nm, b and d) maximum indentation depth 1000 nm.

3.5.2 Depth dependent residual stresses measured on a cross section

The loading and unloading curves on the cross-section pattern for the shot peened sample are shown in Figure 3- 7. Close to the surface, due to the compressive residual stresses, the loading curves were higher than the stress-free sample. Since tensile residual stresses are present in the middle of the sample, the load depth curves are lower than stress-free sample. Figure 3- 8 shows the variation of residual stresses for each indent beneath of the surface by using Eq (3-13) and Eq (3-14). This figure shows that for two-different depths of indentation, h_{max} = 350 nm and 1000 nm, residual stresses are close to the X-ray results. The resulting residual stresses correspond to the maximum indentation depth of 1000 nm has a uniform distribution and less scattered results. The residual stresses value calculated in the deeper area from the edge showed tensile residual stresses at Z = 170 µm beneath of the shot peened surface.

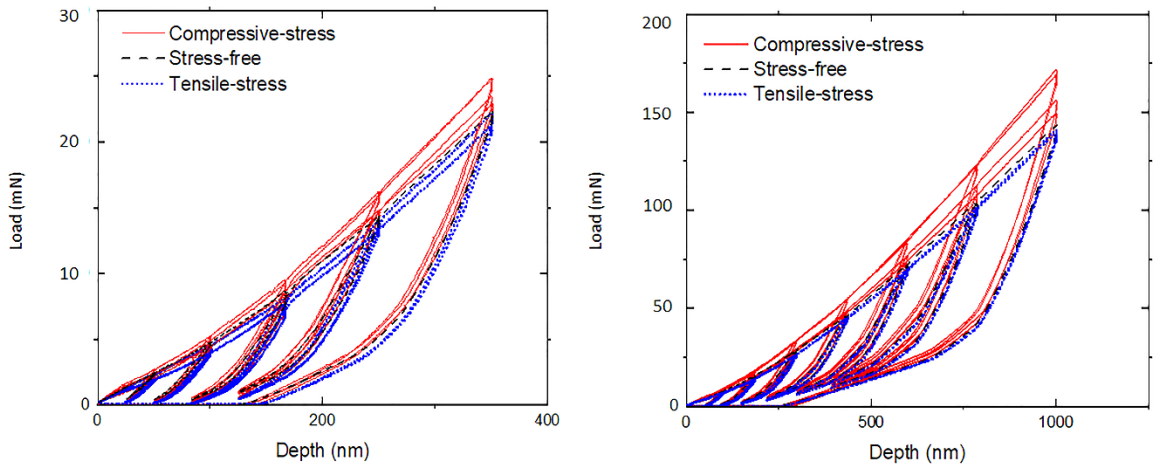

Figure 3- 7 Loading and unloading curves for stressed and stress-free sample on the cross section (color online).

Indentations on the cross-section surface were made at least 50 μm from the edge to avoid any issues of sample preparation or influence from the free surface. In addition, polishing may alter the residual stresses on the surface. However, in the current energy method, this change in stress level from the indentations should be minimized since the comparison is between two polished surfaces for the stress-free sample and peened sample with the same polishing condition. As a consequence, the X-ray result close to the surface on the cross-section in Figure 3- 8 shows a slightly higher residual stress than the nanoindentation method. In general, the stresses measured by indentation on the cross section follow the residual stress trend extracted from the x-ray results, and individual point to point variation is likely due to the local differences in the microstructure (i.e. lack of homogenization) with the indentation when compared to the ≈mm^2 region sampled by the x-ray.

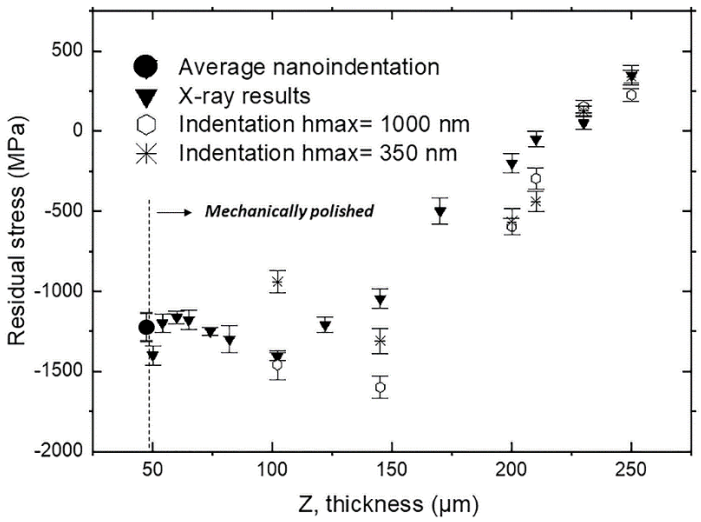

Figure 3- 8 Residual stress profile measured in the cross section. The stresses extracted from the indentation are generally in agreement with the stresses measured via x-ray diffraction. Since the roughness due to peening was removed via mechanical polishing the depth at which that surface was evaluated is noted to be equivalent to ≈50 μm from the original surface. Error bars on the figure represent instrument precision for the x-ray results, and points represent the average of two indentations, with high and low noted as "error bars".

3.5.3 Validation of Suresh model with X-ray technique

In this section residual stress measured with Suresh model has been compared with X-ray technique. Both compressive and tensile residual stresses have been calculated by Eq (2-6) and Eq (2-7). Compressive residual stresses on the shot-peened surface have been shown in Figure 3- 9. In this study X-ray diffraction was performed on the shot-peened surface before nanoindentation examination, resulting in a compressive residual stress of -1490 MPa on the shot peened surface. Typical load-displacement curves for 10 indents on the shot-peened sample and stress-free sample are shown in Figure 3- 5 which they had been used to obtain residual stresses on the substrate. Based on the Suresh and Giannakopoulos model stressed sample and stress-free sample were compared with each other. As we can see in Figure 3- 5, loading curves for compressive residual stresses are higher than the stress-free sample. By using Eq (2-6) the residual stress magnitude can be calculated corresponding to each indent points which they are shown in Figure 3- 9. The average compressive residual stresses measured by X-ray technique on the shot-peened surface was -1240 MPa. Residual stress measurement obtained by Suresh model showed similar behavior to the energy-work method. In this measurement lower indentation depth with 350 nm showed more

scattered results in comparing with 1000 nm indentation depth. The same behavior has been observed in energy-work method. As mentioned in the previous section, each indent point may be impacted by local metallurgical parameters such as defect or boundaries. The higher load (higher indentation depth 1000 nm) due to the larger volume sampled will increase homogenization, as a result changing in each indentation in higher load will be less than the lower indentation load.

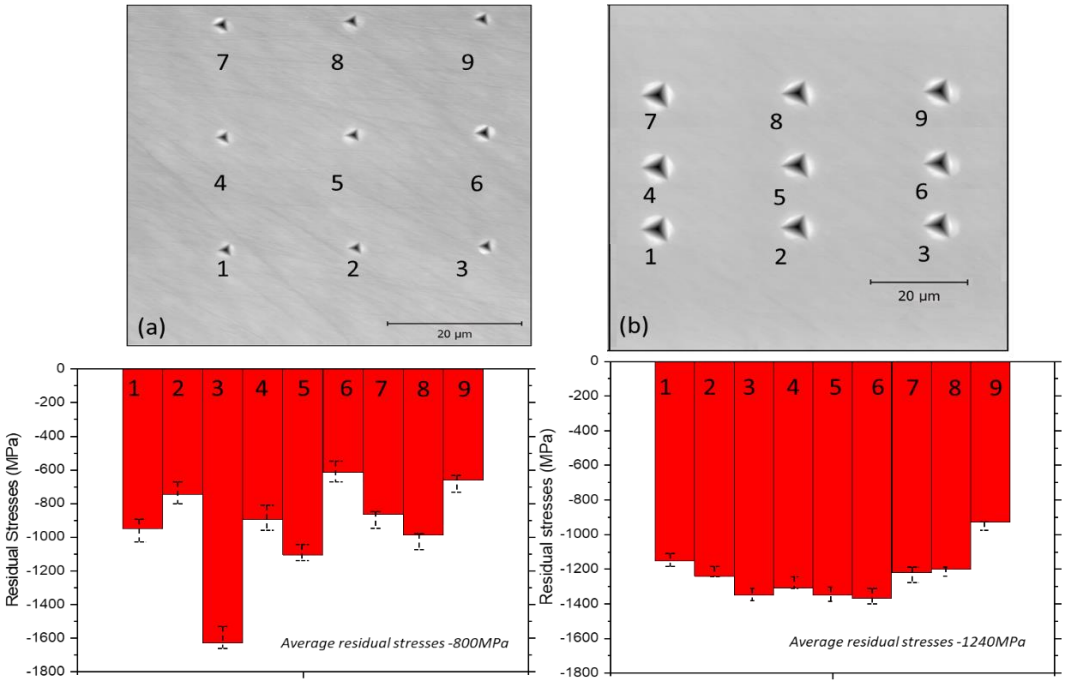

Figure 3- 9 Residual stresses corresponding to the indentation on the shot peened surface obtained by Suresh model, a and c) maximum indentation depth 350 nm, b and d) maximum indentation depth 1000 nm

3.6. Conclusion

The localized residual stresses of a shot peened austempered 52100 steel were evaluated using nanoindentation and x-ray methods. A new approach based on the energy of the indentation has been developed to measure residual stresses after peening process. It is found that unloading response during indentation depends on pre-existing residual stresses for material with strain hardening. The average residual stresses determined using the indentation method on the surface is in good agreement with the x-ray results. It is likely that the wider distribution results for each single indentation, when compared to the x-ray results, is due to localized metallurgical parameters, suggesting that residual stresses on the µm scale may vary significantly more than

would be evident with larger volume sampling methods. The ability to make localized measurements of residual stresses should be useful for future inclusion into crystal plasticity models. The residual stresses obtained by nanoindentation technique on the cross section also showed promising agreement with the x-ray measurement.

Acknowledgments

We wish to thank EI Incorporated, Cummins Fuel Systems, and the Indiana Manufacturing Consortium through the Center for Surface Enhancement Engineering for financial support of this project. We also wish to thank Metal Improvement, Indianapolis IN for shot peening the samples.

CHAPTER 4. SURFACE ROUGHNESS IMPROVMENT AFTER SHOT PEENING AND SURFACE OPTIMIZATION

4.1. Abstract

Shot peening is mainly used to the enhance fatigue life of metallic components. Induced residual compressive stresses on the metallic substrate can prevent crack growth. There is a relationship between stress coverage on the surface and surface roughness. Shot peening influences on surface roughness can be affected by peening size or time. As a result, the surface characteristic impacts the overall mechanical reliability. An ideal condition of shot peening requires a high level of residual stresses and low surface roughness. Generally controlling these two parameters simultaneously in a single shot peening passage is difficult. To improve one of those parameters, the other parameter may be sacrificed. In this research a process is proposed to improve the surface quality and residual stress profile concurrently by using a range of the shot sizes in a single shot peening passage. To predict the surface roughness, 3-D Finite Element Modeling (FEM) has been developed to compare three different shot sizes and mixed shots with simultaneous impact or sequential impacts. FEM modeling has been validated by experimental results. Numerical models predict that mixed shot sizes can create a smoother surface in comparison with monodispersed shot particles. Also, the residual stress profile for mixed shot sizes showed a very broad range of compressive residual stresses in comparison with the largest impact ball size. This newly proposed method can improve the surface quality and the range of the compressive residual stresses in a single-shot peening passage.

4.2. Introduction

Shot peening is a cold working process which has been used to enhance fatigue lifetime and improve the resistance to stress corrosion failure in metallic components. In this surface treatment, multiple small media particles hit the metallic surface in order to induce compressive residual stresses by creating small elastoplastic deformation on the substrate. Shot peening parameters such as velocity, time, incident angle, shot size and shot density have a large influence on the residual stress profile and magnitude [43]. Favorable compressive residual stresses induce fatigue lifetime. In the post-manufacturing process, plastic deformation on the surface due to the shot peening

changes surface topography, therefore, high-velocity impacts on the surface increase surface roughness which can reduce fatigue strength [109]. Numerous studies have been done to enhance fatigue strength by improving surface roughness. The optimization of the shot peening parameters can improve roughness parameters and surface quality.

Various experimental studies have shown with an increasing shot velocity residual stresses on the specimen increase at full peening coverage [110]. As well as experimental data, these results have been shown with numerical analysis [111, 37]. Numerous simulations have been done to simulate shot peening process. Obaid simulated the first finite element simulation for a shot peening process [111]. Al-Hassani et al. performed a finite element simulation based on the 3D scale for single and multiple impacts on the steel substrate [44]. Meguid et al. had comprehensively simulated shot peening parameters such as shot dimension, shot velocity, and substrate mechanical properties [112]. Other mechanical responses after shot peening simulation such as residual stress, plastic strain, and elastic strain have been determined by Meguid as well [112]. Schiffner et al. validated the residual stress profile which was computed by numerical analysis and analytical analysis according to the Hertzian contact theory [57]. There are various numerical analysis that have been performed with random impacts or impacted sequence. The sequence impact with three cycles had been simulated by Kim et al. [113]. They considered average residual stresses over the shot-peened area and the results were compared with experimental residual stress measurement which they found a promising correlation. Gagliano attempted to find a relation between shot peening parameters and residual stresses such as shot size and velocity, then his research has been extended to Almen intensity [36]. The Almen test is a thin strip specimen which is using to control peening intensity and coverage after shot peening. This standard strip is fixed on the rigid body, after peening and removing from the fixture, the arc height must be measured with an Almen gauge to obtain peening intensity. Guagliano and Meguid measured shot peening parameters and Almen intensity [36, 112].

As described above, improving (i.e. decreasing) the roughness parameter is very essential in fatigue enhancement and study the mechanism of crack initiation. After shot peening, surface topography will be changed due to the impingement and waviness which occurs on the shot-peened surface. Indeed, surface roughness parameters are categorized into three classical parameters, namely R_a, R_c, and R_z and many types of researches have been carried out on surface roughness

characterization by utilizing these parameters [48, 38]. Numerical analysis, such as Finite Element Method (FEM) is an effective and practical tool to investigate the resulting surface roughness from impacts. Mylonas et al. [114] developed a numerical analysis based on three-dimensional FE analysis. This work was performed with multi-shot random impacts to obtain 100% plastic coverage. The irregular roughness shape on the surface can act as an active site for crack initiations due to the stress concentration during cyclic loading. Miao et al. [38] used peak to valley parameter to characterize surface roughness by developing numerical analysis. It was shown that surface roughness increased by increasing the number of shots [38]. Bagherifard et al. [115] developed a FEM model and experimental measurements to measure surface roughness for different shot diameters and shot velocities. There have been shown surface roughness increases with increasing shot particles size and velocity [115].

Various roughness parameters Ra, Rc and Rz have been considered to evaluate surface roughness due to the most common choices for surface roughness measurements after shot peening [116, 117]. Definitely, there are many different parameters exist for surface roughness measurement for the study of peakedness and symmetry profile such as kurtosis and skewness. Nonetheless, in this research three important surface roughness parameters were considered in comparing different shot peening conditions [118, 119, 120]. Bagherifard et al measured surface roughness by a profilometer in three-line measurements in the separate areas with the length of 4mm [115]. In this current work surface roughness for different shot particles and mixed-shot particles have been predicted by numerical analysis. Finite element analysis has been calibrated and compared with experimental results with the work of Bagherifard et al. [115]. Results showed that the surface roughness increases with increasing particles size. Also, shot peening with larger impacted particles showed higher residual stresses on the substrate in comparing with the small particles. The achieved results showed mixed balls sizes in comparison with the biggest ball size has a less surface roughness and better surface quality and wide range of residual stress profile which was very close to the biggest ball size performance. These results are very promising to improve both residual stress profile and shot-peened surface quality simultaneously.

4.3. Surface Roughness Measurement

The measurement of the surface roughness is an important step to analyze surface topography. Various descriptions have been developed to measure surface roughness. The first function ascribes as an arithmetic mean value [121]:

$$R_a = \frac{1}{l}\int_0^l |g(x)|\,dx \qquad \text{Equation 4- 1}$$

in this equation, l is the measuring length and g(x) is the height of the peaks. Another well-known roughness characteristic is related to the mean roughness for ten different points, which is defined as [122]:

$$R_c = \frac{1}{5}\left[\sum_1^5 |g_{max}| + \sum_1^5 |g_{min}|\right] \qquad \text{Equation 4- 2}$$

R_c is the mean roughness for five predominant maximum and minimum height respectively in the same measurement length. Finally, the last parameter is the R_z which is related to the distance between the highest peak h_{max} and deepest valley h_{min} within a sampling length [118].

$$R_z = h_{max} + h_{min} \qquad \text{Equation 4- 3}$$

These three parameters have been shown in Figure 4- 1. As can be seen, these three parameters show surface roughness profiles, therefore different shot peening condition can be compared in terms of these roughness parameters. These three parameters are the most commonly reported for surface roughness profile based on the literatures [122, 119]. These parameters provide enough good basis for surface topography measurement. Certainly, for investigating of surface roughness and fatigue phenomena, more complicated models and parameters such as kurtosis, skewness profile [115] and surface characterization based on the notch's depth and distance should be considered. [120, 123].

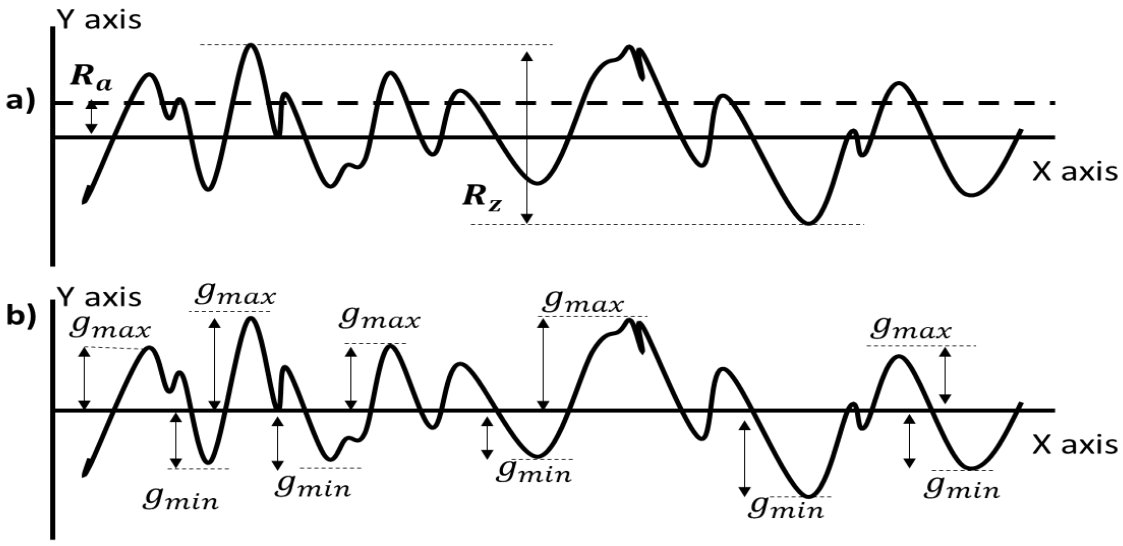

Figure 4- 1 a) Schematic figure arithmetic mean value and distance between highest peak and deepest valley, b) mean roughness for five predominant maximum and minimum height.

4.4. Surface Roughness Modeling

Random shot peening has been simulated by FEM method upon an alloy steel 39NiCrMo$_3$ substrate using a cyclic hardening formulation. The Chaboche hardening model was used for relating stress and strain based on the material properties shown in Table 4- 1 [115, 48]. In this study nonlinear kinematic Chaboche hardening model has been implemented based on the cyclic hardening test [115, 48, 124] which are shown in Eq (4-4) and Eq (5-5).

$$\alpha_i = [\frac{C_i}{Y_i}(1 - e^{-\gamma_i \varepsilon^p})] \qquad \text{Equation 4- 4}$$

$$\alpha_i = \sigma_i - \sigma_i^0 \qquad \text{Equation 4- 5}$$

in these equations α_i is the back-stress for half-cycle and overall back-stress gained by adding all back-stresses which is shown schematically in Figure 4- 2(a), C_i and γ_i are the materials calibration constants.

Table 4- 1 Mechanical properties based on the cycling characteristic [115].

σ_0 MPa	E GPa	ν	C	γ
359	190	0.3	169823	501.8

In this research, finite element simulation performed to simulate the shot peening process by using Abaqus/ Explicit 6-14. Shot particles have been modeled as a rigid steel with three different ball sizes 0.35 mm, 0.43 mm and 0.6 mm respectively. Initial velocity in Z direction considered as an impact direction and perpendicular to the substrate. Shot peening condition for experiment and simulation have been shown in Table 4- 2. Substrate modeled as a rectangular unit cell of 4 mm ×4 mm × 3 mm with all side continuum infinite elements CIN3D8 to avoid elastic shear wave reflection. Along with other researchers [125], it is difficult to obtain very stable equivalent plastic strain PEEQ even by very fine mesh. To obtain reasonable computational time a very fine mesh has been selected as approximately $1/12^{th}$ of the dimple diameter, motivated by Schwarzer et al. [40]. Mesh size between $1/10^{th}$ and $1/15^{th}$ of the dimple size have been used by other researchers for shot peening which they showed reasonable computational time and good quality of the results [126]. Finally, with considering similar modeling conditions for different impact ball-sizes, an error value of PEEQ will be identical for all simulations. Consequently, for roughness comparison results will be faithful.

Table 4- 2 Modeling and Experimental parameters for shot peening.

Simulation FEM Shot size	0.35mm, 0.43mm and 0.6mm
Shot velocity	80 m/s
Experimental [115] Shot size	0.43 mm
Shot velocity	80 m/s

A python subroutine developed to generate random impacts on the surface and create impacts iteration. Each previous impact results transferred automatically to the next simulation/iteration as predefined strain stress for each integration points. This process repeated for *N* number of impacts to obtain more than 100% coverage. During simulation shot particles have been transferred by random vector on the surface area, random X and Y vector's components have been shown as follows:

$$X_1 = A + \text{random. randint } (1.0, 100.0) \times \frac{A+L}{10} \qquad \text{Equation 4- 6}$$

$$Y_1 = A' + \text{random. randint } (1.0, 100.0) \times \frac{A+L}{10} \qquad \text{Equation 4- 7}$$

in these two equations, X_1 and Y_1 are the horizontal and vertical axis for random transfer vectors which are shown in Figure 4- 2(b). A and A' are the positions for the reference point respectively and L is the characteristic length. This random command can create random numbers with the 100µm resolution.

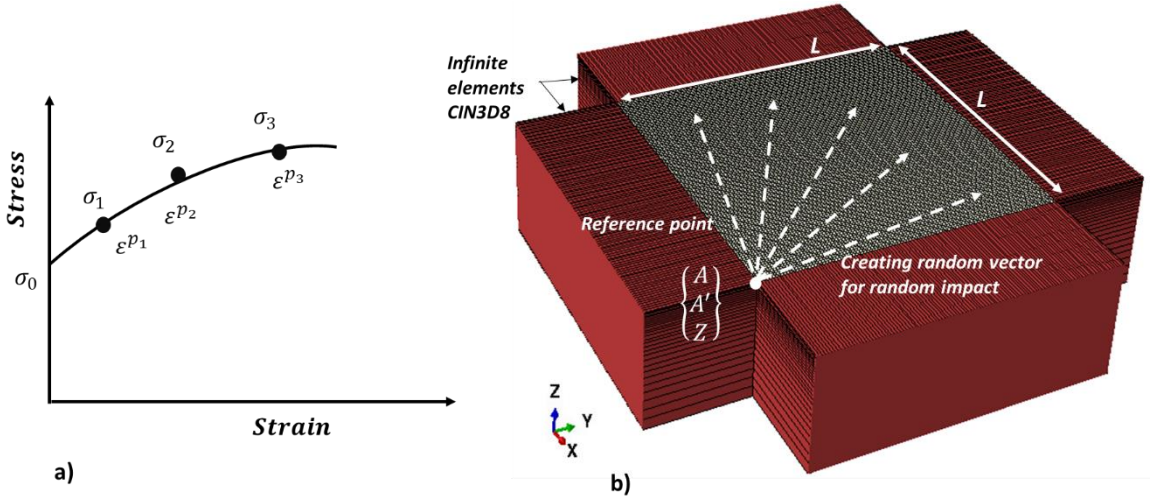

Figure 4- 2 a) Schematic figure of half cycle, stress-strain curve, b) assembling random impact.

4.5. Surface Coverage and Almen Test Modeling

To obtain full coverage of shot peening plastic strain ratio over the whole surface area should be calculated as a surface coverage. Some researchers proposed a mathematical and exponential approach [127] to obtain a number of shots to acquire acceptable surface coverage. In this research, Almen test simulation and the analytical solution have been developed to obtain maximum coverage and the number of shots. This result has been used for surface roughness simulations.

An Almen intensity test is the regular test to assess the intensity and coverage of peening progress. In this technique thin strip called Almen strip that made of steel is fixed on the Almen gage, after shot peening and releasing the strip, residual stress maintains a curved shape. This curvature of the thin strips after shot peening is measured to obtain the exact set of operating parameters. Unequal induced stress generates bending and stretching in the specimen, as a result of that compressive residual stresses needed to reach an equalibrium state. The saturation point

can be determined by plotting the arc height as a function of peening time, in this curve saturation point is equivalent to the time which doubling that time only increases the height by 10%, this time is defined as the Almen intensity.

Finite element random impact modeling (FEM) has been developed with the same python script and procedure which was explained in the previous section. The Almen strip was modeled with C3D8R hexagonal elements, in this simulation the rigid shots are used with three different ball sizes 0.35 mm, 0.43 mm and 0.6 mm respectively. The surface to surface contact was defined between balls and substrate with general contact algorithms. The initial velocity of each shot was the same as the previous section 80 m/s. To accelerate computational time, forty rigid shots have been defined for each Almen simulation which is shown in Figure 4- 3(b). To obtain Almen height two steps were defined. The first step was the random dynamic impact simulation, in this model Almen strip was located on the rigid floor and constrained in peening direction, after peening process, results were transferred to the second step. In the second step, the substrate was removed from the rigid body statistically to obtain relative Almen height which is shown in Figure 4- 3(c). Non-linear geometry was allocated during simulation to control the large distortion and plastic deformation. For boundary conditions, the rigid floor was fixed in all directions (UX=UY=UZ=0) and four rigid fixture were fixed in the in all directions (UX=UY=UZ=0) and substrate was located on the rigid floor and four fixtures Figure 4- 3(a). The Johnson-Cook equation was used for relating stress and plastic strain. In this model material behavior depends on the strain rate and temperature which is shown as the following equation:

$$\sigma = [A+B\varepsilon_p^n)\ [1+C\ln\ (\frac{\dot{\varepsilon_p}}{\dot{\varepsilon_0}})]\ [1-(\frac{T-T_0}{T_M-T})^m] \qquad \text{Equation 4- 8}$$

In this equation A,B,C, m and n are materials constants, material properties and model parameters are shown in Table 4- 3 and Table 4- 4. ε_p is the equivalent plastic strain, $\dot{\varepsilon_0}$ and $\dot{\varepsilon_p}$ are the reference strain rate value and applied strain rate, respectively, T_m, T and T_0 are melting temperature, current temperature in the simulation and reference temperature, respectively.

Table 4- 3 Materials parameters used for Johnson Cook equation [128].

Material parameter	A (MPa)	B (MPa)	n	C	m	$\dot{\varepsilon}_0$	$T_0\ (K)$	$T_m\ (K)$
Steel SAE 1070	1408	600 MPa	0.234	0.0134	1	1	298	1793

Table 4- 4 Physical and materials properties of steel 1070 [129].

σ_0 (MPa)	E (GPa)	ν	ρ (Kg/M^3)	μ (Friction coefficient)
1408	210	0.31	7980	0.3

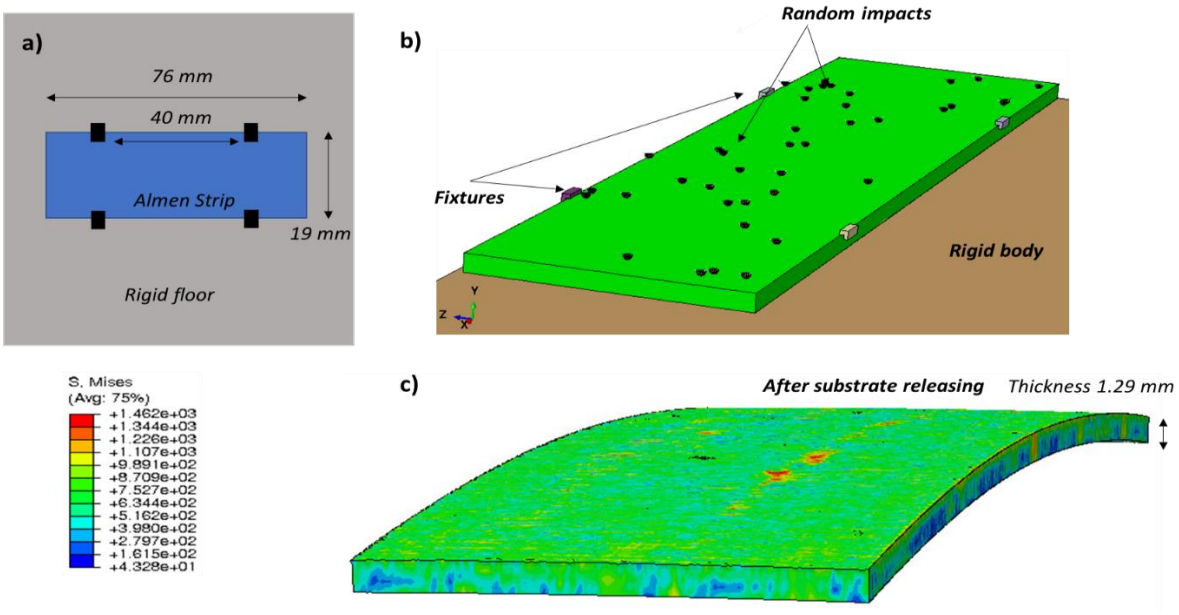

Figure 4- 3 a) schematic view of the Almen test setup, b) three random impact simulation after 40000 impacts, ball-size 0.6 mm and 80m/s shot velocity, c) Almen strip separation from the rigid floor and balancing the internal stresses.

4.5.1 Almen test and analytical analysis

An analytical solution had been developed to validate the numerical solution for Almen height. To obtain an analytical solution, the stress source concept provided by Guechichi et al. has been used in this research. In this solution bending and axial stress should be balanced with the stress source from peening process. All these stress summations should provide residual stresses which

are shown in Eq (4-9). Al-Hassani and Guechichi used a combination of this theory and spherical curvature dent theory which are represented by impact shots [44, 129]. In this analysis, some critical assumptions are made including; impact is normal to the surface, there is no friction between shot impact and substrate, indenter shape is spherical, the materials are isotropic as well as strain-hardening, and the substrate is a semi-infinite body in comparison with the shot size. The Guechichi model shot peening process depends significantly on velocity. This process is related to the multiple impacts and loading and unloading nature of the impact. Hence, shot peening has been considered as a cyclic loading phenomenon. Eventually, Guechichi concluded cyclic time-dependent linear stress field for shot peening process which is shown in Eq (4-10).

$$\sigma_{res} = \sigma_{axial} + \sigma_{bending} + \sigma_{induced} \quad \text{Equation 4- 9}$$

$$\sigma_{el}(t) = \omega(t)\sigma_{max} + [1-\omega(t)]\sigma_{min} \quad \text{Equation 4- 10}$$

In this equation, elastic stress is equal to the maximum and minimum stress during the single cycle of loading. Based on the Guechichi model maximum stress is related to the shot impact and the minimum stress occurs when a shot starts to rebound from the surface. and $\omega(t)$ is a scaler function of time between 0 and 1 [129]. Consequently, total elastic stress can be shown in the following equation:

$$\sigma_{el}(t) = \omega(t)\sigma^{Hertz} \quad \text{Equation 4- 11}$$

In this current research stand-alone software has been developed to obtain Almen height as a function of shot velocity according to the Guechichi and Cao's analytical solutions in python language [130, 129]. The graphical input data panel for this software has been shown in Figure 4-4. According to Figure 4- 4 materials properties of substrate and impact shot should be defined in the software to obtain Almen height as a function of velocity. In this analytical solution shot materials considered as zirconia which material properties have been shown in Figure 4- 4. A developed analytical solution and algorithm are described extensively in Guechichi research [129]. Additionally, all corresponded equations which they have been utilized in this research are summarized in Table 4- 5.

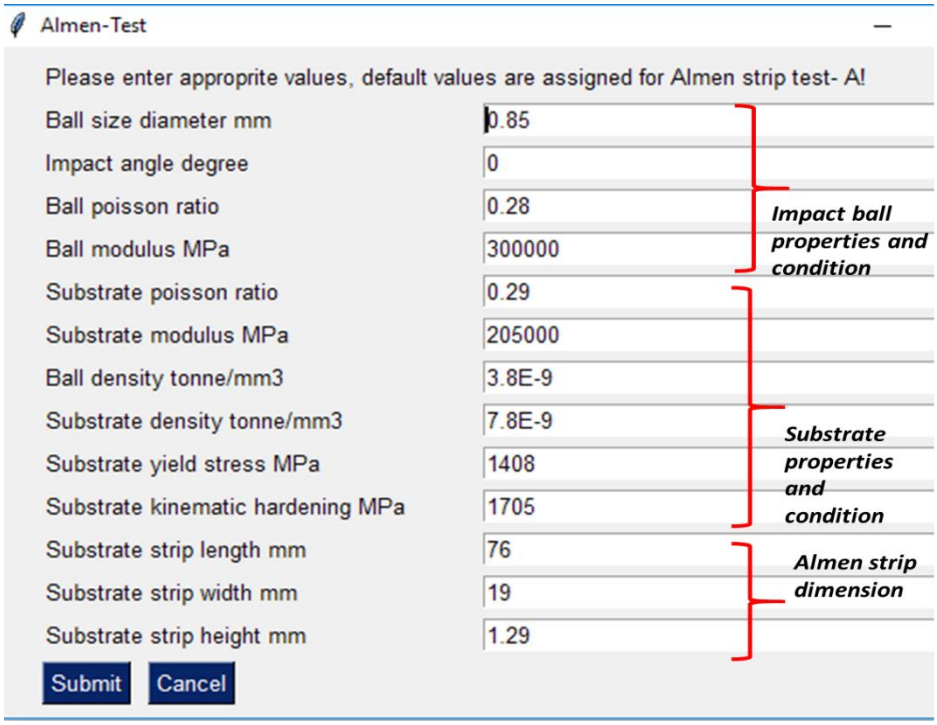

Figure 4- 4 Graphic user interface for analytical solution to obtain Almen height as a function of impact velocity.

Table 4- 5 Summery of all analytical equations used by Guechichi [129] and utilized equations in this research.

Hertz Contact Theory	$P_0 = \frac{1}{\pi}[\frac{5}{2}\pi k\rho v^2 E_0^4]^{\frac{1}{5}}$ Equation 4- 12 $a = \frac{D}{2}\left[\frac{5K\pi\rho V_{nor}^2}{2E_{eq}}\right]^{\frac{1}{5}}$ Equation 4- 13	*ρ = density of the substrate, V = normal velocity, E_0= young modulus. D = ball diameter, K thermal dissipation 0.8. a = radius of elastic contact P_0 = Maximum pressure of elastic contact*
Equivalent modulus	$\frac{1}{E_{eq}} = \frac{1-\vartheta_m^2}{E_m} + \frac{1-\vartheta_s^2}{E_s}$ Equation 4- 14	*E_m and E_s are modulus of the ball and substrate respectively.*

Table 4-5 Continued

Hertzian principal stress	$\sigma_{xx}^{Hertz} = \left[\frac{Z}{a_e}\tan^{-1}\left(\frac{Z}{a_e}\right) - 1\right]p(1+\vartheta) + \frac{pa_e^2}{2(a_e^2+Z^2)}$ Equation 4- 15 $\sigma_{yy}^{Hertz} = \left[\frac{Z}{a_e}\tan^{-1}\left(\frac{Z}{a_e}\right) - 1\right]p(1+\vartheta) + \frac{pa_e^2}{2(a_e^2+Z^2)}$ Equation 4- 16 $\sigma_{zz}^{Hertz} = -p\left[\left(\frac{z}{a_e}\right)^{-1} + 1\right]$ Equation 4- 17	a_e = *radius of elastic contact* *P = Maximum pressure of elastic contact, Z corresponding depth.*
Hertzian stress can be expressed based on the elastic stress *Deviatoric elastic stress tensor*	$\overline{\sigma^{el}}(z) = \overline{\sigma^{Hertzl}}(z) =$ $\begin{bmatrix} \sigma_{xx}^{Hertz}(z) & 0 & 0 \\ 0 & \sigma_{yy}^{Hertz}(z) & 0 \\ 0 & 0 & \sigma_{zz}^{Hertz}(z) \end{bmatrix}$ Equation 4- 18 $s_{ij}^{el}(z) = \sigma_{ij}^{el}(z) - \left(\frac{\sigma_{ij}^{el}(z)}{3}\right)\delta_{ij}$ Equation 4- 19	s_{ij}^{el} *deviatoric elastic stress*
Von Mises criterion *Modified variable* *Defining the new yield stress after shot peening, deviatoric stress after elastic or elastoplastic shakedown*	$f(S,\alpha) = \frac{1}{2}(S - \alpha)^T(S - \alpha) - (R_0 + \Delta R)^2 \le 0$ Equation 4- 20 $\alpha'_{ij} = \alpha_{ij\,(z)} - S_{ij}^{ind}(z)$ Equation 4- 21 $\frac{1}{2}\left(S_{ij}^{el} - \alpha'_{ij}\right)^T\left(S_{ij}^{el} - \alpha'_{ij}\right) \le K^2$ Equation 4- 22 $\alpha'(z) = S_{eq}^{el}(z) - K$ Equation 4- 23 $\alpha'(z) = K$ Equation 4- 24	ΔR *elastic domain increasing related to isotropic hardening,* R_0 *isotropic hardening* $= \sqrt{\frac{2}{3}}$ σ_s, α *internal variable* $\alpha = C\varepsilon^P$, K *= radius of the yield surface* $k = \sqrt{\frac{2H}{3\sigma_s}}$. *H= slope of linear kinematic hardening* *(elastic shakedown)* *(plastic shakedown)*
$\alpha^{ind}(z)$ *Induced residual stresses due to the shot peening* *modified variable*	$\alpha^{ind}(z) = -\varepsilon^p(z)\left(\frac{E_m}{1-\vartheta_m}\right)$ Equation 4- 25	*C is a hardening modulus*

Table 4-5 Continued

Bending stress *Bending moment* *Stretch stress*	$\alpha'(z) = C\ \varepsilon^p(z) - \frac{\sigma^{ind}(z)}{3}$ Equation 4- 26 $\Delta\varepsilon_{eq}^{p}(z) = \Delta\alpha_{eq}(z)(\frac{3(1-\vartheta)}{3C(1-\vartheta)+E})$ Equation 4- 27 $\sigma_{bend} = \frac{12M}{bh^3}\left(\frac{h}{2} - z\right)$ Equation 4- 28 $M = \int_0^k \sigma_{ind}(Z)\left(\frac{H}{2} - Z\right)bdz$ Equation 4- 29 $\sigma_{xx}^{stretch}(z) = -\frac{1}{h}\int_0^{z_{max}} \sigma_{xx}^{ind}(z)\ dz$ Equation 4-30	
Almen arc height	$Arc = \frac{3M\ L_x^2}{2\ E_m h^3}$ Equation 4-31	*M Bending moment, L_x Almen strip length, h Almen thickness, E_m equivalent modulus.*

In this study, the Hertz contact pressure Eq (4-12) was used to calculate Hertz principle stresses and elastic tensor Eq (4-18). Based on Guechichi model, a von Mises criterion is employed as a yield criterion to relate to the residual stress field which is shown in Eq (4-20). Based on the Guechichi model the modified variable can be calculated by the internal variable (back stress) and by using Eq (4-21). For obtaining a modified variable, yield surface should be described by new von Mises function which is shown by Eq (4-22). Based on the Guechichi model materials react as an elastic or plastic shakedown during shot peening process. Elastic shakedown is related to the initial state of non-zero intersection after rebounding for two yield surfaces and without intersection for plastic shakedown. Figure 4- 5 shows elastic and plastic behavior for two materials regarding the initial and final situation.

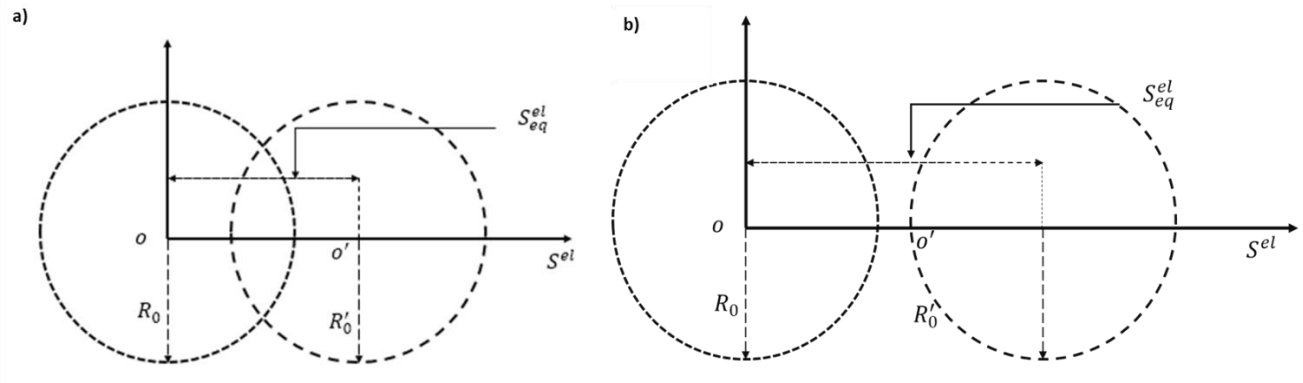

Figure 4- 5 elasto plastic behavior of meterails, a) elastic and b) plastic shakedown with two materials domains, from [129].

In this deformation, the strain rate will affect the final state of the elastic and plastic shakedown. During shot peening, there is a cyclic loading and strain hardening phenomenon. After peening process the initial yield surface will be translated to the new position, consequently, initial yield surface will be restored to the original position when shots are rebounded. Regarding the Von Misses equation, deviatoric stress S_{eq}^{el} is equivalent to elastic stress. Obtaining both parameters; the radius of yield surface k and equivalent elastic stress are so crucial to determine the modified variable. Hence, in the case of elastic shakedown, the value of the S_{eq}^{el} should be higher than the radius of the yield surface and less than $2k$, then modified variable can be shown as the following equation:

$$\alpha'(z) = S_{eq}^{el}(z) - K$$

If the elastic equivalent stress is higher than $2k$, modified variable governed by plastic shakedown which can be shown as [36]:

$$\alpha'(z) = K$$

when elastic equivalent stress is less than k, then induced stress is equal to the zero. Based on the Guechichi model in the thin sample, residual stress is equal to the induced stress, bending stress and stretch stress which is shown in Figure 4- 6. The bending and stretch stress have been shown in Eq (4-28) and Eq (4-30) respectively. Finally, by using Eq (4-31) Almen height can be calculated.

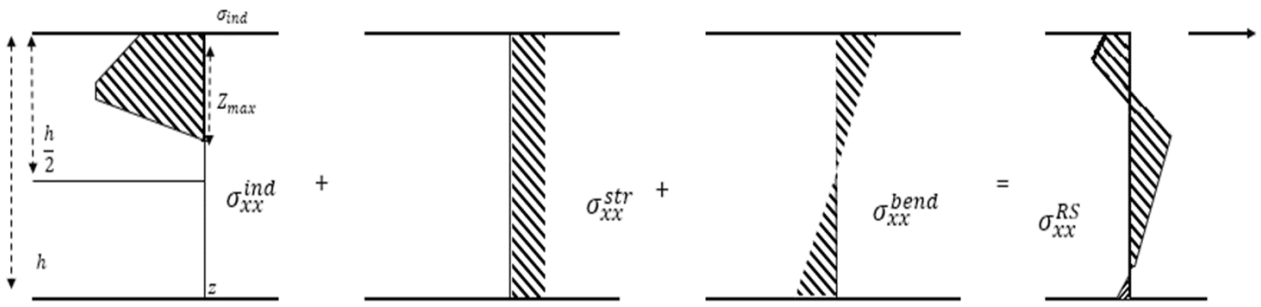

Figure 4- 6 induced stress stretch stress and bending stress profiles.

To predict residual stresses after shot peening an analytical solution has been developed based on the Hertz contact theory in the Python code. The input GUI and material parameters have been shown in Figure 4- 7. In this analytical solution, zirconia ball has been considered as a rigid body which was considered as an analytical rigid body similar to the numerical simulations. In this data input, kinematic hardening was obtained by Eq (4-4) and the corresponding ultimate plastic strain was 0.01.

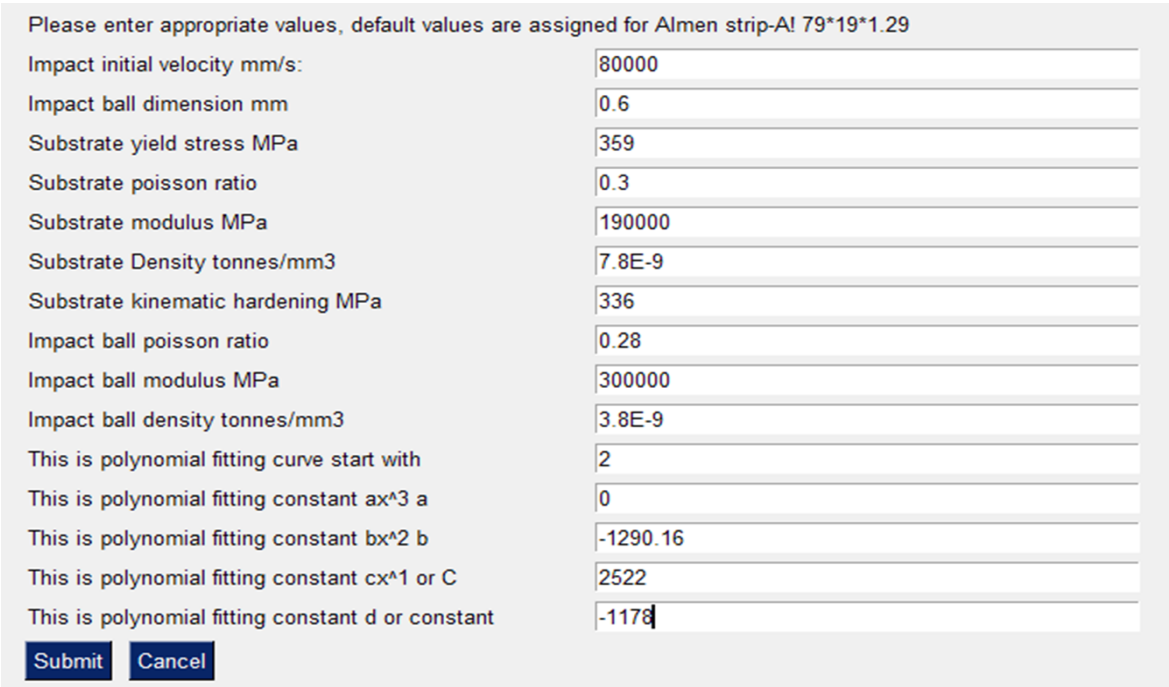

Figure 4- 7 Graphic user interface for analytical solution to obtain residual stresses after shot peening.

4.6. Results and Discussion

4.6.1 Surface coverage and validation of the model

In order to obtain an appropriate number of shots for surface roughness modeling. Almen simulation (FEM) has been used to obtain an appropriate number of shots on the substrate for retrieving 100% shot peening coverage. These results compared with the analytical solution for validating of FEM results. In this case, based on the analytical solution three different shot dimensions 0.35 mm, 0.43 mm, and 0.6 mm were examined respectively. Results for shot velocity as a function of Almen height was shown in Figure 4- 8. As shown in this figure with increasing of the shot velocity Almen height or strip deformation increased due to the internal stresses and higher compressive residual stresses on the substrate. As indicated in Figure 4- 8-a with similar shot velocity different shot sizes creates a quite different deflection due to the different kinetic energy and residual stresses in the Almen strip. As can be seen, with increasing of shot size maximum residual stresses on the substrate and arc height were expanded. Generally, Impact velocity is more effective on the Almen height in comparison with the shot density. Overall, increasing the impact velocity creates higher deflection in compare with increasing ball dimension for a given velocity. For example, with 0.35 mm shot diameter and impact velocity between $100\ m/s$ up to $170\ m/s$ Almen height increases by 35% while in this range velocity increases by 70%. Contrarily, with increasing the shot diameter about 71% (comparing 0.35 mm ball size with 0.6 mm ball size) in the constant velocity $100\ m/s$, Almen height increases by 22%. These results show the most important factor during shot peening is a shot velocity.

Numerical results for Almen test are shown in Figure 4- 8(b). According to the simulations, four different coverages 40%, 60%, 80%, and 100% were conducted by suspending and resuming impacts. As illustrated in this figure, with increasing of number of shots, shown in Table 6, Almen height increased until reaching a steady-state and saturated point. Figure 4- 8(b) shows the number of shots effect upon the resulting deflection and inducing residual stresses. After 80% coverage by doubling the computational time and increasing the number of shots, Almen height variations were less than 8%~10% which were quite similar to the Almen test experience [130]. In the second step, the substrate was removed from the rigid body to obtain corresponding Almen height, which the results are shown in Table 4- 6 and Figure 4- 9. As shown in Table 4- 6 both methods analytical

solution and numerical solution showing good correlation with each other. The arc height between FEM modeling and analytical solution for a given impact velocity were close in both methods. Regarding the results, Almen height and saturation points for given velocity with different shot sizes in FEM modeling can be proved by an analytical solution. Furthermore, these Almen intensities for both analytical solution and numerical solutions are in good agreement with Nordin and Alfredsson experimental and simulation data [131].

According to Figure 4- 8(b) and Table 4- 6 for full Almen strip size, 30100 random impacts are needed to obtain 100% coverage with 0.6 mm shot size. Results for various shot sizes are shown in Table 4- 6. Regarding the Almen test simulations about 250 impacts were needed to obtain 100% coverage with 0.6 mm ball size in a small domain with 4 mm × 4 mm length (Surface roughness simulation). Furthermore, for a shot diameter of 0.43 mm and 0.35 mm, 350 and 480 impacts were considered to obtain full coverage on the same domain-size respectively. In this research for mixed peening coverage 33% of each shot sizes 0.6 mm, 0.43mm and 0.35 mm have been considered to obtain 100% coverage respectively. The order of mixed shot peening and conditions has been shown in Table 4- 6.

Table 4- 6 Almen height calculated with analytical and numerical methods

Ball dimension (mm)	0.6	0.43	0.35
Analytical solution (Arc height mm)	0.24	0.20	0.19
Numerical solution (FEM) Arc height 100% coverage (mm)	0.28	0.21	0.20
Number of shots	30100	53000	76000

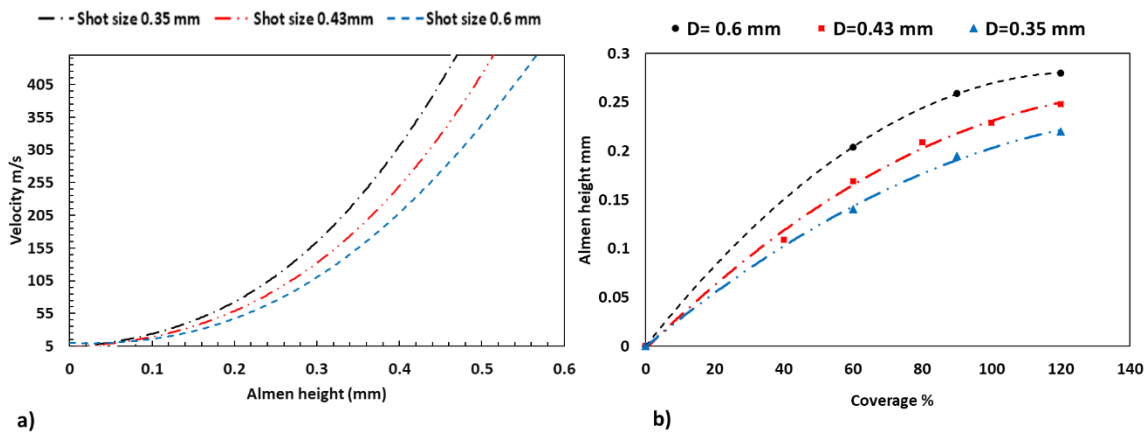

Figure 4- 8 a) Analytical solution for Almen height as a function of velocity, b) FEM results for Almen height as a function of coverage or number of impacts.

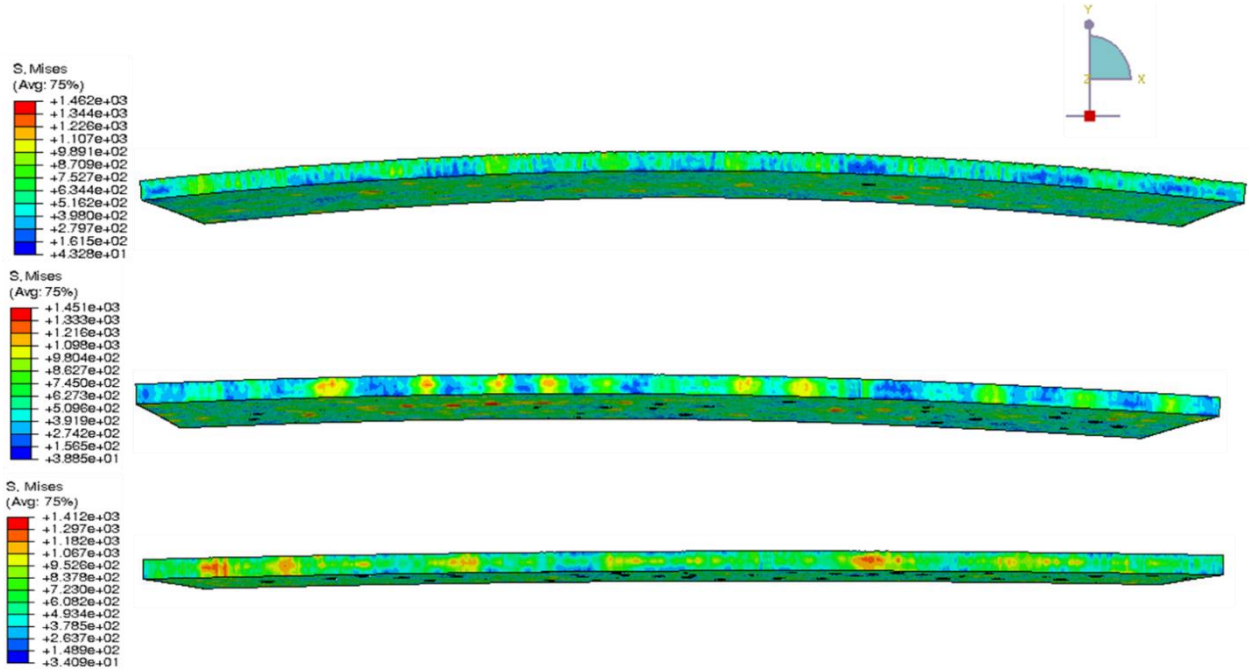

Figure 4- 9 simulation results for Almen deflection and maximum residual stresses for three different shot sizes.

4.6.2 Surface roughness measurement

The results obtained from finite element simulations have been shown in Table 4- 7. Six different simulation results were compared to determine surface roughness parameters with same shot peening modeling. As can be seen in Table 6 there are two major groups of modeling. Single impacts modeling (model-1, model-2, and model-3) and mixed shot peening and sequential

modeling (model-4, model-5, and model-6) respectively. In this research, these two groups are compared with each other to obtain surface roughness. As can be seen in Table 4- 7 model-4 is related to the simultaneous impacts with equal distribution and model-5 and model-6 are sequential impact with equal distributions. However, the differences between model-5 and model-6 are related to the order of the shot diameter of sequential impacts which are shown in Table 4- 7.

Table 4- 7 Shot peening simulations for different setup

FEM modeling	D (mm)	V ($\frac{m}{s}$)	Distribution of Shots % (0.6 mm, 0.43 mm, 0.35 mm)	Sequence
Shot peening model-1	0.6	80	100%, 0%, 0%	n/a
Shot peening model-2	0.43	80	100%, 0%, 0%	n/a
Shot peening model-3	0.35	80	100%, 0%, 0%	n/a
Shot peening model-4	0.6, 0.43, 0.35	80	0.33%, 0.33%, 0.33%	Mixed simultaneous
Shot peening model-5	0.6, 0.43, 0.35	80	0.33%, 0.33%, 0.33%	Sequential impact (0.6 mm→0.43 mm→ 0.35 mm)
Shot peening model-6	0.35, 0.43, 0.6	80	0.33%, 0.33%, 0.33%	Sequential impact (0.35 mm→0.43 mm→ 0.6 mm)

Surface deformation in the Z-axis have been shown in Figure 4- 10 for three individual impacts and three mixed impacts. All simulations performed in the same size and conditions. Surface roughness parameters R_a, R_c, and R_z have been shown in Figure 4- 11. According to the results, increasing the impact ball dimension increases surface roughness parameters due to the higher dimple diameter. During shot peening surface roughness increases with number of impacts. Bagherifard et al. showed this growth in the surface will reach to the steady-state condition due to the dynamic stability and peaks and valleys formation [115, 132]. To validate the simulation results, model-2 has been compared with experimental results with Bagherifard et al. research [115] which is shown in Table 4- 8. Comparing roughness parameters show good correlation between modeling and experimental data. As can be seen in Table 4- 8 the differences between modeling and experimental results for R_a factor is less than 5%. This can be ascribed due to the primary roughness in experimental measurement or higher coverage percentage in shot peening modeling.

Table 4- 8 Validation of modeling results in this research with experimental results obtained by Bagherifard et al [115].

Shot peening	Shot-Diameter (mm)	Velocity (m/s)	Coverage %	Roughness Parameters (μm)
Experimental data [115]	0.43	80	120	R_a = 4.59 [115] R_c = 18.68 [115] R_z = 29.70 [115]
Simulation Model-2	0.43	80	120	R_a = 4.80 R_c = 15.53 R_z = 24.38

According to the section 4.3.1 and Almen test modeling, considering an appropriate number of shots for all simulations will assure modeling to reach more than 120% surface coverage and steady-state condition for surface roughness. In Figure 4- 10- a detailed of roughness parameters show the biggest shot size with 0.6 mm diameter in compare with the smallest shot size 0.35 mm diameter has a 70% higher roughness mean value (R_a). The results indicate that with increasing impact ball dimension with constant velocity, peaks and valleys are growing due to the larger dimple size. According to Figure 4- 11 using mix ball shots, (model-4) reduce roughness parameters in comparison with individual shots. The results obtained from FE simulations showed for mixed shot peening, roughness parameters are less than largest shot size 0.6 mm. The differences for (R_a , R_c, and R_z) are about 32%, 29%, and 38% respectively. But these results indicate that roughness parameters in mixed shot particles are higher in comparison with middle shot size 0.43 mm. The differences for (R_a, R_c, and R_z) are 45%, 31%, and 5% respectively. The last roughness parameter R_z in mixed shot size in comparison with 0.43 mm ball size showed fewer differences. These results can be explained that small ball size decreases the height of the sharp peaks which they are generated by the large shot size. The Sequence impacts in two different orders showed lower roughness parameters in comparison with the single largest shot size. Also, the sequence impacts showed fewer roughness parameters R_a , R_c in compare with mixed shot size about 20% and 12% respectively. The most obvious similarity between mixed shot impact and sequence impacts is related to the R_z factor with 4% ~10% differences.

The R_z factor is related to the differences between the highest peak h_{max} and deepest valley h_{min} within a sampling length. The sequence impact with a big to small order showed the lowest magnitude of R_z due to the reduction of sharp peaks by small ball subsequence impacts. Finally,

this disparities between sequence order with small to big and big to small media in compare with a mixed shot are 4% and 10% respectively. These results indicate mixed shot size has a similar effect on roughness profile in compare with sequence impacts. Also, the mixed shot size in compare with sequence impacts is faster and reliable. This method can be used in a single passage instead of multiple shot peening passages with different media sizes.

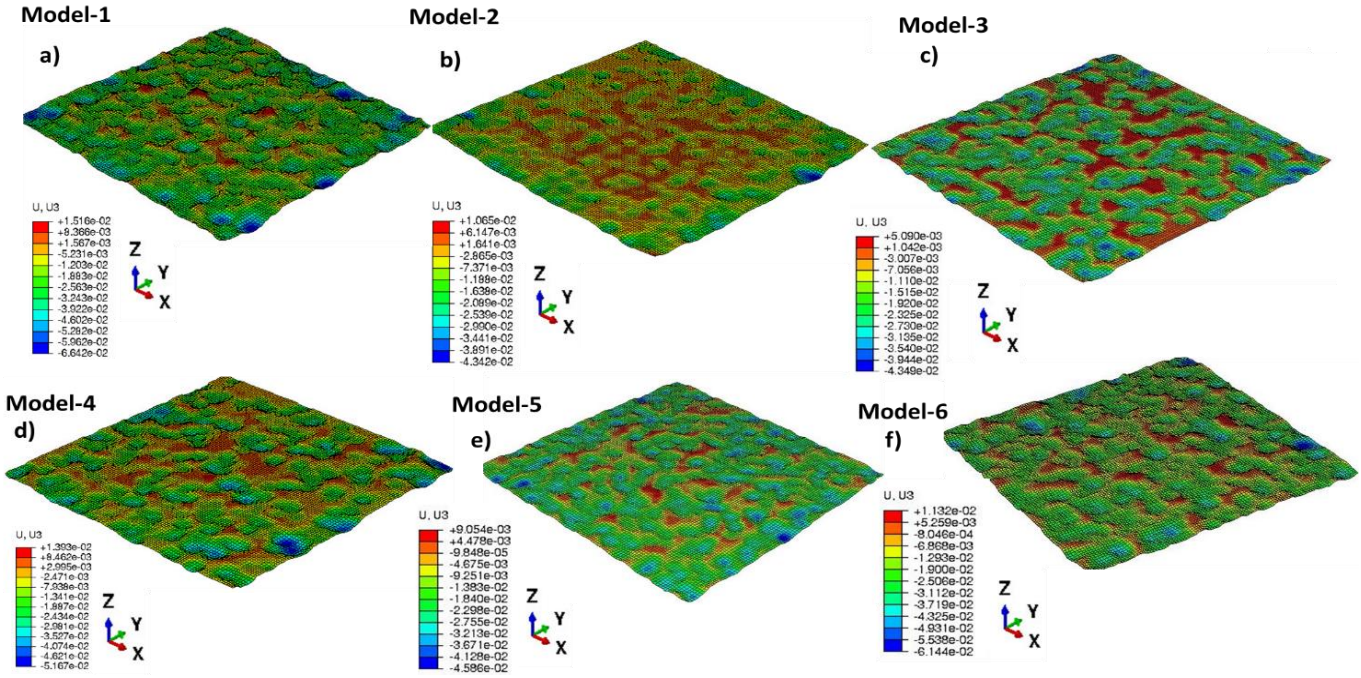

Figure 4- 10 Surface roughness, a) model-1 shot size 0.6 mm, b) model-2 shot size 0.43 mm, c) model-3 sot size 0.35 mm.

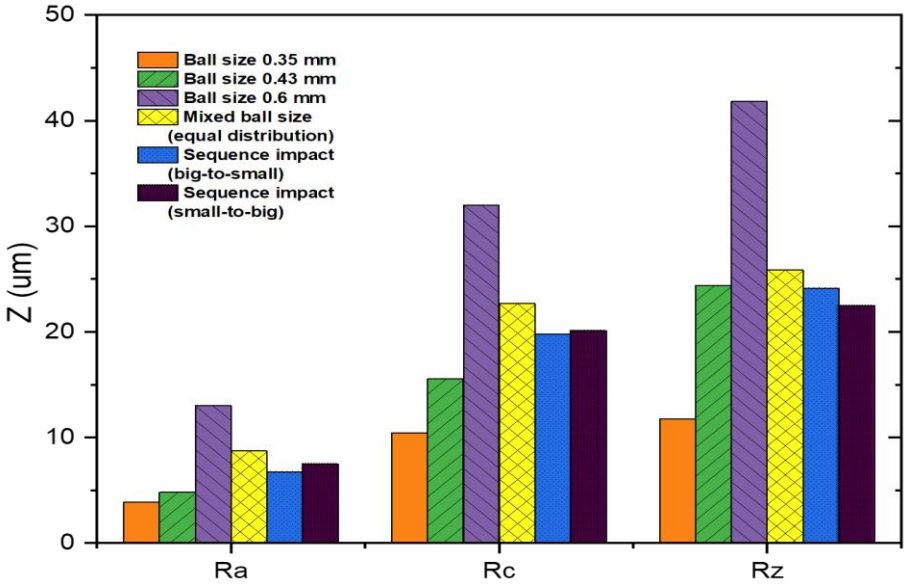

Figure 4- 11 Surface roughness profile for three different roughness parameters R_a , R_c, and R_z.

4.7. Residual Stress Comparison

Figure 4- 12 shows residual stress profiles along the peening direction. In order to compare results, residual stresses were normalized by yield stress. Target material was exposed to shot peening with different shot sizes and mixed shots. According to the results, as can be seen in Figure 4- 12 there is a good correlation between increasing the residual stresses magnitude and increasing the impact shot diameter. In these simulations, the maximum average residual stress values are -480 MPa, -440 MPa and -357 MPa for 0.6 mm, 0.43 mm, and 0.35 mm of shot sizes respectively. Also, the residual stress profile showed a good correlation with shot peening simulation in Bagherifard et al. research [48]. Experimental results showed ~ -510 MPa residual stresses in depth of 0.1 mm with a shot size of 0.6 mm and 90 m/s shot velocity [48]. In this research residual stress was found ~ -470 MPa in depth of 0.1 mm with shot size 0.6 mm and 80 m/s shot velocity. These results indicate good correlation in terms of residual stress prediction. Mixed shot size showed very similar maximum residual stresses in compare with the largest shot size with -387 MPa in the depth of 0.37 mm. Also, the residual stress profile for mixed shot size indicates a wider range of residual stresses which is shown in Figure 4- 12. Both sequence impacts showed very similar residual stress profile in comparison with the largest individual shot size.

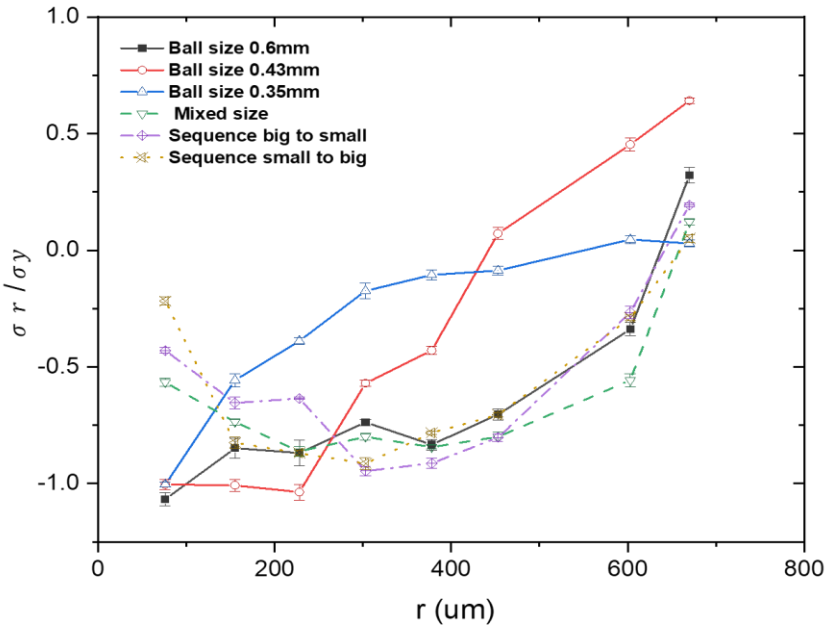

Figure 4- 12 Residual stress profile for various shot size and mixed shot size.

4.7.1 Residual stress comparison between the analytical solution and numerical analysis

The corresponding analytical solutions for induced stress, bending stress and stretch stress for shot velocity 80 m/s and 0.6 mm ball diameter are shown in Figure 4- 13. The summation of induced stress, bending stress and stretch stress cause mechanical balance which is equal to the residual stresses. As can be seen in Figure 4- 13-b (analytical solution), maximum residual stress is about -248MPa and the depth of the maximum residual stress is about 370 μm from the shot-peened surface. It should be noted that in Figure 4- 13 and Figure 4- 12 the depth of the compressive residual stresses in both numerical analysis and analytical solution are less than $400\mu m$ from the shot-peened surface. After thousands of impacts in the numerical simulation, maximum compressive residual stress is -311MPa which is slightly higher than maximum residual stresses in the analytical solution with -248MPa. This difference can be explained due to the cyclic impacts in numerical analysis and hardening theory while in the analytical solution just one single shot impact was considered to predict residual stresses.

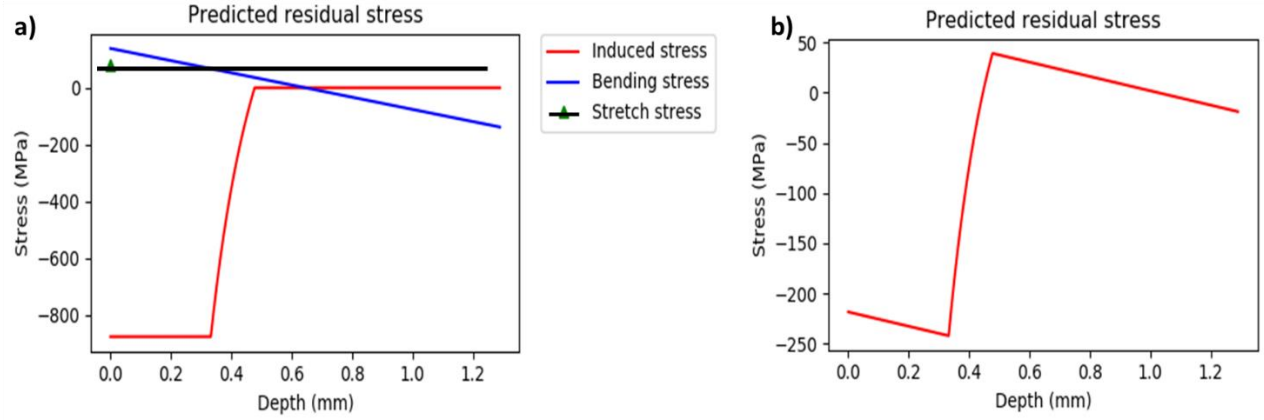

Figure 4- 13 Analytical solution for induced stress, bending stress and stretch stress b) overall residual stresses after summation of all stresses.

4.8. Conclusions

In this research surface roughness profile for different shot sizes and mixed shot, particles have been investigated based on the finite element modeling. Results have been compared with experimental results with the same materials for validation. The results indicate with increasing impact shot dimension, surface roughness parameters are increasing. These results were expected phenomenologically based on other research and experimental data. In this research has been shown by using mixed shot size during shot peening, surface roughness parameters can be reduced extensively. Sequence shot peening with a different order (small to big size) or (big to small size) has the same effect on shot peening roughness parameters. The mixed shot size experimentally can be faster and more reliable instead of doing multiple shot peening with different shot sizes. Residual stress profile showed improvement for a mixed shot size not only in terms of maximum residual stresses but also it showed a wider range of compressive residual stresses which is more desirable for shot peening.

SUMMARY

The current project examined residual stresses after shot peening process with nanoindentation and numerical analysis. Nanoindentation is an experimental technique to reveal the related mechanical behavior of materials while determining residual stresses after cold working or heat treatment. In this research, residual stresses were measured by the nanoindentation technique by comparing the contact area between a stressed sample and stress-free sample. This method has the capability to measure hardness and residual stresses under the impingement surface after shot peening. Residual stresses on the specimen can change the load-displacement curve and indentation impression in comparison to the stress-free sample. Measuring the corrected contact area, hardness and modulus are generally found to be independent of the residual stresses. Based on the contact area model compressive and tensile residual stresses can be found by comparing the relative contacts areas of the stressed sample and stress-free sample. Also, a new approach was developed based on the energy of the indentation to measure residual stresses after peening process. In this model instead of comparing relative contacts areas, the indentation energy between the stressed sample and stress-free sample has been compared to reveal residual stresses. It was determined that unloading response during indentation depends on pre-existing residual stresses in material with strain hardening. The residual stresses of a double-side shot peened thin aluminum sheet was examined by using the nanoindentation contact area method. The generally expected stress profile, with compressive residual stresses on both sides and a slight tensile residual stress in the center, was observed. Due to the thin wall structure and work hardening phenomenon during the first side shot peening an asymmetry stress profile was observed in the part, even having used the same peening processing conditions for both sides. The hardness of the compressively stressed region increased by approximately 10%, but this strain hardened region was constrained to a depth, on the order of the depth over which the compressive residual stresses were present. The asymmetry of the residual stress profile is on the order of 10%; with the first side showing maximum residual stress of approximately 420 MPa and the second side showing maximum residual stress of 470 MPa. On the other hand, there was no significant asymmetry in hardness. Finite element simulation predicted the experimental results and shot peening parameters such as velocity, impact diameter, impact angle and exposure time. Finite element simulation had been

conducted for double sided aluminum sample to simulate experimental residual stress measurement. Both results showed a good correlation in terms of magnitude and depth of the maximum compressive stresses. For aluminum sample hardness and reduced modulus provided data and foundation for crack initiation and crack propagation by hard intermetallic components within shot peened aluminum alloy and un-shot peened sample. The results showed hard particles are cracked due to the shot peening but compressive residual stresses during the fatigue loading prevents crack propagation from hard particles into the metallic matrix. The localized residual stresses of a shot peened austempered 52100 steel were measured by using nanoindentation energy formulated method. Also, nanoindentation results were validated by X-ray technique. It was found that the average residual stresses extracted using the indentation method on the surface was in good agreement with the x-ray results. Wider distribution results for every single indentation were observed in comparison with the x-ray results. This was attributed to localized metallurgical parameters, suggesting that residual stresses on the micro scale may vary significantly more than would be evident with larger volume sampling methods. The residual stresses obtained by nanoindentation technique on the cross section also showed promising agreement with the x-ray measurement. Finally, surface roughness profile for different shot sizes and mixed shot, particles were investigated based on the finite element modeling for surface roughness optimization. In this research, Almen test simulation was developed to create a link between model shot energy to Almen strip intensities to obtain a number of shot particles during surface roughness modeling. The results showed with increasing impact shot dimension, surface roughness parameters were increasing. These results were expected phenomenologically based on other research and experimental data. In this research was shown by using mixed shot size during shot peening, surface roughness parameters can be reduced extensively. Sequence shot peening with a different order (small to big size) or (big to small size) had the same effect on shot peening roughness parameters. Residual stress profile showed improvement for a mixed shot size not only in terms of maximum residual stresses but also it showed a wider range of compressive residual stresses which is more desirable for shot peening. The results have been compared with experimental results with the same materials for validation.

APPENDIX A. ALMEN-TEST RANDOM IMPACT CODE PYTHON 2.7

```
# -*- coding: mbcss -*-
from part import *
from material import *
from section import *
from assembly import *
from step import *
from interaction import *
from load import *
from mesh import *
from optimization import *
from job import *
from sketch import *
from visualization import *
from connectorBehavior import *
import random
import time
for z in range(0, 2500):
    X = 0.0 + random.randint(1.0,100.0) * 2.5 / 10.0
    Y = 0.0 + random.randint(1.0,100.0) * 1.9 / 10.0
    mdb.models['Model-1'].ConstrainedSketch(name='__profile__', sheetSize=200.0)
    mdb.models['Model-1'].sketches['__profile__'].rectangle(point1=(0.0, 0.0),
        point2=(76.0, 1.29))
    mdb.models['Model-1'].Part(dimensionality=THREE_D, name='Substrate', type=
        DEFORMABLE_BODY)
    mdb.models['Model-1'].parts['Substrate'].BaseSolidExtrude(depth=19.0, sketch=
        mdb.models['Model-1'].sketches['__profile__'])
    del mdb.models['Model-1'].sketches['__profile__']
```

```
mdb.models['Model-1'].parts['Substrate'].Surface(name='Bottom-surf',
    side1Faces=
    mdb.models['Model-1'].parts['Substrate'].faces.getSequenceFromMask((
    '[#8 ]', ), ))
mdb.models['Model-1'].ConstrainedSketch(name='__profile__', sheetSize=20.0)
mdb.models['Model-1'].sketches['__profile__'].ConstructionLine(point1=(0.0,
    -10.0), point2=(0.0, 10.0))
mdb.models['Model-1'].sketches['__profile__'].FixedConstraint(entity=
    mdb.models['Model-1'].sketches['__profile__'].geometry[2])
mdb.models['Model-1'].sketches['__profile__'].ArcByCenterEnds(center=(0.0, 0.0)
    , direction=CLOCKWISE, point1=(0.3, 0.0), point2=(0.0, -0.3))
mdb.models['Model-1'].sketches['__profile__'].CoincidentConstraint(
    addUndoState=False, entity1=
    mdb.models['Model-1'].sketches['__profile__'].vertices[1], entity2=
    mdb.models['Model-1'].sketches['__profile__'].geometry[2])
mdb.models['Model-1'].Part(dimensionality=THREE_D, name='Ball-1', type=
    ANALYTIC_RIGID_SURFACE)
mdb.models['Model-1'].parts['Ball-1'].AnalyticRigidSurfRevolve(sketch=
    mdb.models['Model-1'].sketches['__profile__'])
del mdb.models['Model-1'].sketches['__profile__']
mdb.models['Model-1'].ConstrainedSketch(name='__profile__', sheetSize=20.0)
mdb.models['Model-1'].sketches['__profile__'].ConstructionLine(point1=(0.0,
    -10.0), point2=(0.0, 10.0))
mdb.models['Model-1'].sketches['__profile__'].FixedConstraint(entity=
    mdb.models['Model-1'].sketches['__profile__'].geometry[2])
mdb.models['Model-1'].sketches['__profile__'].ArcByCenterEnds(center=(0.0, 0.0)
    , direction=CLOCKWISE, point1=(0.3, 0.0), point2=(0.0, -0.3))
mdb.models['Model-1'].sketches['__profile__'].CoincidentConstraint(
    addUndoState=False, entity1=
    mdb.models['Model-1'].sketches['__profile__'].vertices[1], entity2=
```

```
    mdb.models['Model-1'].sketches['__profile__'].geometry[2])
mdb.models['Model-1'].Part(dimensionality=THREE_D, name='Ball-2', type=
    ANALYTIC_RIGID_SURFACE)
mdb.models['Model-1'].parts['Ball-2'].AnalyticRigidSurfRevolve(sketch=
    mdb.models['Model-1'].sketches['__profile__'])
del mdb.models['Model-1'].sketches['__profile__']
mdb.models['Model-1'].ConstrainedSketch(name='__profile__', sheetSize=20.0)
mdb.models['Model-1'].sketches['__profile__'].ConstructionLine(point1=(0.0,
    -10.0), point2=(0.0, 10.0))
mdb.models['Model-1'].sketches['__profile__'].FixedConstraint(entity=
    mdb.models['Model-1'].sketches['__profile__'].geometry[2])
mdb.models['Model-1'].sketches['__profile__'].ArcByCenterEnds(center=(0.0, 0.0)
    , direction=CLOCKWISE, point1=(0.3, 0.0), point2=(0.0, -0.3))
mdb.models['Model-1'].sketches['__profile__'].CoincidentConstraint(
    addUndoState=False, entity1=
    mdb.models['Model-1'].sketches['__profile__'].vertices[1], entity2=
    mdb.models['Model-1'].sketches['__profile__'].geometry[2])
mdb.models['Model-1'].Part(dimensionality=THREE_D, name='Ball-3', type=
    ANALYTIC_RIGID_SURFACE)
mdb.models['Model-1'].parts['Ball-3'].AnalyticRigidSurfRevolve(sketch=
    mdb.models['Model-1'].sketches['__profile__'])
del mdb.models['Model-1'].sketches['__profile__']
mdb.models['Model-1'].ConstrainedSketch(name='__profile__', sheetSize=20.0)
mdb.models['Model-1'].sketches['__profile__'].ConstructionLine(point1=(0.0,
    -10.0), point2=(0.0, 10.0))
mdb.models['Model-1'].sketches['__profile__'].FixedConstraint(entity=
    mdb.models['Model-1'].sketches['__profile__'].geometry[2])
mdb.models['Model-1'].sketches['__profile__'].ArcByCenterEnds(center=(0.0, 0.0)
    , direction=CLOCKWISE, point1=(0.3, 0.0), point2=(0.0, -0.3))
mdb.models['Model-1'].sketches['__profile__'].CoincidentConstraint(
```

```
    addUndoState=False, entity1=
    mdb.models['Model-1'].sketches['__profile__'].vertices[1], entity2=
    mdb.models['Model-1'].sketches['__profile__'].geometry[2])
mdb.models['Model-1'].Part(dimensionality=THREE_D, name='Ball-4', type=
    ANALYTIC_RIGID_SURFACE)
mdb.models['Model-1'].parts['Ball-4'].AnalyticRigidSurfRevolve(sketch=
    mdb.models['Model-1'].sketches['__profile__'])
del mdb.models['Model-1'].sketches['__profile__']
mdb.models['Model-1'].parts['Ball-1'].Surface(name='ball1-surf', side1Faces=
    mdb.models['Model-1'].parts['Ball-1'].faces.getSequenceFromMask(('[#1 ]',
    ), ))
mdb.models['Model-1'].Part(name='Ball-5', objectToCopy=
mdb.models['Model-1'].parts['Ball-1'])
                                        .
                                        .
    mdb.models['Model-1'].rootAssembly.Instance(dependent=ON, name='Ball-40-1',
    part=mdb.models['Model-1'].parts['Ball-40'])
#mdb.models['Model-1'].rootAssembly.translate(instanceList=('Ball-4-1',),
                                       .
                                        .
                                        .
mdb.models['Model-1'].rootAssembly.translate(instanceList=('Ball-40-1',),
                                    vector=(X40, r, Y40))
mdb.models['Model-1'].rootAssembly.Instance(dependent=ON, name='Ball-1-1',
    part=mdb.models['Model-1'].parts['Ball-1'])
                                        .
                                        .
mdb.models['Model-1'].rootAssembly.Instance(dependent=ON, name='Ball-40-1',
    part=mdb.models['Model-1'].parts['Ball-40'])
mdb.models['Model-1'].RigidBody(name='Constraint-3', refPointRegion=Region(
```

```
    referencePoints=(
    mdb.models['Model-1'].rootAssembly.instances['Ball-1-1'].referencePoints[3],
    )), surfaceRegion=
    mdb.models['Model-1'].rootAssembly.instances['Ball-1-1'].surfaces['ball1-surf'])
mdb.models['Model-1'].RigidBody(name='Constraint-n', refPointRegion=Region(
    referencePoints=(
    mdb.models['Model-1'].rootAssembly.instances['Ball-40-1'].referencePoints[3],
    )), surfaceRegion=
    mdb.models['Model-1'].rootAssembly.instances['Ball-40-1'].surfaces['Ball4-surf'])
```

APPENDIX B. ALMEN ANALYTICAL SOLUTION CODE PYTHON 3.6

```
import os
import sys
from PyQt5.QtWidgets import QApplication, QWidget, QPushButton, QMessageBox
from scipy.integrate import quad
from PyQt5.QtGui import QIcon
from PyQt5.QtCore import pyqtSlot
import numpy as np
import matplotlib
from pylab import*
import math
import numpy.matlib as M
import matplotlib.pyplot as plt
import PySimpleGUI as sg
window = sg.Window('Almen-Test')
class App(QWidget):
    def __init__(self):
        super().__init__()
        self.title = 'PyQt5 messagebox - pythonspot.com'
        self.left = 10
        self.top = 10
        self.width = 320
        self.height = 200
        self.initUI
    @property
    def initUI(self):
        self.setWindowTitle(self.title)
        self.setGeometry(self.left, self.top, self.width, self.height)
```

```
        sys.exit()
            layout = [
            [sg.Text('Please enter approprite values, default values are assigned for Almen strip test- A!')],
            [sg.Text('Ball size diameter mm', size=(30, 1)), sg.InputText('0.85', key='DD')],
            [sg.Text('Impact angle degree', size=(30, 1)), sg.InputText('0', key='alphaa1')],
            [sg.Text('Ball poisson ratio', size=(30, 1)), sg.InputText('0.28', key='posnB1')],
            [sg.Text('Ball modulus MPa', size=(30, 1)), sg.InputText('300000', key='modlsB1')],
            [sg.Text('Substrate poisson ratio', size=(30, 1)), sg.InputText('0.29', key='posnM1')],
            [sg.Text('Substrate modulus MPa', size=(30, 1)), sg.InputText('205000', key='modlsM1')],
            [sg.Text('Ball density tonne/mm3', size=(30, 1)), sg.InputText('3.8E-9', key='roB1')],
            [sg.Text('Substrate density tonne/mm3', size=(30, 1)), sg.InputText('7.8E-9', key='roM1')],
            [sg.Text('Substrate yield stress MPa', size=(30, 1)), sg.InputText('1408', key='sigmay1')],
            [sg.Text('Substrate kinematic hardening MPa', size=(30, 1)), sg.InputText('1705', key='CC')],
            [sg.Text('Substrate strip length mm', size=(30, 1)), sg.InputText('76', key='Lx1')],
            [sg.Text('Substrate strip width mm', size=(30, 1)), sg.InputText('19', key='w1')],
            [sg.Text('Substrate strip height mm', size=(30, 1)), sg.InputText('1.29', key='h1')],
            [sg.Submit(), sg.Cancel()]]
        event, values = window.Layout(layout).Read()
        #kk = float(input("Efficiency ex. 0.85: "))
        #vv = float(input("Impact initial velocity ex. 30000mm/s: " ))
        DD11 = float(values['DD'])
        alphaa11 = float(values['alphaa1'])
        posnB11 = float(values['posnB1'])
        modlsB11 = float(values['modlsB1'])
        posnM11 = float(values['posnM1'])
        modlsM11 = float(values['modlsM1'])
```

```
        roB11 = float(values['roB1'])
        roM11 = float(values['roM1'])
        sigmay11 = float(values['sigmay1'])
        CC1 = float(values['CC'])  # Modulus of kinematic hardening
        Lx11 = float(values['Lx1'])
        w11 = float(values['w1'])
        h11 = float(values['h1'])
        ii = arange(0, 0.6, 0.01)
        for Al in (ii):
            v = 4000
            z1= 0.001
            k = 0.8
            s = 1
            modlsEQ = 1 / (((1 - (posnM) ** 2) / modlsM) + ((1 - (posnB) ** 2) / modlsB))
                K = ((2 / 3)) ** (0.50) * sigmay
                Vn = v * np.sin(90 - alphaa)
                p0 = ((5 * k * modlsEQ ** 4 * roB * (Vn) ** 2) / (2 * pi ** 4)) ** (0.2)  # Elastic
contact pressure
                a = (D / 2) * ((5 * k * pi * roB * (Vn) ** 2) / (2 * modlsEQ)) ** (0.2)  # Impact
dimple size
                sigmaxx = p0 * (1 + posnM) * ((z / a) * ((pi / 2) - (np.arctan(z / a))) - 1) + (
                (p0 * a ** 2) / (2 * (a ** 2 + z ** 2)))  # stress in xx axis hertz contact
                sigmayy = p0 * (1 + posnM) * ((z / a) * ((pi / 2) - (np.arctan(z / a))) - 1) + (
                (p0 * a ** 2) / (2 * (a ** 2 + z ** 2)))  # stress in yy axis hertz contact
                sigmazz = -((p0 * a ** 2) / (a ** 2 + z ** 2))  # stress in zz axis hertz contact
                sigmael = array([[sigmaxx, 0, 0], [0, sigmayy, 0], [0, 0, sigmazz]])  # Hertz Tensor
                tr = trace(sigmael)  # trace
                sel = sigmael - np.array([[tr / 3, 0, 0], [0, tr / 3, 0], [0, 0, tr / 3]])  # Herz deviatoric
stress
                seq = (2 * (sel[0, 0]) ** 2 + (sel[2, 2]) ** 2) ** (0.5)
                    b =1
```

```
            M0 =  M00[0]
            M2.append(abs(M0))
            M1 = stressind2*sum(M2)
            arc = ((3 * abs(M1) * Lx ** 2) / (2 * modlsM * h ** 3))
            finalVelocity1 = v
               depth1 = z
               AlmenHeight1 = arc
               z1 = 0
               v = v + 400
               z1 = 0
         strainp = alphaz * ((3 * (1 - posnM)) / (3 * C * (1 - posnM) + modlsM))
         stressind2 = (-strainp * (modlsM / (1 - posnM)))
         stressindT2.append(stressind2)
      finalVelocity.append((finalVelocity1) / 1000)
      AlmenHeight.append(AlmenHeight1)
      depth.append(depth1)
print(finalVelocity)
print(AlmenHeight)
# print(depth)
fig = plt.figure()
plt.subplot(1, 2, 1)
plt.plot(AlmenHeight, finalVelocity, 'ro')
plt.title('Almen height')
plt.xlabel('Almen height (mm)')
plt.ylabel('Velocity (m/s)')
plt.subplot(1, 2, 2)
plt.plot(depth, finalVelocity, 'ro')
plt.title('Maximum depth of residual stress')
plt.xlabel('Residual stress Depth (mm)')
plt.ylabel('Velocity (m/s)')
```

```
plt.tight_layout()
plt.show()
sys.exit()
```

APPENDIX C. RESIDUAL STRESS ANALYTICAL SOLUTION CODE PYTHON 3.6

```
import os
import sys
from PyQt5.QtWidgets import QApplication, QWidget, QPushButton, QMessageBox
from PyQt5.QtGui import QIcon
from PyQt5.QtCore import pyqtSlot
import numpy as np
import matplotlib
from pylab import*
import math
import numpy.matlib as M
import matplotlib.pyplot as plt
from scipy.integrate import quad
import PySimpleGUI as sg
window = sg.Window('Almen-Test')
window = sg.Window('Almen-Test')
layout = [
    [sg.Text('Please enter appropriate values, default values are assigned for Almen strip-A! 79*19*1.29')],
    [sg.Text('Impact initial velocity mm/s:', size=(40, 1)), sg.InputText('80000', key='VV')],
    [sg.Text('Impact ball dimension mm', size=(40, 1)), sg.InputText('0.4', key='DD')],
    [sg.Text('Substrate yield stress MPa', size=(40, 1)), sg.InputText('803', key='sigmayy')],
    [sg.Text('Substrate poisson ratio ', size=(40, 1)), sg.InputText('0.3', key='posnMM')],
    [sg.Text('Substrate modulus MPa', size=(40, 1)), sg.InputText('200000', key='modlsMM')],
    [sg.Text('Substrate Density tonnes/mm3', size=(40, 1)), sg.InputText('7.8E-9', key='roMM')],
    [sg.Text('Substrate kinematic hardening MPa', size=(40, 1)), sg.InputText('2773', key='Ckinematic')],
```

```
    [sg.Text('Impact ball poisson ratio', size=(40, 1)), sg.InputText('0.31', key='posnBB')],
    [sg.Text('Impact ball modulus MPa', size=(40, 1)), sg.InputText('210000', key='modlsBB')],
    [sg.Text('Impact ball density tonnes/mm3 ', size=(40, 1)), sg.InputText('7.8E-9', key='roBB')],
    [sg.Text('This is polynomial fitting curve start with', size=(40, 1)), sg.InputText('2',
key='powerinput')],
    [sg.Text('This is polynomial fitting constant ax^3 a', size=(40, 1)), sg.InputText('0',
key='aaa')],
    [sg.Text('This is polynomial fitting constant bx^2 b', size=(40, 1)), sg.InputText('-3125.7',
key='bbb')],
    [sg.Text('This is polynomial fitting constant cx^1 or C', size=(40, 1)), sg.InputText('5222.13',
key='ccc')],
    [sg.Text('This is polynomial fitting constant d or constant', size=(40, 1)), sg.InputText('-
1939.69', key='ddd')],
    [sg.Submit(), sg.Cancel()]
]
event, values = window.Layout(layout).Read()
vv1 = float(values['VV'])
DD1 = float(values['DD'])
sigmayy1 = float(values['sigmayy'])
posnMM1 = float(values['posnMM'])
modlsMM1 = float(values['modlsMM'])
roMM1 = float(values['roMM'])
Ckinematic1 = float(values['Ckinematic'])
posnBB1 = float(values['posnBB'])
modlsBB1 = float(values['modlsBB'])
roBB1 = float(values['roBB'])
powerinput1 = float(values['powerinput'])
aaa1 = float(values['aaa'])
bbb1 = float(values['bbb'])
ccc1 = float(values['ccc'])
ddd1 = float(values['ddd'])
```

```
power = powerinput1

C = Ckinematic1

Lx = 76

w = 19

h = 1.29

j =1

j =1                                                    #Second Counter

#Contact elastic calculation

arc = 0

z1=0

modlsEQ = 1/(((1-(posnM) ** 2)/modlsM)+ ((1-(posnB) ** 2)/modlsB))
#compliance of modulus

    t = (h - z1) / 1000

    Vn = v * np.sin(90 - alphaa)  # Normal velocity

    p0 = ((5 * k * (modlsEQ) ** 4 * roB * (Vn) ** 2) / (2 * pi ** 4)) ** (1 / 5)  # Elastic contact
pressure

    a = (D / 2) * ((5 * k * pi * roB * (Vn) ** 2) / (2 * modlsEQ)) ** (1 / 5)  # Impact dimple size

    K = ((2 / 3)) ** (0.5) * sigmay  # slope of the placticity

    sigmaxx = p0 * (1 + posnM) * ((z / a) * ((pi / 2) - (np.arctan(z / a))) - 1) + ((p0 * a ** 2) / (2 *
(a ** 2 + z ** 2)))  # stress in xx axis hertz contact

    sigmayy = p0 * (1 + posnM) * ((z / a) * ((pi / 2) - (np.arctan(z / a))) - 1) + ((p0 * a ** 2) / (2 *
(a ** 2 + z ** 2)))  # stress in yy axis hertz contact

    sigmazz = -((p0 * a ** 2) / (a ** 2 + z ** 2))  # stress in zz axis hertz contact

    sigmael = array([[sigmaxx, 0, 0], [0, sigmayy, 0], [0, 0, sigmazz]])  # Hertz T

    tr = trace(sigmael)  # trace

    sel = sigmael - np.array([[tr / 3, 0, 0], [0, tr / 3, 0], [0, 0, tr / 3]])  # Herz deviatoric stress

    seq = (1 / 2 * ((sel[0, 0] - sel[1, 1]) ** 2 + (sel[1, 1] - sel[2, 2]) ** 2 + (sel[2, 2] - sel[0, 0]) **
2)) ** (0.5)

Iyy = (1/3)*(w * h ** 3)

stressbending = (ans/ Iyy) *((h/2)-np.array(length))

plt.figure(1)
```

```
plt.subplot(221)
plt.plot(length, stressindT2, '-r')
polynomial=polyval(p,length)
plt.plot(length,polynomial, '-b', label=p)
plt.title('Polynomial fitting')
plt.legend(loc='lower left', fontsize = 'xx-small')
plt.xlabel('Depth (mm)')
plt.ylabel('Stress (MPa)')
RS = (stretchstress+(-stressbending)+stressindT2)
plt.subplot(222)
plt.plot(length, RS, '-r')
plt.title('Predicted residual stress')
plt.xlabel('Depth (mm)')
plt.ylabel('Stress (MPa)')
plt.subplot(223)
plt.plot(length, stressindT2, '-r' , label="Induced stress")
plt.plot(length, -(stressbending), '-b', label="Bending stress")
plt.plot(0, stretchstress, 'g^', label="Stretch stress")
plt.title('Predicted residual stress')
plt.xlabel('Depth (mm)')
plt.ylabel('Stress (MPa)')
plt.legend(bbox_to_anchor=(1.05, 1), loc=2, borderaxespad=0.)
plt.tight_layout()
```

LIST OF REFRENCES

[1] H. Wohlfahrt, "The influence of peening conditions on the resulting distribution of residual stress," *Proceedings of the 2nd International Conference on Shot Peening,* p. 316331, 1984.

[2] S. Al-Hassani, "An engineering approach to shot peening mechanics," *International conference shot peening,* pp. 275-282, 1984.

[3] R. Seifi and D. S. Majd, "Effects of plasticity on residual stresses measurement by hole drilling method," *Mechan. Mater,* vol. 53, p. 73, 2012.

[4] M. Mahmoodi, M. Sedighi and D. Tanner, "Investigation of through thickness residual stress distribution in equal channel angular rolled Al 5083 alloy by layer removal technique and X-ray diffraction," *Mater. Des,* no. 40, p. 516, 2012.

[5] O. Oladijo, A. M. Venter, L. A. Cornish and N. Sacks, "X-ray diffraction measurement of residual stress in WC-Co thermally sprayed coatings onto metal substrates," *Surf. Coatings Technol,* vol. 206, p. 4725, 2012.

[6] H. IlkerYelbay, I. Cam and C. Gur, "Non-destructive determination of residual stress state in steel weldments by Magnetic Barkhausen Noise technique," *NDT&E Int,* vol. 43, p. 29, 2010.

[7] S. Suresh, A. E. Giannakopoulos and J. Alcal_a, "Spherical indentation of compositionally graded materials theory and experiments," *Acta Materialia,* vol. 45, p. 1307, 1997.

[8] T. A. Venkatesh, K. J. Van Vliet, A. E. Giannakopoulos and S. Suresh, "Determination of elasto-plastic properties by instrumented sharp indentation guidelines for property extraction," *Scripta Material,* vol. 42, p. 833, 2000.

[9] A. E. Giannakopoulos and S. Suresh, "Theory of indentation of piezoelectric materials," *Acta Material,* vol. 47, pp. 21-53, 1999.

[10] L. N. Zhu, B. S. Xu, H. D. Wang and C. B. Wang, "Microstructure and nanoindentation measurement of residual stress in Fe based coating by laser cladding," *J. Mater. Sci,* vol. 47, pp. 21-22, 2012.

[11] W. C. Oliver and G. M. Pharr., "Influences of stress on the measurement of mechanical properties using nanoindentation Experimental studies in an aluminum alloy," *J. Mater. Res,* vol. 11, p. 752, 1996.

[12] A. Bolshakov, W. C. Oliver and G. M. Pharr, "Influences of stress on the measurement of mechanical properties using nanoindentation, II. Finite element simulations," *J. Mater. Res,* vol. 11, p. 76, 1996.

[13] L. N. Zhu, B. S. Xu, H. D. Wang and W. C. B, "Measurement of Residual Stresses Using nanoindentation Method," *Solid. Mater. Sci. Eng,* vol. 40, pp. 77-89, 2015.

[14] L. N. Zhu, B. S. Xu, H. D. Wang and C. B. Wang, "Effect of residual stress on the nanoindentation response of (100) copper single crystal," *Mater. Chem. Phys,* vol. 136, p. 561, 2012.

[15] S. Suresh and A. E. Giannakopoulos, "A New Method for Estimating Residual Stresses by Instrumented Sharp Indentation," *Acta Mater,* vol. 46, pp. 5755-5767, 1998.

[16] Y. H. Lee and D. Kwon, "Estimation of biaxial surface stress by instrumented indentation with sharp indenters," *Acta Material,* vol. 52, p. 1555, 2004.

[17] J. G. Swadener, B. Taljat and G. M. Pharr, "Measurement of residual stress by load and depth sensing indentation with spherical indenters," *J. Mater. Res,* vol. 16, p. 2091, 2001.

[18] W. Oliver and G. Pharr, "An improved technique for determining hardness and elastic modulus using load and displacement sensing indentation experiments," *J. Mater. Res,* vol. 7, no. 6, pp. 1564-1583, 1992.

[19] W. C. Oliver and G. M. Pharr, "Measurement of hardness and elastic modulus by instrumented indentation Advances in understanding and refinements to methodology," *J. Mater Res,* vol. 19, p. 3, 2004.

[20] Y. T. Cheng and C. M. Cheng, "Scaling approach to conical indentation in elastic-plastic solids with work hardening," *Appl. Phys. Lett,* vol. 73, p. 614, 1998.

[21] M. K. Khan, M. E. Fitzpatrick, S. V. Hainsworth and L. Edwards, "Effect of residual stress on the nanoindentation," *Computat. Mater. Sci,* vol. 50, p. 2967, 2011.

[22] J. C. Hay, A. Bolshakov and G. M. Pharr, " A critical examination of the fundamental relations used in the analysis of nanoindentation data," *J. Mater. Res,* vol. 14, pp. 22-96, 1999.

[23] T. Y. Tsui, W. C. Oliver and G. M. Pharr, "Influences of stress on the measurement of mechanical properties using nanoindentation Experimental studies in an aluminum alloy," *J. Mater. Res,* vol. 11, p. 752, 1996.

[24] L. Zhu, B. Xu, D. Wng and B. Wang, "Effect of residual stress on the nanoindentation responce of (100) copper single crystal," *Mater, chem. phys,* vol. 136, p. 561, 2012.

[25] W. Oliver and G. Pharr, "Measurment of hardness and elastic modulus by instrument indentation: Advances in understading and refinements to methodology.," *J. mater. Res,* p. 3, 2004.

[26] M. Thomas and M. Jackson, "The role of temperature and alloy chemistry on subsurface deformation mechanisms during shot peening of titanium alloys," *Scripta Mater,* vol. 66, p. 1065–1068, 2012.

[27] C. A. Taylor, M. F. Wayne and C. W. K, "Residual stress measurement in thin carbon films by Raman spectroscopy and nanoindentation.," *Thin Solid Films,* vol. 429, p. 190, 2003.

[28] M. Khabou, T. Castex and L. Inglebert, "The effect of material behavior law on the theoretical shot peening results," *European Journal Of Mechanics,* vol. 9, no. 1989, pp. 537-549, A/ Solid.

[29] Y. F. Obaid, "A rudimentary analysis of improving fatigue life of metals by shot peening," *Journal of Applied Mechanics,* vol. 57, pp. 307-312, 1990.

[30] S. Shen and S. Alturi, "analytical model for shot peening induced residual stresses," *Materials and Continua,* vol. 42, pp. 75-85, 2006.

[31] K. L. Johnson, Contact mechanics, Cambridge University Press, Cambridge UK: Cambridge University Press, 1985.

[32] M. Frija, T. Hassine, R. Fathallah, C. Bouraoui and A. Dogui, "Finite element modelling of shot peening process: Prediction of the compressive residual stresses the plastic deformations and the surface integrity," *Mater Sci Technol,* vol. 426, pp. 173-180, 2006.

[33] L. Lillamand, "Cyclic modelling of the mechanical state produced by shot peening," *Fatigue Fract Mater Struct,* vol. 24, pp. 93-104, 2001.

[34] K. J. Miller, "Materials science perspective of metal fatigue resistance," *Materials Science Technology,* vol. 9, p. 453, 1993.

[35] P. K. Sharp and G. Clark, Report DSTO-RR-0208. Aeronautical and Maritime Research Laboratory, Australia: Feshermand Bend , 2001.

[36] M. Guagliano, "Relating Almen intensity to residual stresses induced by shot peening: a numerical approach," *Journal of Materials Processing Technology,* vol. 110, pp. 277-286, 2001.

[37] S. A. Meguid, G. Shagal and J. Stranart, "D FE analysis of peening of strain-rate sensitive materials using multiple impingement model," *International Journal of Impact Engineering,* vol. 27, pp. 119-134, 2002.

[38] H. Y. Miao, H. Larose, C. Perron and L. M, "On the potential applications of a 3D random finite element model for the simulation of shot peening,," *Adv Eng Softw,* vol. 40, no. 10, pp. 1023-1038, 2009.

[39] S. T. Al-Hassani, K. Kormi and D. C. Webb, "Numerical simulation of multiple shot impact," *Proceedings of the 7th international conference on shot peening,* pp. 217-227, 1999.

[40] J. Schwarzer, V. Schulze and O. Vohringer, "Evaluation of the Influence of Shot Peening Parameters on Residual Stress Profiles using Finite Element Simulation," *Mater Sci Forum,* vol. 462, pp. 3951-3956, 2003.

[41] C. Ould, E. Rouhaud and M. François, "Kinematic Hardening Finite Elements Model to Evaluate Residual Stresses in Shot-Peened Parts, Local Measurements by X-Ray Diffraction," *Mater Sci Forum,* vol. 524, pp. 161-166,, 2006.

[42] E. Rouhaud and D. Deslaef, "nfluence of Shots' Material on Shot Peening, a Finite Element Model," *Mater Sci Forum,* vol. 404, pp. 153-158, 2002.

[43] S. Kyriacou, "Shot-peening mechanics a theoretical study," *Proceedings of the 6th International Conference on Shot Peening,* pp. 506-516, 1996.

[44] T. S. Al-Hassani, K. Kormi and D. C. Webb, "Numerical simulation of multiple shot," in *7th International conference on Shot Peening (ICSP),*, Warsaw, Poland,, 1999.

[45] S. A. Meguid, Mechanics of shot peening, UMIST.UK: Thesis , 1975.

[46] S. Baragetti, "Three-dimensional finite-element procedures for shot peening residual stress field prediction," *Int J Comput Appl Tech,* vol. 14, pp. 51-63, 2001.

[47] M. Klemenz, V. Schulze and O. Vöhringer, "Finite Element Simulation of the Residual Stress States after Shot Peening," in *7th European Conference on Residual Trans Tech Publications*, Uetikon-Zürich, 2006.

[48] S. Bagherifard, R. Ghelichi and M. Guagliano, "A numerical model of severe shot peening (SSP) to predict the generation of a nanostructured surface layer of material," *Surface & Coatings Technology,* vol. 204, pp. 4081-4090, 2010.

[49] J. Cammett, P. Prevéy and N. Jayaraman, "The effect of shot peening coverage on residual stress, cold work and fatigue in a nickel-base superalloy," in *ICSP-9,* Paris, France, 2005.

[50] S. Ma, X. Zhang, Y. Lian and X. Zhou, "Simulation of high explosive explosion using adaptive material point method," *Computer Modeling in Engineering & Sciences,* vol. 39, no. 2, pp. 101-124.

[51] M. Elbestawi and M. EITobgy, "Three dimensional elastoplastic element model for residual stresses in the shot peening process," *Proc. Instn Mech. Engrs,* vol. 218, no. 11, pp. 1471-1481, 2001.

[52] M. Grujicic, B. Pandurangan, C. F. Yen and B. A. Cheeseman, "Modifications in the AA5083 Johnson-Cook Material Model for Use in Friction Stir Welding Computational Analyses," *Modifications in the AA5083 Johnson-Cook Material Model for Use in Friction Stir Welding Computational Analyses,* vol. 21, no. 11, pp. 2207-2217, 2012.

[53] A. Yonezu, R. Kusano, T. Hiyoshi and X. Chen, "A Method to Estimate Residual Stress in Austenitic Stainless Steel Using a Micro indentation Test," *JMEPEG,* vol. 24, pp. 362-372, 2015.

[54] J. K. Li, M. Yao, D. Wang and R. Z. Wang, "Mechanical approach to the residual stress field induced by shot peening," *Materials Science and Engineering A,* vol. 147, pp. 167-173, 1991.

[55] K. Mori, K. Osakada and M. N, "Finite element analysis of peening process with plastically deforming shot," *Journal of Materials Processing Technology,* vol. 45, pp. 607-612, 1994.

[56] A. Levers and A. Prior, "Finite element simulation of shot peening," *The Shot Peener,* vol. 9, pp. 14-16, 1995.

[57] K. Schiffer and C. H. Droste gen, "Simulation of residual stresses by shot peening," *Computers and Structures,* vol. 72, pp. 329-340, 1999.

[58] J. Schwarzer, V. Schulze and O. Vöhringer, "Evaluation of the influence of shot parameters on residual stress profiles using element simulation," *Materials Science Forum,* vol. 426, pp. 3951-3956, 2003.

[59] T. J. Kim, N. S. Kim, S. C. Park and W. W Jeong, "Finite Element Analysis of Shot Peening Effected by Multiple Impacts," *KSME(A),* vol. 426, pp. 2656-2661, 2002.

[60] T. Kim and H. Lee, "A 2D FE Model for Unique Solution of Peening Residual Stress in Single Shot Impact," *KSME(A),* vol. 32, pp. 362-370, 2008.

[61] C. Hardy, C. N. Baronet and G. V. Tordion, "The elasto-plastic indentation of a half-space by a rigid sphere," *Int. J. Numer Methods Eng,* vol. 3, pp. 451-462, 1971.

[62] J. Edberg, L. Lindgren and K. Mori, Shot peening simulated by two different finite element formulations, , theory methods and applications, Rotterdam: Balkema, 1995.

[63] O. Hatamleh, I. V. Rivero and J. Lyons, "Evaluation of Surface Residual Stresses in Friction Stir Welds Due to Laser and Shot Peening," *JMEPEG,* vol. 16, pp. 549-553, 2007.

[64] G. Genzel, I. A. Denks, R. Coelho, D. Thomas, R. Mainz, A. D and K. M, "Exploiting the features of energy-dispersive synchrotron diffraction for advanced residual stress and texture analysis," *J. Strain Analysis,* vol. 46, p. 67, 2011.

[65] M. Crofta, I. Zakharchenko, Z. Zhong, Y. Gurlak, J. H. Hastings, R. Holtz, M. DaSilva and T. Tsakalakos, "Strain field and scattered intensity profiling with energy dispersive x-ray scattering," *Journal of applied physics,* vol. 92, pp. 870-880, 2002.

[66] A. Tekaya, H. A. Ghulman, T. Benameur and S. Labd, "Cyclic Nanoindentation and Finite Element Analysis of Ti/TiN and CrN Nanocoatings on Zr-Based Metallic Glasses Mechanical Performance," *JMEPEG,* vol. 23, pp. 4259-4270, 2014.

[67] A. Bolshakov, W. C. Oliver and G. M. Pharr, "Influences of stress on the measurement of mechanical properties using nanoindentation, II, Finite element simulations.," *J. Mater. Res,* vol. 11, p. 760, 1996.

[68] L. N. Zhu, B. S. Xu, H. D. Wang and W. C. B, "Measurement of Residual Stresses Using nanoindentation Method," *Solid. Mater. Sci. Eng,* vol. 40, pp. 77-89, 2015.

[69] P.-L. Larsson, "On the Influence of elastic deformation for residual stress determination by sharp indentation testing," *JMEPEG,* vol. 26, pp. 3854-3860, 2017.

[70] S. Larsson and C. Per-Lennart, "On the determination of residual stress and strain fields by sharp indentation testing, Part I Theoretical and numerical analysis," *Acta mater,* vol. 49, pp. 2179-2191, 2001.

[71] J. C. Hay, A. Bolshakov and G. M. Pharr, "A critical examination of the fundamental relations used in the analysis of nanoindentation data," *J. Mater. Res,* vol. 14, pp. 22-96, 1999.

[72] M. Nishikawa and H. Soyama, "Two-step method to evaluate equibiaxial residual stress of metal surface based on micro indentation tests," *Mater. Des,* vol. 32, p. 3240, 2011.

[73] M. Tanaka, M. Hasegawa, A. F. Dericioglu and Y. Kagawa, "Measurement of residual stress in air plasma-sprayed Y2O3-ZrO2 thermal barrier coating system using micro-Raman spectroscopy," *Mater. Sci. Eng A,* vol. 419, p. 262, 2006.

[74] E. Rouhaud, D. Deslaef, J. Lu and L. Chaboche, Modeling of residual stress, shot peening, Handbook on Residual Stress, Society of Experimental Mechanics, 2005.

[75] I. Altenberger, Mechanical surface treatment, shot peening, in: Jian Lu (Ed.), Society of Experimental Mechanics, 2005.

[76] W. M. Alberto, A. Nicolas, R. A. Lebensohn and S. M, "Effect of microstructure on strain localization in a 7050 aluminum alloy: Comparison of experiments and modeling for various textures," *Materials Science and Engineering,* vol. 661, pp. 187-197, 2016.

[77] D. J. Chadwick, S. Ghanbari, B. D. F and S. Michael, "Crack incubation in shot peened AA7050 and mechanism for fatigue enhancement," *Fatigue & Fracture of Engineering Materials & Structures,* vol. 41, pp. 71-83, 2017.

[78] Xiao, "Numerical simulation of stress peen forming with regular indentation," *Procedia Engineering,* vol. 81, pp. 867-872, 2014.

[79] W. Cao, R. Fathallah and L. Castex, "Correlation of Almen arc height with residual stresses in shot peening process," *Mater. Sci. Technol,* vol. 11, pp. 967-973, 1995.

[80] Y. Lu, S. Kurapati and F. Yang, "Finite element analysis of cylindrical indentation for determining plastic properties of materials in small volumes," *J. Phys. D: Appl. Phys,* vol. 41, 2008.

[81] M. Liu, C. Lu, K. A. Tieu, C. T. Peng and K. C, ", A combined experimental-numerical approach for determining mechanical properties of aluminum subjects to nanoindentation," *Sci. Rep,* vol. 5, p. 1507, 2015.

[82] A. F. Bower, N. A. Fleck, A. Needleman and N. Ogbonna, "Indentation of a power law creeping solid," *Proc. R. Soc. Lond. A,* vol. 441, pp. 97-124, 1993.

[83] G. W. König, Life Enhancement of Aero Engine Components by Shot Peening opportunities and Risks, 3th ed, Weinheim, Germany: Wiley-VCH, 2003.

[84] R. Seifi and D. S. Majd, " Effects of plasticity on residual stresses measurement by hole drilling method," *Mechan. Mater,* vol. 53, p. 73, 2012.

[85] M. Mahmoodi, M. Sedighi and D. Tanner, "Investigation of through thickness residual stress distribution in equal channel angular rolled Al 5083 alloy by layer removal technique and X-ray diffraction," *Mater. Des,* no. 40, p. 516, 2012.

[86] S. Suresh and A. E. Giannakapulos, "A new method for estimating residual stresses by instrumented sharp indentation," *Acta mater,* vol. 46, pp. 5755-5767, 1998.

[87] j. Swadener, B. Taljat and G. M. Pharr, "Measurment of residual stress by load and depth sensing indentation with spherical indenters," *J. Mater. Res,* vol. 16, 2001.

[88] Q. N. Meng, M. Wen, C. Q. Hu, S. M. Wang, K. Zhang, J. S. Lian and W. Zheng, "Influence of the residual stress on the nanoindentation-evaluated hardness for zirconium nitride films," *Surf. Coatings Technol,* vol. 206, pp. 32-50, 2012.

[89] A. Bolshakov, W. C. Oliver and G. M. Pharr, "Influences of stress on the measurment of mechanical properties using nanoindentation: II. Finite element simulations.," *J. Mater. Res,* vol. 11, p. 760, 1996.

[90] Z. H. XY and X. Li, "Influence of equi-biaxial residual stress on unloading behaviour of nanoindentation," *Acta Materialia,* vol. 53, p. 1913, 2005.

[91] M. K. Khan, M. Fitzpatrick, S. V. Hanisworth and L. Edwards, "Effect of residual stress on the nanoindentation responce of aerospace aluminum alloyu," *Comput. Mater. Sci,* vol. 50, p. 2967, 2011.

[92] L. Zhu, B. Xu, H. D Wang and C. Wang, "Measurment of mechanical properties of 1045 steel with significant pile-up by sharp indentation," *J. Mater. Sci,* vol. 46, p. 1083, 2011.

[93] M. K. Khan, M. E. Fitzpatrick, S. V. Hainsworth and L.Edwards, "Effect of residual stress on the nanoindentation response of aerospace aluminium alloys," *Computat. Mater. Sci,* vol. 50, p. 2967, 2011.

[94] S. Carlsson and P. Larsson, "On the determination of residual stress and strain fields by sharp indentation testing.: Part I: theoretical and numerical analysis," *Acta Mater,* vol. 49, p. 2179, 2001.

[95] Q. Wang, K. O. A, H. I. B, S. Nakano and H. Ogiso, "Indentation method to measure the residual stress induced," *Nucl. Instrum Methods B,* vol. 242, pp. 88-92, 2006.

[96] Youkendou, "X-ray Stress Measurement method," *Japan Sociey of Materials Science,* vol. 54, 1981.

[97] Y. Yoshioka, S. Ohya and T. Shinkai, "INFLUENCE OF IMAGE PROCESSING CONDITIONS OF DEBYE," *J. JSNDI,,* vol. 39, p. 666, 1990.

[98] T. SASAKI and Y. HIROSE, "INFLUENCE OF IMAGE PROCESSING CONDITIONS OF DEBYE SCHERRER RING IMAGES IN X-RAY STRESS MEASUREMENT USING AN IMAGING PLATE," *JCPDS-International Centre for Diffraction Data,* 1997.

[99] S. Taira and K. Tanaka, "Local Residual Stress near Fatigue Crack Tip," *The Society of Materials Science,* vol. 27, p. 251, 1978.

[100] G. Pharr and A. Bolshakov, "Understanding nanoindentation unloading curves," *J Mater Res,* vol. 17, pp. 2660-2671, 2002.

[101] M. Shrshorov, S.I.Bulychev and V.O.Alekhin, "Work of plastic and elastic deformation during indenter indentation," *Sov. Phys Dokl,* vol. 26, pp. 769-771, 1981.

[102] S. V. Hainsworth, H. W. Chandler and T. F. Page, "Analysis of nanoindentation load-displacement loading curves," *J. Mater.Res,* vol. 11, p. 8, 1996.

[103] M. M. Chaudhri, "Subsurface strain distribution around Vickers," *Acta Mater,* pp. 46, 3047, 1998.

[104] D. Tabor, The Hardness of solid, Oxford: Oxford University Press, 1951.

[105] W. D.Nix and H. Gao, "Indentation size effects in crystaline materials: a low for strain gradient plasticity," *J. Mech. Phys. Solids,* vol. 46, no. 3, pp. 411-425, 1998.

[106] B. Wolf and A. Richter, "The concept of differential hardness in depth sensing," *New Journal of Physics,* vol. 5, 2003.

[107] B. Wolf, A. Richter and M. Gunther, "Approaches of quantifying the entire load–depth curve in terms of hardness," *Z. Metal,* vol. 94, pp. 807-812, 2003.

[108] A. Rydin and P. Larsson, "On the correlation Between Residual Stresses and GlobalIndentation Quantities: Equibiaxial Stress Field," *Tribol. Lett,* pp. 31-42, 2012.

[109] P. K. Sharp, J. Q. Clayton and G. Clark, "The fatigue resistance of peened 7050-T7451 aluminum alloy-repair and re-treatment of a component surface," *Fatigue & Fracture of Engineering Materials & Structures,* vol. 17, no. 3, pp. 243-252, 1994.

[110] H. Miao, D. Demers, L. S, P. C and L. M, "Experimental studyof shot peening and stress peen forming," *J Mater Process Technol,* no. 210, pp. 2089-2102, 2010.

[111] F. Y. Al-Obaid, "Three dimensional dynamic finite element analysis for shot peening," *Computers and Structures,* vol. 36, no. 4, pp. 681-689, 1990.

[112] S. Meguid, G. Shagal and J. Stranart, "Finite element modelling of shot-peeningresidual stress," *J Mater Process Technol,* vol. 92, pp. 401-404, 1999.

[113] T. Kim, H. E. Lee, H. Lee and S. Cheong, "An area-average approach to peening residual stress under multi-impacts using a three-dimensional symmetry-cell finite element model with plastic shots," *Materials and Design,* vol. 31, pp. 50-59, 2010.

[114] G. I. Mylonas and G. Labeas, "Numerical modelling of shot peening process and corresponding products: Residual stress, surface roughness and cold work prediction," *Surface & Coatings Technology,* vol. 205, pp. 4480-4494, 2011.

[115] S. Bagherifard, R. Ghelichi and M. Guagliano, "Numerical and experimental analysis of surface roughness generated by shot peening," *J. Appl. Surf. Sc,* vol. 258, pp. 6831-6840, 2012.

[116] R. Clausen and J. Stangenberg, "Roughness of shot-peened surfaces – definition and measurement," in *The 7th International Conference on Shot Peening ICSP7*, Warsaw, Poland, 1999.

[117] J. Schmahling, F. A. Hamprecht and H. DMP, "three-dimensional measure of surface roughness based on mathematical morphology," *Int. J. Machine Tool Manuf,* vol. 46, pp. 1764-1769, 2006.

[118] J. B. 0601:, Geometrical Product Specification (GPS) – Surface Texture: Profile Method – Terms, Definitions and Surface Texture Parameters, FOREIGN STANDARD,, 2001.

[119] E. S. Gadelmawla, M. M. Koura, T. M. A. Maksoud, I. M. Elewa and H. H. Soliman, "Roughness parameters," *J. Mater. Process. Technol,* vol. 123, pp. 133-145, 2002.

[120] M. D. Sangid, J. A. Stori and P. M. Ferriera, "Process characterization of vibrostrengthening," *Int J Adv Manuf Technol,* vol. 53, no. 5-8, pp. 561-575, 2010.

[121] V. Baˇcová and D. Draganovskám, "Analyses of the quality of blasted surfaces," *Mater Sci,* vol. 1, no. 40, pp. 125-131, 2004.

[122] J. B. 0031, Geometrical Product Specifications (GPS) – Indication of Surface Texture in Technical Product Documentation, TOKYO: Japanese STANDARD, 2003.

[123] M. Sangid, J. A. Stori and P. M. Ferriera, "Process characterization of vibrostrengthening and application to fatigue enhancement of aluminum aerospace components—part I. Experimental study of process parameters," *The International Journal of Advanced Manufacturing Technology,* vol. 53, no. 5-8, pp. 545-560, 2011.

[124] J. Shit, S. Dhar and S. Acharyya, "Modeling and Finite Element Simulation of Low Cycle FatigueBehaviors of 316," *Procedia Engineering,* vol. 55, pp. 774-779, 2013.

[125] W. Y. Li, H. Liao, C. Li, G. Li, C. Coddet and X. Wang, "On high velocity impact of micro-sized metallic particles in cold spraying," *Appl. Surf. Sci,* vol. 253, pp. 2852-2862, 2006.

[126] M. Zimmerman, V. Schulze, H. U. Baron and L. D, "A Novel 3D Finite Element Simulation Model for the Prediction of the Residual Stress State after Shot Peening," *Proc. of the 10th International,* p. 63, 2008.

[127] D. Kirk and M. Y. Abyaneh, "Theoretical basis of shot peening coverage control," *Shot,* vol. 9, no. 2, pp. 28-30, 1995.

[128] H. Dianyin, Y. Gao, F. Meng, J. Song, Y. Wang, M. Ren and R. Wang, "A unifying approach in simulating the shot peening process using a 3D random representative volume finite element model," *Chinese Journal of Aeronautics,* vol. 30, no. 4, pp. 1592-1602, 2017.

[129] H. Guechichi, L. Castex and M. Benkhettab, "An Analytical Model to Relate Shot Peening Almen Intensity to Shot Velocity," *Mechanics Based Design of Structures and Machines,* vol. 41, pp. 79-99, 2013.

[130] W. Cao, R. Fathallah and L. Castex, "Correlation of Almen arc height with residual stresses in shot peening process," *Materials Science and Technology,* vol. 11, no. 9, pp. 967-973, 2013.

[131] E. Nordina and B. Alfredsson, "Measuring shot peening media velocity by indent size comparison," *Journal of Materials Processing Technology,* vol. 235, pp. 143-148, 2016.

[132] V. Baˇcová and D. Draganovskám, "Analyses of the quality of blasted surfaces," *Mater. Sci,* vol. 40, no. 1, pp. 125-131, 2004.

[133] J. Tan, M. Zhan, S. Liu, T. Huang, J. Guo and Y. H, "A modified Johnson–Cook model for tensile flow behaviors of 7050-aluminum alloy at high strain rates," vol. 631, pp. 214-219 , 2015.

[134] G. W. König, "Life Enhancement of Aero Engine Components by Shot Peening: Opportunities and Risks," in *Shot peening,* MTU Aero Engines, Munich, Germany, WILEY-VCH GmbH & Co.KGaA, 2002, p. 13.

[135] T. S. Al-Hassani, K. Kormi and D. C. Webb, "Numerical simulation of multiple shot," in *7th International conference on Shot Peening (ICSP),* Warsaw, Poland,, 1999.